MONTHLY NOTICES

OF THE

ROYAL ASTRONOMICAL SOCIETY

Volume 120 No. 5 1960

Published and Sold by the

ROYAL ASTRONOMICAL SOCIETY
BURLINGTON HOUSE
LONDON, W.1

Price £1 4s. 0d.; in U.S.A. $3.50

Subscription for volume: £6; in U.S.A. $18

The Geophysical Journal

OF THE

ROYAL ASTRONOMICAL SOCIETY

Editors

A. H. Cook
M.A., Ph.D., F.R.A.S., F.G.S.
National Physical Laboratory
Teddington

T. F. Gaskell
M.A., Ph.D., F.R.A.S.
British Petroleum Company
London

Price £1 per number; in U.S.A. $3. Annual Subscription £3; in U.S.A. $9

Volume 3 No. 2 June 1960

CONTENTS

P. J. Winter and H. D. Valliant, Relative gravity determinations in the Prairie provinces with Dominion Observatory bronze pendulum apparatus.

F. F. Evison, On the growth of continents by plastic flow under gravity.

D. E. Weston, The low-frequency scaling laws and source levels for underground explosion and other disturbances.

C. W. F. Everitt, Rock magnetism and the origin of the Midland Basalts.

C. Bull and E. Irving, The palaeomagnetism of some hyperbyssal intrusive rocks from South Victoria Land, Antarctica.

A. L. Hales and D. I. Gough, Isostatic anomalies and crustal structure in the Southern Cape.

E. C. Bullard, The automatic reduction of geophysical data.

J. Proudman, The condition that a long-period tide shall follow the equilibrium-law.

B. Gutenberg, PKIKP and pseudo-PKIKP phases at distances of less than 140°.

K. E. Bullen, A new method of deriving seismic velocity distributions from travel-time data.

Research Note

R. J. Donato, Seismic model experiments on the shape and amplitude of the refracted wave.

Note on Progress in Geophysics

G. Jobert, Current research in geophysics in France.

Report of Meeting

Geophysical Discussion of the Royal Astronomical Society, 1960 January 22.

Orders should be addressed to:

The Assistant Secretary

Royal Astronomical Society, Burlington House, London, W.1

MONTHLY NOTICES
OF THE
ROYAL ASTRONOMICAL SOCIETY
Vol. 120 No. 5

RADIO-ECHO OBSERVATIONS OF SOUTHERN HEMISPHERE METEOR SHOWER ACTIVITY FROM 1956 DECEMBER TO 1958 AUGUST

A. A. Weiss

(Communicated by E. G. Bowen)

(Received 1959 September 8)

Summary

A further survey of southern hemisphere meteor activity, extending from 1956 December to 1958 August, has been made with the 67 Mc/s narrow-beam equipment. The faintest detectable meteor trail has an electron line density of $1{\cdot}3 \times 10^{11}$ electrons/cm. The potentialities of radio equipments for the detection of weak meteor showers are demonstrated by an objective statistical analysis of echo counts. Weaker showers can be detected by the present equipment only if they transit within 30° of the zenith. The statistical analysis reveals an inherent clustering in the ecliptical component of sporadic meteors, and there is some evidence for very weak or short-lived showers which do not satisfy all the criteria laid down for an accepted shower. Radiants and echo rates for fifteen accepted and seven possible showers are tabulated and discussed. Echo rates measured at different equipment sensitivities for four showers indicate in all cases a deficiency, relative to sporadic meteors, in the numbers of fainter meteors in these streams.

1. *Introduction.*—This paper deals with the meteor showers detected during a radio survey of meteor activity at Adelaide. With the exception of a few short breaks, the survey was continuous from 1956 December to 1957 December inclusive, and again from 1958 April to August. No records were obtained during 1958 January–March. These observations continue the survey of Southern Hemisphere meteor activity which has proceeded intermittently since mid-1952 (Weiss (**1**, **2**) hereafter referred to as Papers I and II).

The potentialities of radio equipments in the identification and measurement of weak showers is a subject which has received little attention in the literature. For this reason a considerable part of this paper is devoted to a discussion of the factors which determine whether or not a given shower is detectable with the narrow-beam equipment in use, and to a description of the method developed to minimize the subjective element in the identification of the weaker showers. This is followed by factual data on all showers identified during the survey.

The application of an objective method of analysis of data, collected with an equipment whose inherent resolving power is superior to that of the previously used 27 Mc/s wind equipment, has resulted in the recognition of several new showers, which were either missed or regarded as uncertain in previous surveys.

2. *Equipment.*—The 67 Mc/s radiant equipment is basically the same as that used in 1953 and described in Paper I, except that the peak pulse power has been increased to 50 kW. The discrimination afforded between noise impulses and meteor echoes by transmission of double pulses 100-μsec apart

was supplemented in 1957 by a jitter on the time-base of the recording tube, which resulted in the quadrupling of each echo. This however was found to be unnecessary, and ample discrimination was obtained in 1958 by retaining the time-base jitter and transmitting a single pulse 25-μsec wide. The time of occurrence and slant range of each echo were recorded.

The axes of the two identical beamed aerial arrays are directed at elevation 9° along azimuths 35°·5 S of E (N aerial) and 14° N of E (S aerial). Half-power beam widths are $\pm 3°{\cdot}5$ in azimuth and $\pm 4°{\cdot}5$ in elevation. The collecting sectors of these two aerials, which contain the radiants of all the detectable meteors, are narrow sectors stretching from horizon to horizon along great circles perpendicular to the beam axes. The daily rotation of the Earth sweeps these collecting sectors across that part of the celestial sphere which is visible from Adelaide, so that each portion of the visible celestial sphere is sampled twice per 24 hours, once by each sector. Each collecting sector crosses a point source in from 1 to 2 hours, except when the source lies close to the south celestial pole, where the times of passage are much longer. The time-difference between reception of echoes from a given source in the two aerials is a unique function of the declination of the source. Curves for the determination of meteor shower radiants from measured times of reception of echoes from the two sectors are given in Paper I. The finite beam widths of the aerials result in a variation of echo range with time, as the collecting sectors pass across the source; typical range–time envelopes have already been published (**3**).

3. *Calibration of the equipment.*—The average sporadic echo rate is about 700 per day in each channel.

The electron line density in the faintest detectable meteor trail has been estimated by two indirect methods. A limiting line density of $1{\cdot}2 \pm 0{\cdot}2 \times 10^{11}$ electrons/cm has been deduced for 1957 October to December from a comparison of echo rates at different equipment sensitivities (**4**). The second method, based on shower meteor fluxes, will be described in detail.

Following the procedure already applied to the 27 Mc/s wind equipment (**5**), the echo rate N_r for the radiant equipment has been determined as a function of the meteor particle flux F, at those times when the direction of maximum equipment response lies in the echo plane, i.e. when the direction of flight of the meteor particles proceeding from an individual radiant is normal to the direction of maximum response. This direction lies in the azimuth of the beam axis and at elevation 10°·5; the slight displacement from the direction of the axis of the aerial beam is due to the variation of returned echo power with slant range of the reflection point. Assuming an inverse power law for the differential distribution of meteor masses, the integral flux function F becomes*

$$F(\alpha_r) = (c/(s-1))\alpha_r^{1-s} \qquad (1)$$

where α_r is the maximum electron density in the trail at the limit of detection in the direction of maximum response. The ratio $N_r/F\,(\mathrm{km})^2$ is plotted in Fig. 1 as a function of radiant zenith angle χ for three values of s. If the flux F can be measured independently, α_r can be found at once from (1). The Geminid meteor stream is most suitable for this calibration; the maximum echo rate is remarkably constant from year to year, and the mass distribution is well

* It is assumed that the ionizing efficiency of a meteor is independent of its mass.

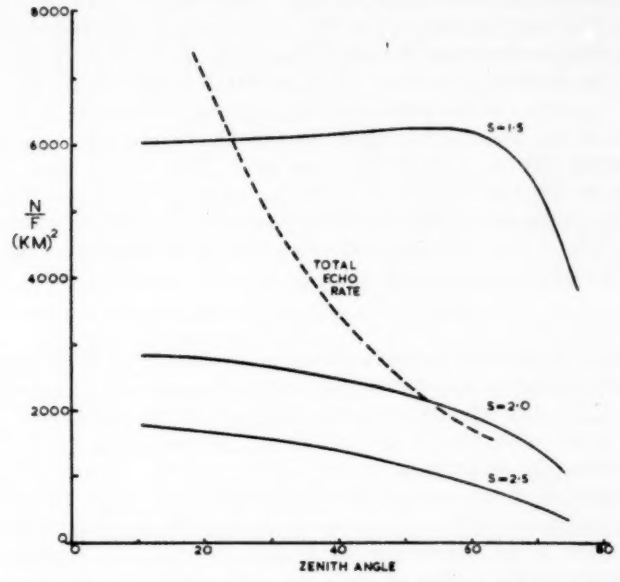

FIG. 1.—*The echo rate N for the radiant equipment, as a function of the zenith angle of the radiant at the time when the direction of the meteor flight is normal to the direction of maximum equipment response. F is the integral meteor flux, and s is the mass distribution parameter (see equation (1)). The total echo rate (broken curve) is the relative number of echoes received whilst the radiant lies within the collecting sector of the aerial; it is drawn for sporadic meteors, s=2·0.*

determined ($s \sim 1{\cdot}5$ in the brightness range which contributes most of the echoes). Now the 27 Mc/s wind equipment has been calibrated absolutely, and equation 6 (*a*) of reference (**5**) gives the relation between N_w and $F(\alpha_w)$ for this equipment when $\chi = 70^\circ$ and $\alpha_w = 3{\cdot}5 \times 10^{11}$ electrons/cm. With $s = 1{\cdot}5$,

$$\alpha_r = 3{\cdot}5 \times 10^{11} \left(\frac{f}{3050}\right)^2 \left(\frac{N_w}{N_r}\right)^2 \text{ electrons/cm}, \qquad (2)$$

$N_w = 24$/hr (Paper II). The ratio $f = N_r/F(\alpha_r)$ is to be taken from Fig. 1 at the zenith angle of the Geminid radiant at the time of detection at maximum response, and N_r is the instantaneous echo rate at this time, which may be ascertained from the range–time plots. For the *N* aerial, $\chi = 75^\circ$, $f = 4050$ km², $N_r = 54$/hr (1957), leading to $\alpha_r = 1{\cdot}21 \times 10^{11}$ electrons/cm. For the S aerial, $\chi = 70^\circ$, $f = 5230$ km², $N_r = 66$/hr, $\alpha_r = 1{\cdot}35 \times 10^{11}$ electrons/cm. These results are insensitive to a small error in the value of *s*, and to the finer details of the aerial polar diagrams. The calibration, of course, applies only to 1957 December, but the shower echo rates for 1956 and 1957 were almost identical.

A mean value of $\alpha_r = 1{\cdot}3 \times 10^{11}$ electrons/cm agrees satisfactorily with the above-quoted independent estimate of $1{\cdot}2 \times 10^{11}$. The fact that this latter calibration applies to a different period lends considerable weight to the supposition that the equipment sensitivity was essentially constant over the whole of the survey.

The limiting line density $\alpha_r = 1{\cdot}3 \times 10^{11}$ electrons/cm is the line density of the faintest trail segment detected by the equipment; it corresponds to a meteor some three magnitudes below the visual threshold. It is not at the same time the maximum line density in the trail which is detected most frequently. Because the effective aperture of the aerial increases with the line density at the reflection point, then in the range of maximum line densities from α_{max} to $\alpha_{max} + d\alpha_{max}$ the equipment collects a maximum number of trails when $\alpha_{max} \sim 2\alpha_r$. This result may be derived as follows. Again assuming the elementary integral distribution (1), the actual differential distribution of the maximum line densities of all trails detected by the equipment, regardless of the position of the reflection point on the trail, may be written as

$$N\,d\alpha_{max} = W(\alpha_{max})\alpha_{max}^{-s}\,d\alpha_{max}. \qquad (3)$$

The weighting function W is proportional to the volume of space within which a trail, whose maximum line density lies in the range α_{max} to $\alpha_{max} + d\alpha_{max}$, may be detected. It depends on the polar diagram of the aerial, and has been calculated by an extension of the numerical approach adopted by Clegg (**6**) in determining the collecting area for a point radiant. The extension of the weighting factor W from a surface to a volume has been made because with the fixed aerial system in use the collecting area appropriate to a point radiant moves across the whole of the aperture of the aerial as the radiant is carried across the collecting sector by the motion of the earth. In other words, the characteristics of shower echoes are determined as an average over the whole of the range–time envelope. Differential distributions for the echo rate for three values of s are given in Fig. 2, along with the curve for a meteor distribution of the form

$$N\,d\alpha_{max} = W\alpha_{max}^{-[1{\cdot}5+0{\cdot}453\log(\alpha_{max}/\alpha_r)]}\,d\alpha_{max}$$

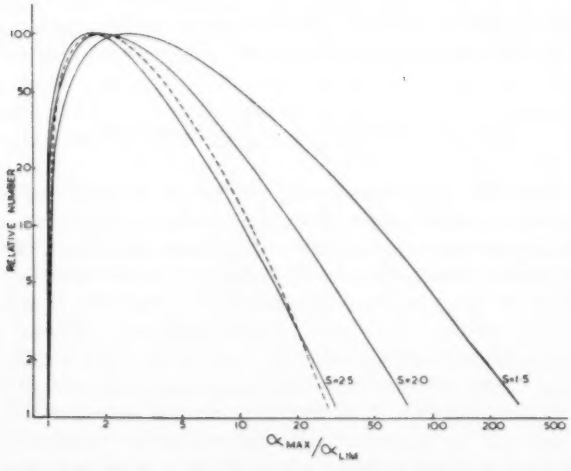

FIG. 2.—*Differential distributions of the numbers of meteor trails with maximum line densities in the range α_{max} to $\alpha_{max} + d\alpha_{max}$, as detected by the radiant equipment. Full lines are for constant values of the mass distribution parameter s. The broken line is for $s = 1{\cdot}5 + 0{\cdot}453\ log\ (\alpha_{max}/\alpha_{lim})$. α_{lim} is the equipment threshold.*

which, apart from the particular numerical values, is a possible representation of the mass distribution data for such showers as the Geminids and the Perseids. It is seen that the location of the maximum in the echo rate distribution is not strongly dependent on the mass distribution of the incident meteors, and lies about 1 magnitude above the equipment threshold.

The computations leading to Fig. 2 apply strictly only to a radiant which transits at the zenith. However, collecting areas examined during the preparation of Fig. 1 were found to be quite insensitive to the zenith angle of the radiant, and it is expected that the curves of Fig. 2 will apply with good accuracy to all radiants other than those which transit at low elevation.

The polar diagrams of most conventional aerial systems, if reduced to constant half-power widths, are very similar in the vicinity of the beam axes. The above conclusion, that the position of the maximum in the differential echo rate distribution as a function of radio brightness lies about 1 magnitude above the equipment threshold, should therefore not be limited to the Adelaide radiant equipment. It is a general result which will apply to the majority of radio equipments used in meteor studies.

4. *The recognition of shower activity.*—A detailed discussion of what is understood by the term "meteor shower" has already been given elsewhere (3). This question will not be pursued here, as the context of this paper should make clear the significance attached to this term.

Shower activity is detected and measured against a background of sporadic meteor activity, whose fluctuations set the ultimate limit to recognition of shower activity. The background activity has strong diurnal and seasonal variations, on which are superimposed the essentially random fluctuations which are examined in detail in Section 5. The sporadic rate ranges from a maximum of 100 echoes/hr near mid-day in March to a minimum of 2 echoes/hr near sunset in September. The corresponding range in the absolute value of the statistical fluctuations in the sporadic echo count precludes any constant threshold for shower detection; the chances of discovery are heavily weighted in favour of radiants with longitudes within $\pm 60^\circ$ of the antapex. Most showers in fact are detected from 22 hr through midnight to 10 hr L.T., when the sporadic rate is also high (average 40/hr), and the limiting echo rate at which a shower is detectable is 20–30/hr.

The method of searching the records for shower activity is based on an objective statistical analysis of the echo counts (3). The problem, as already mentioned, is one of disentangling rate increases due to shower activity from random fluctuations in the background count. Briefly, the echoes detected in each half-hourly period are counted, and the probability of obtaining any particular count is ascertained on the assumption that the background count is random and follows Poisson's distribution. The validity of Poisson's distribution has been established already for periods up to 10 min duration (3). During the present survey additional evidence, not described here, has been obtained that this distribution is valid also for echo counts in 30 min periods.

Periods of high count, which may include shower activity, are further scrutinized by plotting individual echoes in a range–time plot. Only those periods giving recognizable range–time envelopes are accepted as certainly including shower activity, unless the existence of the shower has been demonstrated independently by other observers. This reservation is made

because the clarity of a range–time envelope depends on the diffuseness of the radiant, and is also severely prejudiced by intermittent activity, which seems to be characteristic of some of the weaker showers, although this patchiness can be overcome to some extent by integration of the records for successive days.

In addition to considerations of meteor particle flux, time of detection, and radiant structure, the probability of detection of a shower is influenced strongly by the declination of the radiant, through a dependence of echo rate on zenith angle of the radiant at the time of passage through the collecting sector. Fig. 1 illustrates this dependence for those special instants when the direction of maximum equipment response lies in the echo plane. This is not the most useful representation, as the total number of echoes received whilst the radiant lies inside the collecting sector depends also on the shape of the range–time envelope and the duration of the passage, both of which are determined by the declination of the radiant. The concentrated Sun and anti-Sun sources of sporadic meteors (**7, 8**) afford the most reliable indication of this variation of total echo rate with zenith angle of the radiant. The mean total echo rate from these sources, as found in the present survey, is sketched in Fig. 1. Since this refers to sporadic meteors, the value of s is probably close to 2·0, but there is no reason to doubt that a similar strong variation of total echo rate would apply also to showers whose s-values may differ from 2·0.

It is therefore to be expected that the probability of detection of a shower will increase as the elevation of the radiant at transit increases from the northern horizon to the zenith. Beyond this to the south, the probability of detection will fall off rapidly, not only because of decreasing echo rates for a given flux, but also because the rapidly increasing duration of the passage of the radiant across the collecting sector may result in more, rather than less, confusion with the background count.

The tendency for the radiants of the weaker showers of Table III and of the possible showers of Table VII to group in the vicinity of $\delta = -35^\circ$ is a clear indication that the radiant type of equipment is most sensitive to showers whose radiant declination is approximately equal to the latitude of the observing station. A similar, spurious grouping of declinations near $\delta = -35^\circ$ could arise from a subjective bias in pairing periods of high activity on the two aerials to determine possible shower radiants, in that there is a natural tendency to group together periods of high activity which are close together in time. The more objective type of analysis adopted here makes such a bias very improbable.

5. *The statistics of echo counts.*—Levels of significance were set at 5 per cent, 1 per cent and 0·1 per cent, and a detailed analysis made of the occurrence of all cells (of $\frac{1}{2}$-hr period in time) whose count was either significantly high or significantly low. Data for both aerials have been pooled. For further details of the method of analysis, see (**3**).

The result of this analysis for the 5 per cent level is illustrated in Fig. 3 (*a*). All cells in which recognized shower activity occurred have been excluded. The unexpected shape of Fig. 3 (*a*) is therefore not due to shower activity which, as previously noted, occurs mainly from 22 hr to 10 hr L.T.; its implications are mentioned below, after discussion of other possible causes. Data for the whole period of the survey have been combined, as there is no apparent seasonal influence on the frequency of significant counts. The echo rate, Fig. 3 (*c*), is also an average over both aerials. The diurnal variation in occurrence of cells

significant at the 1 per cent and the 0·1 per cent levels is substantially the same as at the 5 per cent level. Their absolute numbers are of course lower (Table I), but not as low as would be expected from proportionality to the level of probability. Although many of the cells occupied by showers give a highly significant excess count, the overall contribution of showers to the total number of significant cells only becomes appreciable at probability levels $\leqslant 1$ per cent.

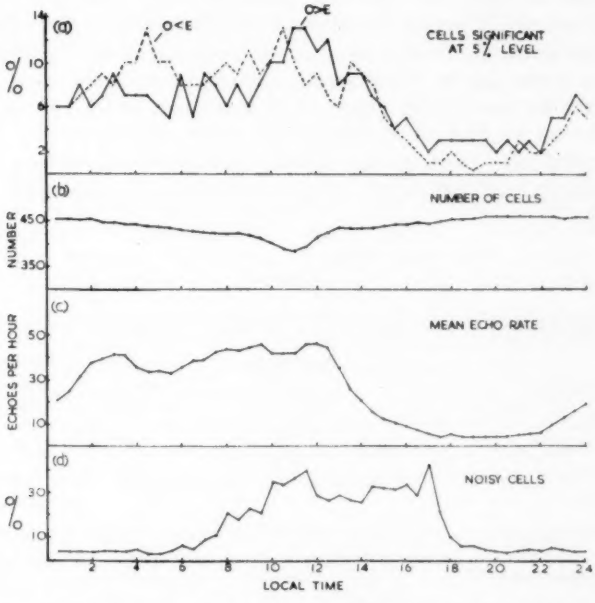

FIG. 3.—*The diurnal variation in the percentage of half-hourly cells whose echo counts are significantly high ($O > E$) or significantly low ($O < E$) at the 5 per cent level, compared with some other characteristics of the cells. Cells whose echo count is possibly reduced by interference are classified as noisy.*

The dip in the number of cells per half-hour around 11 hr L.T. (Fig. 3 (*b*)), and a general tendency for the number of cells to be lower during the day than the night, are caused by a combination of a regular mid-morning film change, and essential equipment maintenance. Cells occupied by showers amount to less than 5 per cent of the whole and their exclusion from the statistical analysis is unnoticed in Fig. 3 (*b*). This is a further striking example of the insignificant contribution of recognizable shower activity to the total meteor echo rate integrated over the basic period of one year.

One of the difficulties encountered in the application of statistical methods to the study of echo counts springs from cells whose counts may be in error due to extraneous causes. Of these causes of loss of rigour in the statistics, interference by noise impulses is by far the most serious. Contamination of the records by man-made interference, against which echo discrimination in the form of doubling and even quadrupling the meteor echo at times proved powerless, was a continuing problem during the survey, but fortunately the effect on the echo

statistics is determinable. All cells possibly, but not necessarily, affected by noise were noted; the counts for these "noisy" cells may either be correct or low, but never high.

The average distribution of noisy cells throughout the day is shown in Fig. 3 (*d*). Their incidence differs markedly from that of the cells of significantly low count. There is also no correlation between the total number of noisy cells for a given month, and the total number of cells of significantly low count for that month. Remembering that the echo count in a cell affected by noise is not thereby necessarily incorrect, the absence of correlations in these two instances suggests that noise interference is of minor consequence to the statistics. This is of course borne out by the general similarity between the incidence of cells of high and of low count (Fig. 3 (*a*)). It is only when we turn to the last column of Table I that we find clear evidence of meteor echoes lost by interference. Amongst noisy cells, there is some loss of significantly high counts, and a much stronger gain in significantly low counts which also increases with the level of significance.

TABLE I

Observed probabilities of occurrence of cells significant at different levels of expectation

Category	per cent	Including showers per cent	Excluding showers per cent	Percentage of noisy cells per cent
O > E	5	7·9	6·4	10
	1	3·3	2·1	11
	0·1	1·4	0·60	9
O < E	5		6·2	24
	1		2·0	27
	0·1		0·51	31
Total number of cells		21180	20380	15

Whilst a high order of accuracy cannot be claimed, it seems reasonable to conclude that Fig. 3 correctly depicts the general pattern of the diurnal variation in significant cells, that this pattern is identical for high and low counts, but that there is a small excess, say 10–20 per cent, of high counts over low counts.

The extent to which this excess of high count cells is indicative of permanent shower activity may be judged by examining the records for repetition of significant cells at identical times from one year to the next. This comparison is made in Table II between 1957 and 1958 for the months of May and July. As before, times of accepted shower activity have been omitted. A coincidence is scored only if the significant cells occur at identical times in the two years. Expected numbers of coincidences have been calculated on the assumption that significant cells are uniformly distributed in time throughout the day. Since in fact most significant cells are grouped into about 16 hr (Fig. 3) the expectations in Table II could well be increased by a factor of 2, in which case the number of coincidences between events in 1957 and in 1958 is no more than would be expected on a chance basis. The fact that coincidences between cells of low count are no less frequent than those between cells of high count supports this conclusion.

TABLE II

Observed and expected coincidences between significant cells for corresponding months in successive years

Category		1957–58 May		1957–58 July	
		Expect	Observe	Expect	Observe
	per cent				
O > E	5	5·3	9	1·6	5
	1	0·6	3	0·09	0
	0·1	0·06	1	0·005	0
O < E	5	3·1	7	1·7	3
	1	0·3	3	0·09	1
	0·1	0·02	0	0·000	0

Despite this negative result, the small excess of high count cells is probably real, and as such must originate in minor shower activity. Regardless of the reality of this excess, its very smallness implies that any attempt to identify all, or even a major portion of, periods of high count with shower activity is misleading. Lists of minor showers compiled on this basis will be virtually meaningless. At the 5 per cent level of significance, the fluctuations in the total echo count, after accepted showers have been excluded, are essentially random. At the 1 per cent and 0·1 per cent levels the fluctuations are greater than can be attributed to a purely random influx of meteors. The excess fluctuations, which are strongest when the concentrations in apparent radiants of sporadic meteors towards the Sun and the anti-Sun lie in the collecting sectors, are presumably to be associated with some inherent clustering amongst the ecliptical component of sporadic meteors.

6. *The accepted showers.*—Table III lists those showers which gave definite range–time envelopes, or are otherwise regarded as certain.

TABLE III

Accepted showers detected from 1956 December to 1958 August

Shower	Date of maximum activity	Duration (days)	Radiant α	Radiant δ	Maximum hourly echo rate
			°	°	
η-Aquarids	May 7	8	339	+ 2	30
Sagittarids	June 11	5	304	−35	30
Arietids, ζ-Perseids, β-Taurids	June	...	...	...	60
Phoenicids	July 14	15	32	−48	30
δ-Aquarids	July 29	26	342	−17	110
Capricornids	July	> 30	320	−20	100
Pisces Australids	July	> 30	335	−20	
Cetids	July	> 20	351	−18	
Sextantids/Leonids	September 29	9	155	0	30
Orionids	October 21	2	...	...	8
Puppids/Velids	December 6	9	140	−50	50
Phoenicids	December 5	1	15	−55	20
Geminids	December 14	8	114	+34	60

(*a*) *η-Aquarids.*—Radiant coordinates and estimates of radiant area are given in Table IV. There is some intermittent activity prior to May 3 and after May 10, which is probably attributable to this stream. The diffuseness of the radiant increases progressively as the Earth moves through the stream. Echo rates are plotted in Fig. 4; maximum activity occurs at $\odot = 45°$.

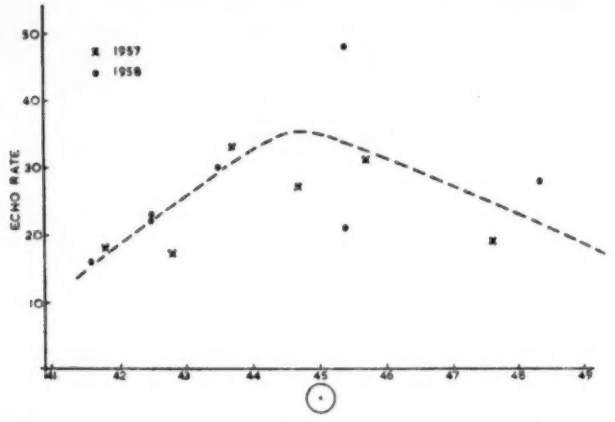

FIG. 4.—*Echo rates (shower echoes falling within range-time envelopes) for the η-Aquarid shower, as a function of solar longitude.*

The η-Aquarids is one of the more prominent visual showers. In comparison, the echo rate of 30/hr, at a zenith angle at tranist of 30°, for an equipment whose threshold is $\alpha = 1{\cdot}3 \times 10^{11}$ electrons/cm (visual brightness $M_v = \sim 7{\cdot}0$), seems rather low. However, after rejection of 40 per cent of long-enduring echoes on the grounds that their amplitudes showed obvious irregularities, a minimum of 20 per cent of the echoes detected in the 1957 apparition had durations exceeding 0·36 sec, corresponding to $\alpha \sim 1{\cdot}4 \times 10^{13}$ electrons/cm, $M_v \sim 2{\cdot}0$. The visual prominence of this shower is therefore not surprising, and the comparatively low echo rates obtained at the higher sensitivity can only mean that this stream is deficient in small meteors, i.e. the mass distribution parameter $s \ll 2{\cdot}0$ for $\alpha_{max} < 10^{13}$ electrons/cm.

TABLE IV

The radiant of the η-Aquarid shower

Date	Radiant co-ordinates		Radiant area*	
	1957	1958	1957	1958
May 3	}	...	C	VC
4	} 339, −2	338, −1	C	VC
5	}	338, −3	C	VC
6		339, −3	...	C
7		339, +2	VD	D
8		340, +2	...	D
9		...	D	...
10		340, +3	...	D

* C = compact, D = diffuse

(*b*) *Sagittarids.*—This is a newly discovered shower of which there is no trace in the 27 Mc/s wind equipment records for 1952, 1953, 1954 or 1956. The radiant coordinates are: 1957, 307°, −35°; 1958, 301°, −36°. The radiant is compact and the echo rate about 30/hr. Fig. 5, which is typical of the range–time plots generated by the weaker showers, serves to illustrate the degree of contrast between the background echoes and those belonging to a shower which is approaching the limit of resolution of the equipment.

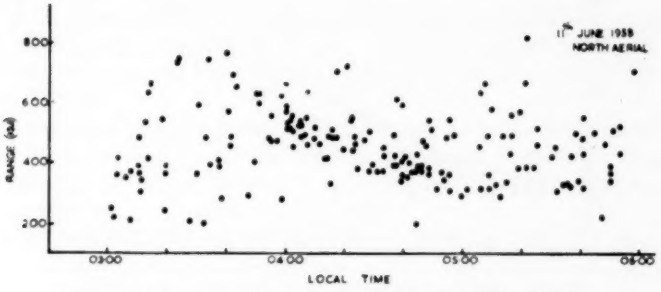

FIG. 5.—*A typical range-time plot of echoes for the Sagittarids shower.*

(*c*) *June daytime streams.*—The records for 1957 and 1958 June are marked by strong activity—echo rates up to 60/hr in excess of normal—from 06–09 hr L.T. on the N aerial and from 10–13 hr on the S aerial. Range–time plots are disappointing in that no shower envelopes can be delineated. The times of activity, however, require $\delta = +20°$ to $+30°$, and this activity is therefore identified with the June daytime showers: the Arietids, ζ-Perseids and later in the month the β-Taurids. Although the first two showers are active simultaneously, the radiants differ in R.A. by 20°, and if compact their resolution should be within the capacity of the equipment. Failure to resolve them, and the absence of well-marked range–time envelopes, suggest that the radiants are diffuse rather than compact, especially as the Geminid shower, whose radiant is compact and which transits still further to the north, gives reasonably good envelopes.

Activity near the end of June, associated with the β-Taurid stream, was strong in 1958 but weak almost to undetectability in 1957. Similar variability is evident in previous surveys (see Paper II).

(*d*) *Phoenicids.*—The 1958 ephemeris for this previously unreported shower is plotted in Fig. 6, in which each individual radiant is joined to the point on the mean radiant path corresponding to the longitude of the Sun at which it was determined. The radiant coordinates are

$$\alpha = 31°{\cdot}1 + 1{\cdot}05(\odot - 109°{\cdot}6), \qquad \delta = -47°{\cdot}9 + 0{\cdot}54(\odot - 109°{\cdot}6).$$

For 1957, a mean radiant of 31°, −44° was determined for July 12–17. The hourly echo rates of Fig. 7 indicate a marked asymmetry in activity across the stream, with a fairly sharp maximum at $\odot = 112°$. The equipment sensitivity was identical for the two years. The activity is patchy and the radiant tends to be diffuse.

In the 1953 survey with the radiant equipment, activity of up to 13 echoes/hr was observed on the S aerial on July 9, 10 and 13 between 07 and 10 hr, and

again on the N aerial on July 16 from 08 to 11 hr. The fragmentary nature of the recordings did not at that time warrant the assumption that this activity proceeded from only one radiant. With the confirmation now available, the earlier records have been re-examined, and a radiant at 30°, −43° has been determined. Further the 27 Mc/s wind equipment recordings for 1954 and

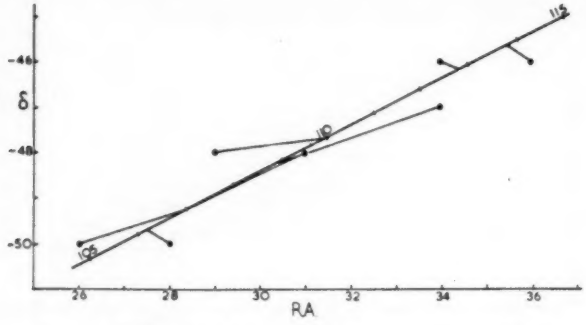

FIG. 6.—*Radiant ephemeris for the Phoenicid shower, 1958 July.*

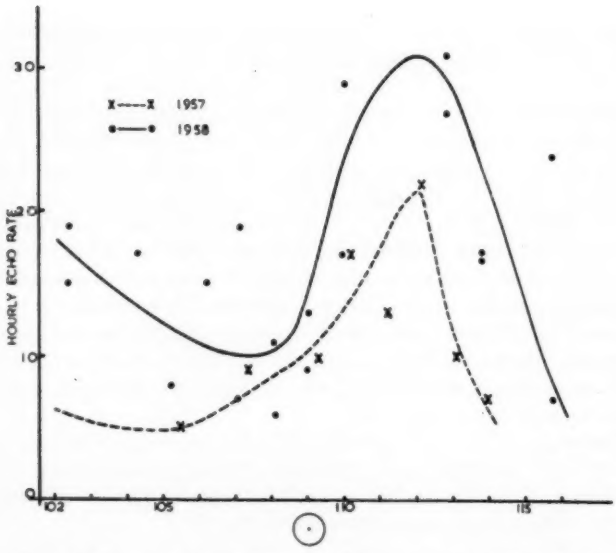

FIG. 7.—*Hourly echo rates for the July Phoenicid shower, as a function of solar longitude.*

1956 show an increased activity, up to 8 echoes/hr, centred on July 13, which could be due to a radiant which transits near 08 hr. This is sufficiently close to the transit time of from 06·49 to 07·12 found from the radiant equipment to identify this activity also with the Phoenicid radiant.

Having now been detected during each of the five surveys made between 1953 and 1958, this shower may be classed as permanent.

(*e*) δ-*Aquarids.*—Radiant measurements for 1953, 1957 and 1958 have been combined. A least squares fit gives for the radiant coordinates over the period July 20–August 10:

$$\alpha = 342^\circ{\cdot}2 + 0^\circ{\cdot}77(\odot - 126^\circ{\cdot}0),$$
$$\delta = -16^\circ{\cdot}6 + 0^\circ{\cdot}19(\odot - 126^\circ{\cdot}0).$$

Maximum activity of 110 echoes/hr occurs at $\odot = 124^\circ{\cdot}5$. The echo durations contain some evidence for a deficiency of more massive particles near the centre of the stream.

The three minor showers (Capricornids, Pisces Australids, Cetids) whose presence was suspected in 1953, have been confirmed. Their combined activity is approximately equal to, and rises to maximum at about the same time as, that of the δ-Aquarids.

A detailed report on this group of showers will be made in a separate paper.

(*f*) *Sextantids-Leonids.*—At the time of detection of this new shower only the N aerial was in use, and resort to matching of theoretical envelopes to the echo range–time plot was necessary in order to measure the declination. For $\delta \sim 0$ this is, unfortunately, not a particularly accurate process. The radiant of 155°, 0° is considered accurate to only ±8° in right ascension and ±10° in declination. The fitted envelope is shown in Fig. 8, superimposed on contours of constant echo rate. The radiant area is evidently compact. Peak activity of about 30 echoes/hr persisted from September 29 to October 3.

No trace of activity due to this shower could be found in previous surveys.

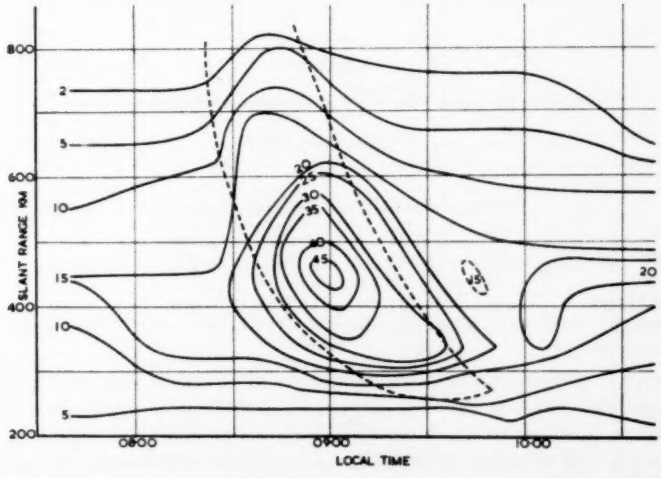

FIG. 8.—*Contours of constant echo rate at the time of the 1957 Sextantid/Leonid shower. The numbers on the contours are the total numbers of echoes (shower plus background) received in 10 min intervals of time for 100 km intervals of slant range, summed over the 9 days from September 26 to October 4. The broken curve is the range-time envelope for a radiant at* $\alpha = 155^\circ$, $\delta = 0^\circ$.

(*g*) *Puppids/Velids.*—If there were not clear evidence for this shower in previous surveys, and support for this view in an unpublished survey by Ellyett (private communication), there would be some hesitation in ascribing this activity (December 1–9) to a shower. The activity is intermittent, with a

maximum of about 50 echoes/hr near December 6, but the radiant is so ill-defined that range–time envelopes cannot be delineated, nor can an accurate radiant be determined. A tentative radiant at 140°, −50° differs considerably from the estimate of 124°, −36° reached from the wind equipment data (Paper II).

(*h*) *Phoenicids.*—This shower, which made an isolated appearance on the night of 1956 December 5, has already been described (**9**). It has not recurred.

(*i*) *Geminids.*—Five years' observations, extending from 1952 to 1957, have been summarized elsewhere (**10**). It is worthwhile noting here that a mean radiant at 113°·4, +31°·4 at ☉ = 260°·2, and a maximum activity at ☉ = 260°·8, agree with the results of Bullough's analysis (**11**) of the extensive Jodrell Bank radio measurements.

7. *The echo rates.*—It is a striking feature of the echo rates listed in Table III that most of the accepted showers should be so close to the detection threshold of 20–30 echoes/hr. Two reasons may be advanced for this. Firstly, the majority of the stronger showers have radiants to the north of the ecliptic and are either invisible or unfavourably situated for detection at Adelaide. The second factor is illustrated by the comparisons of echo rates in Table V. Sporadic echo rates are daily averages for the months in which the showers occurred. The percentage of echoes with $\alpha > 1{\cdot}4 \times 10^{13}$ electrons/cm is measured as in Section 6(*a*). Although some uncertainty is introduced by comparing data for different years, Table V indicates that for all the showers tabulated the increase in frequency with increasing magnitude is less rapid than is the case for sporadic meteors; this rule applies also to the Quadrantids and the Perseids (**15**). In fact, the only shower which seems to violate this rule is the daytime Arietids, but if we

TABLE V

Comparison of shower echo rates at different equipment sensitivities

Shower	Hourly echo rates (1)		Hourly echo rates (2)		Percentage of echoes (1) with durations >0·36 sec.	
	Shower	Sporadic	Shower	Sporadic	Shower	Sporadic
Geminids	60	33	24	3·9	9	7
δ-Aquarids	110	23	30	3·6	12	7
η-Aquarids	30	25	...	...	20	7
Phoenicids (July)	29	23	13	3·6	...	...
Years of survey	1957–58		1953		1957–58	
α_{lim} (electrons/cm)	$1{\cdot}3 \times 10^{11}$		...		$1{\cdot}4 \times 10^{13}$	

TABLE VI

Comparison of Adelaide and Jodrell Bank echo rates

	Arietids		Geminids		Sporadic
	Hourly rate	Elevation at transit	Hourly rate	Elevation at transit	echo rate
Adelaide	55	32	60	24	50
Jodrell Bank	75(*a*)	60	70(*a*)	68	8(*b*)
Mass parameter *s* (*c*)	2·7		1·6		2·0

(*a*) Rates for 1952–53, reduced to 1950 sensitivity; references (**11**), (**12**), (**13**).
(*b*) Reference (**14**).
(*c*) $7 > M_r > 5$ Browne *et al.* (**15**).

may assume even approximately constant shower activity from year to year, then Table VI suggests that in this case also the echo rate at the higher sensitivity of the present survey is less than would be expected from the *s*-values. The relative sensitivities of the two equipments are given roughly by the ratio of the sporadic rates. The corrections required to reduce the echo rates of Table VI to the zenith are difficult to assess, but a low rate for the Arietids at the Adelaide level of sensitivity seems very likely.

8. *The possible showers.*—It has been shown in Section 5 that the fluctuations in the echo rate, after subtraction of accepted shower activity, are substantially random, with a small excess of periods with high counts. A selection of the more prominent times of high echo count is listed in Table VII, as possible showers. This tabulation includes only those events in which high counts appeared on both aerials with a time-difference of less than 3 hr, persisted for at least 1 hr in each aerial, and contained at least one cell significant at the 1 per cent level. These are just the characteristics expected of shower activity, but none of these events is classified as a certain shower because in no case could range–time envelopes be discerned in the plots of individual echoes.

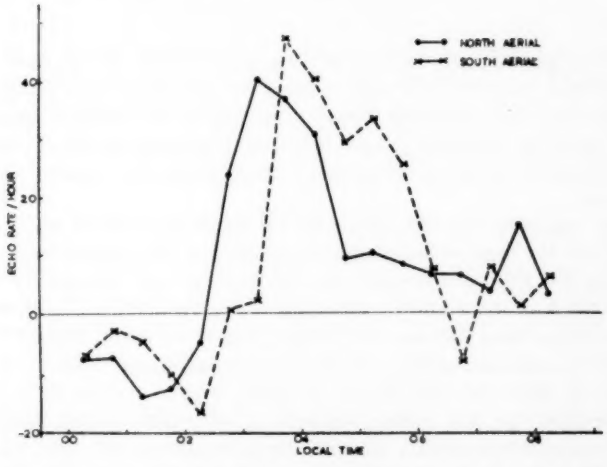

FIG. 9.—*Echo rates (excess over normal background count) for* 1958 *May* 31, *illustrating a possible shower.*

This list of possible showers is both provisional and incomplete. Some of the events may be chance coincidences of periods of high count which happen to meet the conditions stated above. Again, comparisons of records for 1957 and 1958 for the months of May and July resulted in inclusion in this list of some periods which in one year alone did not meet all of the above conditions. From 1957 August to November the equipment operated with only one channel, which automatically excluded from the list any high counts noted over this interval.

As an indication of the type of event listed in Table VII, the echo counts (excess over normal) for 1958 May 31 are illustrated in Fig. 9. If this is a shower it lasted for less than two days, as the echo counts on the following and preceding days were normal.

TABLE VII

List of possible meteor showers

Year	Dates	Approximate transit (L.T.)	Approximate radiant α	Approximate radiant δ	Maximum echo rate per 1/2-hr
			°	°	
1956	Dec 5–6	21·42	36	−39	12
1957	Mar 31–Apr 8	10·07	340	−32	34
1957	Apr 3–4	21·42	153	−39	11
1957	Apr 22–23	02·20	241	−44	22
1957	May 3–12	10·12	13	−18	34(*a*)
1958	May 1–12				21
1957	May 31	02·58	289	−18	21
1958	May 31				23 (*b*)
1957	July 11	10·20	80	−44	14
1958	July 10–11				9

(*a*) Accompanied by an abnormally large number of long-enduring echoes.
(*b*) See Fig. 9.

Some sixty periods of high count, which persisted for at least 1 hr and contained at least one cell significant at the 1 per cent level, but which appeared in one aerial only, have also been noted. Judging by the reclassifications already made as a result of comparing 1958 with 1957 records, some of these events might be regarded as possible showers if recordings in other years were available for comparison.

We may conclude that the detection of minor showers is well within the potentialities of the type of radio equipment used in the present survey. Their identification will require an objective, but perhaps not necessarily statistical, approach to the data and a survey extending over several years. Even when these requirements have been fulfilled, an effective search for minor showers is sharply restricted by the aperture of the system—in our case minor showers are virtually undetectable if their radiants transit at zenith angles greater than 30°. The effective aperture for the major showers is of course much larger. This limitation as to aperture applies in some form or other to all radio equipments, indeed in most cases more strongly than to visual or photographic observations.

The less rapid increase in echo rate with decreasing line density of electrons in the trail, for shower meteors as compared with sporadics, may suggest that the efficiency of a search for weak meteor showers would be improved by operation at low sensitivity. However, at the low echo rates so obtained the statistical fluctuations would be high and could easily offset the gains to be expected from the relatively higher shower echo rates.

Acknowledgment.—The author wishes to thank Mr J. W. Smith for his great assistance in the uninterrupted operation of the equipment over the period of the survey.

Division of Radiophysics, C.S.I.R.O.,
Department of Physics,
University of Adelaide:
1959 *September* 25

References

(1) A. A. Weiss, *Aust. J. Phys.*, **8**, 148, 1955.
(2) A. A. Weiss, *Aust. J. Phys.*, **10**, 299, 1957.
(3) A. A. Weiss, *J. Atmosph. Terr. Phys.*, **14**, 19, 1959.
(4) T. R. Kaiser, *Advanc. Phys.*, **2**, 495, 1953.
(5) A. A. Weiss, *Aust. J. Phys.*, **10**, 397, 1957.
(6) J. A. Clegg, *M.N.*, **112**, 399, 1952.
(7) A. A. Weiss, *Aust. J. Phys.*, **10**, 77, 1957.
(8) G. S. Hawkins and J. P. M. Prentice, *Astron. J.*, **62**, 234, 1957.
(9) A. A. Weiss, *Aust. J. Phys.*, **11**, 113, 1958.
(10) A. A. Weiss, *Aust. J. Phys.*, **12**, 315, 1959.
(11) K. Bullough, *Jodrell Bank Ann.*, **1**, 68, 1954.
(12) M. Almond, K. Bullough and G. S. Hawkins, *Jodrell Bank Ann.*, **1**, 13, 1952.
(13) G. S. Hawkins and M. Almond, *M.N.*, **112**, 219, 1952.
(14) G. S. Hawkins, *M.N.*, **116**, 92, 1956.
(15) I. C. Browne, K. Bullough, S. Evans and T. R. Kaiser, *Proc. Phys. Soc. Lond.*, **69**, 83, 1956.

THE LUNAR SURFACE AS AN IMPACT COUNTER

E. J. Öpik

(Received 1959 October 19)

Summary

The dust cover of the Moon sticks to mountain slopes and cannot possess any degree of fluidity. It is probable that only a limited migration of the dust from the slopes into adjacent valleys takes place, caused by meteor bombardment. The material of the micrometeors cannot escape from the Moon and is expected to form a layer of the order of 40 gr/cm², accumulating over the *maria* and protecting them from further erosion by small meteors.

Large meteorites are not stopped by the dust and produce meteor craters; at a velocity of 20 km/sec the ratio of crater to projectile diameter is estimated to be about 20.

812 crater diameters, measured over an area of 465,000 km² in Western Mare Imbrium, show a frequency distribution which is close to that predicted from the present population of interplanetary space and a time interval of $4{\cdot}5 \times 10^9$ years. It is concluded that since the formation of Mare Imbrium the population of interplanetary space has not changed appreciably; a tentative explanation is given.

---

1. *The nature of the lunar surface and crater formation.*—The craters of the Moon can be regarded as imprints testifying to the last stage of the building-up of this, and probably other members of the terrestrial group of planets. Their origin by way of impact stands practically beyond doubt, as contrasted by a few small cones pointed out by Kuiper (1954, and verbal communication 1959) whose relief appears to be similar to terrestrial volcanoes, and which may be either the relics of early volcanic activity, or the outcome of secondary processes following the impact of bodies of asteroidal dimensions. The eruption of gases from the central peak of Alphonsus as described by Kozyrev (1959) may well be an example of such long-enduring after-effects. On the other hand, the topography of the Moon lacks any indications of orogenic processes of the terrestrial type, such as the still continuing Alpine foldings and concomitant volcanoes along the tectonic arcs. Nor could such activity be expected to take place on the Moon, on account of the practical absence of erosion; the orogenic cycles on Earth are the result of unbalancing by large-scale erosion and sedimentation, absent from the Moon.

Of course, the possibility of large-scale erosion has been suggested, in the form of creep or flow of lunar dust (Gold 1955). A critical consideration of observational evidence indicates, however, that large-scale flow actually does not take place. The presence of dust (probably due to battering by meteors) is revealed by bolometric observations of temperature changes during lunar eclipses (Pettit and Nicholson 1930, 1940), which indicate a layer at least 5 cm thick of low-conducting material which can only be dust *in vacuo*, or a similar porous substance (Wesselink 1948). The observations of 1927 (Pettit and Nicholson 1930) were made on a spot in the rugged region 48″ from the southern limb; for purely geometrical reasons, only mountain slopes turned toward the observer could have contributed to the measured radiation. The presence of the dust layer on these

slopes, as revealed by the bolometric curve, refutes its fluidity postulated by Gold; whatever the cause, the dust sticks to its place of origin (as indicated by some experiments, dust particles *in vacuo* become welded together at the points of contact, which may offer an explanation), being disturbed only by meteoric bombardment; and this can cause displacement but on a very limited scale, a gradual diffusion from the mountain slopes into the nearest valleys. It can be estimated that, with the actual content of micro-meteoric material in interplanetary space, and a ratio of mass eroded to meteoric mass of about 100, a dust layer of the order of 20 metres could have been battered out of an exposed rock surface during the lifetime of the Moon (assumed to be $4{\cdot}5 \times 10^9$ years). The estimate follows from a theory of meteor impact (Öpik 1936, 1958a) with 5 km/sec as the impact velocity, and an accretion of 0·01 gr/cm² per one million years, or one-quarter that estimated for the Earth (Öpik 1956). However, a layer of 0·2 gr/cm² would already protect the underlying surface against further erosion by micrometeors, so that, if the dust is not removed, subsequent erosion could have been caused only by the larger and faster meteors whose total mass is relatively small; an upper limit of some 100 cm for the eroded layer can be set in this case.

The dust may be supposed to consist of a mixture of locally pulverized surface rock, and of the products of destruction of micrometeors. These, identified as zodiacal particles, at a velocity of impact of the order of 5 km/sec (Öpik 1956), may become partly or completely vaporized at impact, but the velocities of the vapour molecules will be mostly less than the velocity of escape (2·3 km/sec), because most of the kinetic energy will be absorbed by the medium or go into the heat of vaporization. The vaporized material will return to the lunar surface and be deposited there, providing thus another means of cementation of the lunar dust. A layer of meteoric material of the order of 40 gr/cm² may have been produced in such a manner during the lifetime of the Moon. This layer would suffice to cover the Moon with a uniform coating, efficiently protecting the rock surface from further erosion.

The differences in reflecting power of different portions of the lunar surface indicate, however, that such uniformity has not been achieved. If we assume that, as the result of meteoric impact, the mountain slopes of the *continents* are currently relieved of the excess of dust which collects in the adjacent valleys, there will be intense erosion of the slopes and the dust will mainly consist of local material, with but a moderate proportion of meteoric substance intermingled; this will refer also to the valleys between the mountains where the material from the slopes is collected. On the contrary, in the extended plains of the *maria* the dust remains *in situ*, erosion is prevented by the protective layer, and the amount of deposit of meteoric origin will greatly exceed that originally ground off from local rock. If the meteoric deposit is dark, the rock powder bright, the difference in coloration between the *continents* and the *maria* can be explained. We note that the conclusion about the continuing erosion of mountain slopes necessarily follows if a considerable fraction of the meteoric material is retained by the Moon.

As to the ray systems of Tycho, Copernicus and others, they may be due partly to spray of a light-coloured material, partly to a ruggedness of their surface, perhaps to cracks whose slopes are still subject to erosion.

In the eclipse of 1939 a central region of the Moon was observed bolometrically (Pettit and Nicholson 1940). The temperature curve indicated thermal properties of the lunar soil that were similar to those of the previous observation. About 25

per cent of the observed area was covered by a *mare* surface. As pointed out by Gilvarry (1958), 25 per cent of bare rock (lava) surface would have considerably influenced the temperature variation, making it less steep; hence he rightly concludes that the *maria* are covered with dust. However, contrary to his further conclusions, this does not contradict the lava theory of the *maria*; a lava surface, like that of any other rock, if exposed to the vacuum and meteorite impact, will ultimately be covered by a dust layer. The eclipse observations indicate only the existence of the thermally insulating layer of dust, without producing evidence relating to the nature of the underlying rock or rubble.

It appears, thus, that the whole surface of the Moon is covered by dust due mainly to the bombardment by meteors. On mountain slopes the layer must be thin, in the *maria* much thicker but hardly more than the equivalent of some 40 gr/cm². To meteorites exceeding 100 cm in diameter such a dust presents an insignificant obstacle, and craters will be produced as at impact into solid rock.

TABLE I

Depth of erosion and crater diameter, in units of the spherical equivalent diameter of the projectile

(Assumed density of surface rock = 2·5; of stone meteorite = 3·9; of iron = 7·8)

	Stone Meteorite		Iron Meteorite	
Velocity	20 km/sec	5 km/sec	20 km/sec	5 km/sec
Depth of erosion	2·5	2·2	4·0	3·6
Crater diameter	18	9·5	20	10·5

From the theory of meteorite impact into solid surface (Öpik 1958 a), the data as given in Table I are derived. The crater diameter (measured from rim to rim) as determined by the volume of crushed rock is not supposed to depend much on gravity, but for large craters more rubble will fall back and remain inside the crater which will therefore appear shallower than small craters. We note that there is but a very slight dependence of the crater to projectile diameter ratio on the density of the projectile. This is because the increase in crater volume, due to increased density of the projectile, is achieved mainly at the expense of depth, and only to a minor degree of the area of the crater. It is admissible, therefore, in the statistics of lunar craters, to deal solely with diameters, disregarding the densities or masses of the projectiles.

The figures are supposed to represent a close-order estimate, perhaps to 20 per cent in the linear dimensions. From a special analysis (Öpik 1958 b) it appears that crater-producing collisions are at present expected to take place chiefly with the members of the Appollo group of asteroids, and with comet nuclei, predominantly non-periodic comets, both groups being represented in almost equal numbers. The average impact velocity may be estimated roughly to be 20 km/sec for the first group, and higher for the second. We may assume 20 km/sec in Table I, the higher velocity of the comets being compensated by the smaller density of their nuclei, and conventionally accept a ratio of crater diameter to projectile diameter equal to 20, with the understanding that the mass of the projectile should be calculated with a density of meteoric stone, i.e. of 3·9.

The *continents* are much more densely covered with craters than the *maria*. According to current concepts this means that the *contintents* correspond to an earlier stage as compared with the *maria*. These latter are believed to be caused by impacts of large projectiles toward the end of formation of the Moon's surface features; in this process, the previously formed topographic features (still partly

recognizable in the so-called ghost craters) have been levelled out. The craters of the *maria* are thus formed during the period starting with the end of formation of the Moon's surface and ending with present time, therefore reflecting the history of the Moon under conditions of surrounding space which were more or less similar to those prevailing now—contrary to the more chaotic conditions of the preceding primitive stage. The statistics of craters in the *maria* can thus be directly compared with what is known of the frequency of stray bodies in the vicinity of the Earth and, among other things, can be used as a quantitative check of the mechanical theory of formation of meteor craters. Needless to say, quantitative tests in such matters can be relied upon only as to the order of magnitude.

2. *The distribution of crater diameters in Western Mare Imbrium.*—Rim to rim diameters of craters were measured and counted by the author on a print of the well-known photograph made with the 100-inch Mt Wilson reflector on 1919 September 15, (scale 1 mm = 4·32 km); by courtesy of Mt Wilson Observatory, the print was reproduced in the *Irish Astronomical Journal* (Fitzgerald 1953). Craters down to 1·2 km diameter appear to be completely recorded on the original print; on the half-tone reproduction in the *Journal*, made to three-quarter size, the limit of completeness is about 2·4 km. The limit of recognition of small craters is uniform all over the photograph, irrespective of the distance from the terminator (which passes just beyond the western edge of Mare Imbrium). The diameters were measured with a millimetre scale, in the direction of the major axis of the projected crater image. Allowing for the conditions of illumination, subjective judgement had to be applied, to determine the position of the crater rim; it was felt that no systematic errors of importance could have originated from this source, as well as from resolving power; the latter conclusion was confirmed by re-measuring the diameters on the half-tone print. The probable error of the scale readings was $\pm 0{\cdot}11$ km or $\pm 0''{\cdot}05$, and this also may be assumed to be the probable error in the diameters of the small craters. For larger craters the error may be greater, due to judgement errors caused by irregularities in the rim topography. Altogether 812 craters ranging in diameter from 0·6 to 73·4 km were recorded. The counts were made along twelve strips stretching in an east–west direction, the southernmost strip No. 1 running just north of Eratosthenes, the northernmost strip No. 12 south of Plato and bordering on Sinus Iridum but excluding the latter. "Epicontinental" areas such as that south-east of Archimedes and the rugged region around Autolycus were also excluded but the floor of Archimedes with eight counted craterlets was included. Areas completely immersed in shadow (Cassini) were also excluded. The areas quoted in the second column of Table II refer to the portions of Mare Imbrium in which counts were actually made. In the third column, $\overline{\cos \alpha}$ is the ratio of projected to true area of the strip. In the fifth column, ρ, the recorded surface density of craters of all sizes, shows a systematic decrease from south to north which far exceeds the sampling error. The southern edge of Mare Imbrium is more thickly populated by craters than the rest of the surface of this *mare*; this may be due to a greater proportion of objects of the pre-mare stage having survived there. There is no significant difference in the relative number of small and large craters (below and above 2·5 km diameter) in the southern portion of the *mare*, as compared with the rest.

Table III summarizes the distribution of crater diameters for the entire region. From the general run of the counts it appears that the data are complete down to a diameter of 1·19 km.

TABLE II

Number of all craters recorded

n = observed number; S = area of strip, in square kilometres; $\overline{\cos \alpha}$ = average projection ratio; $\rho \pm p.e.$ = number per 10,000 km² and its sampling error $\pm \rho/\sqrt{2n}$

Strip No.	S, km²	$\overline{\cos \alpha}$	n	$\rho \pm p.e.$	Remarks
1	20,000	0·93	88	$44 \pm 3{\cdot}5$	Southernmost strip
2	21,300	0·92	64	$30 \pm 3{\cdot}0$	Contains half-destroyed crater wall, diam. 24·2 km (counted)
3	18,300	0·92	40	$22 \pm 2{\cdot}5$	
4	24,500	0·89	62	$25 \pm 2{\cdot}5$	
5	28,600	0·88	58	$20 \pm 2{\cdot}0$	Contains Timocharis and Lambert.
6	39,800	0·87	78	$20 \pm 1{\cdot}5$	Contains Archimedes and Autolycus.
7	54,500	0·85	71	$13 \pm 1{\cdot}0$	Middle strip; contains Aristillus.
8	51,700	0·82	50	$10 \pm 1{\cdot}0$	
9	44,600	0·80	84	$19 \pm 1{\cdot}5$	
10	49,100	0·79	70	$14 \pm 1{\cdot}5$	Contains Piton; Cassini excluded.
11	49,800	0·75	69	$14 \pm 1{\cdot}5$	Contains Leverrier and Helicon.
12	62,500	0·70	78	$12 \pm 1{\cdot}0$	Northernmost strip, with Pico.
Total	464,700		812	$17{\cdot}5 \pm 0{\cdot}4$	

TABLE III

Distribution of crater diameters in Mare Imbrium

area = 465,000 square kilometres; n = number within limits; N = cumulative number

Diameter, km	n	N	Diameter, km	n	N
∞		0	5·40		35
	1			19	
70·6		1	4·10		54
	0			21	
55·5		1	3·35		75
	1			36	
43·0		2	2·92		111
	1			97	
34·3		3	2·48		208
	2			135	
27·0		5	2·05		343
	4			75	
21·4		9	1·84		418
	1			96	
16·6		10	1·62		514
	0			101	
12·7		10	1·40		615
	6			118	
9·72		16	1·19		733
	3			48	
7·99		19	0·97		781
	7			31	
6·70		26	0·64		812
	9			0	
5·40		35	0·00		812

The number dn within the limits of diameter of the craters, or the projectiles which caused them, from x to $x + dx$ can be assumed to be defined by the conventional frequency function

$$dn = Cx^{-p}\,dx, \qquad (1)$$

where the exponent p or the "frequency index" is normally a positive number. The expression is an idealization which cannot be conveniently applied to small

counted numbers, on account of sampling fluctuations. Its integral from infinity to x can be used instead to represent the cumulative number, N, with a satisfactory degree of stability even in the case of very small numbers,

$$N = N_0 x^{-s} \qquad (2)$$

where s, for obvious reasons always positive, can be called the *population index* *. In the case of strict validity of equation (1) we have evidently

$$s = p - 1, \qquad (3)$$

an idealization which, however, seldom applies in real cases. It is preferable to define the population index directly by eqn. (2), even with s variable according to circumstances. Usually but a slow variation of s with x would ocur. The population index reflects the history of the population and its mode of origin. Thus, fragmentation will tend to increase the number of small objects, and to yield a large value of s (meteors); condensation, on the other hand, leading to the building up of large masses (planets, stars), would tend toward small values of the population index. The population index of the Mare Imbrium craters (or their projectiles), as compared with that of other populations (from various sources, partly unpublished), is given in Table IV.

TABLE IV

Population index (s) of diameters (x)

Population	x	$s \pm p.e.$	s
Mare Imbrium craters	1·14– 2·48 km	1·70 ± 0·07	
	2·48– 5·40 km	2·24 ± 0·15	
	5·40–12·7 km	1·49 ± 0·22	
	12·7 –34·3 km	1·22 ± 0·35	
	34·3 –70·6 km	1·52 ± 0·50	
	1·14–34·3 km	1·64 ± 0·10	
Micrometeors	10^{-4}–10^{-2} cm		1·6–1·8
Visual Meteors			
In cometary orbits	2×10^{-1} cm		3·3
In asteroidal orbits	1 cm		4·2
Asteroids	2–90 km		1·59
	90–360 km		2·5
Appollo Group asteroids	0·4–2·8 km		(2·7:)
Comet nuclei	> 6 km		2·1 ± 0·2
Meteorites	50–10^4 cm		3·3
In the Solar System			
Planets and Satellites	200– 4,000 km		0·5
	4,000–64,000 km		0·5

The population index of the lunar craters is 1·6, or nearly equal to that of the smaller asteroids; the range of the projectile diameters is, however, very different, from 0·06 to 1·7 km for the hypothetical lunar projectiles, thus linking up, at their upper limit, with the smallest observable asteroids.

3. *Comparison with the contemporary population of the Earth's vicinity.*—From an analysis based on observed data bridged over by inter- and extrapolation (Öpik 1958 b) the frequency of collisions of the Earth with objects of different size has been estimated. At a relative velocity of about 20 km/sec the condensing action of

* The population index, under the name of "gradient", has been successfully used by Vaucouleurs (1956) in the analysis of stellar populations.

the Earth's gravitational field amounts to an increase in the number of impacts in a ratio of only 1·3 to one; for the Moon the frequency of impacts per unit area may be thus assumed equal to 80 per cent that for the Earth. In Table V is given the estimated cumulative number of impacts (N_{theor}) upon a lunar area of 465,000 km² over a period of 4,500 million years, corresponding to the present-day frequency (Öpik 1958 b); this is compared with the cumulative number (N_{obs}) of craters in Mare Imbrium registered over the same area; the projectile diameters are assumed equal to one-twentieth of those of the craters.

TABLE V

Cumulative number of impacts on Mare Imbrium (465,000 km²) *in* $4{\cdot}5 \times 10^9$ *years*

Diameter of projectile, lower limit, km	0·060	0·124	0·270	0·64	1·72	3·53
N_{obs}	733	208	35	10	3	1
N_{theor}	1050	202	35	5·0	0·44	0·10
Ratio N_{obs}/N_{theor}	0·70	1·03	1·0	2·0	7	10

The observed numbers are in close agreement with the theoretical figures except for the large craters whose numbers are in excess of the expected ones. The agreement is closer than could have been expected from the character of the estimates. The assumed crater to projectile diameter ratio, as well as the frequency of meteoritic bodies in the diameter range 0·06–0·27 km are based on rough theoretical and very scanty observational data; the very close agreement can, therefore, only be a matter of chance. Nevertheless, the conclusion appears to be justified that the craters in Mare Imbrium can be accounted for by bombardment at a more or less uniform rate during $4{\cdot}5 \times 10^9$ years by stray bodies of the same kind, and of the same space density, as those populating the solar system in the vicinity of the Earth's orbit at present. The observed excess in the numbers of large projectiles, or large craters in Table V can be ascribed to survival of the larger formations, which may have withstood the events connected with the formation of the *mare*; they belong thus, probably, to the pre-mare stage.

The conclusion is somewhat unexpected; the stray bodies are continually swept away by the planets, and their number is expected to decrease exponentially with time; in the beginning there should have been very much more stray bodies than at present, and the number of impacts should have been considerably greater than that calculated from the present-day density.

However, a plausible explanation can be given to this puzzling result. The accretion of the planetary masses most probably proceeded at the expense of debris and gas placed more or less in the region where the planetary orbits ultimately stabilized. The projectiles which battered the surface of the Moon in the pre-mare stage must have belonged to the same category, circling the sun in orbits of small eccentricity and inclination, say $e = 0{\cdot}1$, $\sin i = 0{\cdot}1$, $a \cong 1$ astr. unit. Formulae of collisional probabilities (Öpik 1951) yield in such a case a collisional lifetime with respect to the Earth of the order of 2×10^6 years. These "planetesimal" fragments must have been removed rapidly long ago, and no trace of them remains at present; the surrounding space was swept clean of them already at the time of the major collisions which produced the lunar *maria*. [These collisions may have been caused by moonlets which, like the Moon itself, originally, may have been

formed as independent planets on the Earth's orbit (cf. Gerstenkorn 1955) drifting very slowly toward each other (because the periods of revolution were almost equal) and colliding after the other fragments were swept away.]

The lifetimes of the objects of the Appollo group, of the order of 10^8 years, are also too short for them to be regarded as remnants of the primordial fragments; they rather are continually replenished from outside, to replace those swept away, and an equilibrium density of them has established itself in our surroundings (Öpik 1951). A source of these objects must exist which is not easily depleted. The source may be partly in the asteroidal region, whence cumulative perturbations in close approaches to Mars will deflect some of them toward the inner portions of the solar system. Another, more inexhaustible source is in the cloud of comets surrounding the solar system to distances of the order of 10^5 astron. units (Oort 1950); from the outskirts they are efficiently removed by stellar perturbations (Öpik 1932), but in their bulk they are very stable. A comet of $a = 10^4$ astron. units which happens to enter the inner regions of the solar system has a collisional lifetime of the order of 10^{12} years, thus very much longer than the solar system; the lifetime of the Mars asteroids is of the order of 10^{10} years. With such lifetimes the supply of stray objects toward the inner portions of the solar system may have remained constant, indeed, during all the time of the existence of the solar system since its rapid condensation.

If this is so, the surfaces of the lunar *maria* can be regarded as a counter which, over the ages, has registered the impacts of stray bodies and from which conclusions can be made on the present-day distribution of diameters and number density of these bodies.

This research was supported in part by the Geophysical Research Directorate of the Air Force Cambridge Research Center.

Department of Physics,
University of Maryland
(On leave from Armagh Observatory):

1959 *September* 29.

References

(1) Fitzgerald, A. P., 1953, *Irish Astr. J.*, **2**, 160.
(2) Gerstenkorn, H., 1955, *Zeits. f. Ap.*, **36**, 245.
(3) Gilvarry, J. J., 1958, *Ap. J.*, **127**, 751.
(4) Gold, T., 1955, *M.N.*, **115**, 585.
(5) Kozyrev, N. A., 1959, *Priroda* No. 3, 84.
(6) Kuiper, G. P., 1954, *Proceed. Nat. Ac. Sc.*, **40**, 1096.
(7) Oort, J. H., 1950, *B.A.N.*, **11**, 91.
(8) Öpik, E., 1932, *Proceed. Amer. Ac. Arts and Sc.*, **67**, 169; *Harvard Repr.* No. 79.
(9) Öpik, E., 1936, *Tartu Obs. Publ.*, **28**, No. 6.
(10) Öpik, E. J., 1951, *Proceed. Roy. Irish Acad.*, **54** A, 165; *Armagh Obs. Contrib.* No. 6.
(11) Öpik, E. J., 1956, *Irish Astr. J.*, **4**, 84; *Armagh Obs. Contrib.* No. 19.
(12) Öpik, E. J., 1958 a, *Irish Astr. J.*, **5**, 14; *Armgah Obs. Contrib.* No. 24.
(13) Öpik, E. J., 1958 b, *Irish Astr. J.*, **5**, 34.
(14) Pettit, E., and Nicholson, S. B., 1930, *Ap. J.*, **71**, 102.
(15) Pettit, E., and Nicholson, S. B., 1940, *Ap. J.*, **91**, 408.
(16) Vaucouleurs, G. de, 1956, *Irish Astr. J.*, **4**, 13.
(17) Wesselink, A. J., 1948, *B.A.N.*, **10**, 351.

THE SPATIAL ANALYSIS OF MAGNETIC FIELDS IN SUNSPOTS

P. J. Treanor, S.J.*

(Communicated by the Director of the University Observatory, Oxford)

(Received 1959 August 31)

Summary

A review of existing methods of determining the strength and direction of magnetic fields in sunspots, as a function of position and depth within the spot shows that these have given fragmentary and somewhat discordant results. In particular, little is known of the direction of the magnetic vector.

A new method of determining this quantity is described. By means of a Babinet compensator, polarization fringe systems are produced in the components of a normal Zeeman triplet. From the phase difference of the σ-component fringes, the constants of the elliptical polarization at each point in the spot are determined, and the orientation of the lines of force deduced. The method minimizes the effect of instrumental polarization; the reduction is simple and fairly short.

An experimental test on four sunspots has been carried out, using the Oxford 35 m solar tower and 12 m spectrograph with a Babcock grating. Measurements of field direction were made, using the triplet λ6173 (Fe I); the associated field strengths were determined from the same line and from λ6149, a weak line of Fe II. The resulting field-strength variation is in agreement with Broxon's parabolic law, but in contrast with Joy and Nicholson's measures of direction, 40 per cent of the flux is found to be confined within a cone of unit solid angle. Comparisons of field-strength at λ6173 (Fe I) and λ6149 (Fe II) suggest that the gradient in depth does not exceed 1 oersted/km.

Introduction.—It has long been recognized (**3**) that the physical processes operative in sunspots present a problem in magneto-hydrodynamics, for the correct investigation of which it is necessary to have an accurate observational picture of the magnitude and direction of the magnetic fields and the velocity fields in sunspots, as a function of position and depth within a typical spot. It is now just fifty years since Hale first interpreted the splitting of sunspot lines in terms of the Zeeman effect, and so laid the foundations of quantitative magnetic measurements of sunspot fields (**7, 8**), and since Evershed (**4**) discovered the effect named after him, in which he interpreted variations in the wave-length of the same line in different parts of a spot in terms of radial and tangential velocity streams. During this time much work has been done in the development of techniques and in systematic measurements and yet it cannot be said that the present position regarding these basic data is at all coherent or satisfactory.

1. *Existing methods and results.*—The methods which have been used almost universally for determining the magnetic fields of sunspots have been derived from procedures described in a classical paper of Hale and Nicholson (**9**).

* Skynner Research Fellow in Astronomy, Balliol College, Oxford.

To determine the field strength, the observation consists essentially of the measurement of the splitting of a Zeeman triplet, from which the total magnetic field in which the line originates is determined by the relation

$$\Delta\lambda = gCH\lambda^2 \qquad (1)$$

where λ denotes the wave-length, g the splitting factor, C is a constant, and H the field strength. The practical difficulty in this basically simple measurement is due to the fact that the splitting for average spot fields is of the same order of magnitude as the line width, so that even with high dispersion and resolving power the components are only properly separated at the centre of large spots. Hale solved this problem by reducing to a practical form a procedure first used by Zeeman to detect small magnetic splittings in laboratory spectra. In the case of a normal triplet, viewed along the field, the central π-component is absent while the outer σ-components are circularly polarized with opposed directions of rotation. Consequently one or the other can be extinguished when the triplet is viewed through a quarter-wave plate and a Nicol whose plane of transmission makes an angle of $\pm 45^\circ$ to the wave-plate axis. In this way the difficult measurement of an unresolved doublet can be replaced by the determination of the relative positions of two undisturbed lines. Hale constructed a mosaic of quarter-wave strips so oriented that alternate components appeared in adjacent strips. This method permits rapid visual or photographic measurements, and forms the basis of a long series of field measurements by Hale and Nicholson and their successors at Mount Wilson. In an important paper (**31**), von Klüber refined the method of Hale and applied it to extensive photographic measurements, and his techniques form the basis of a series of determinations of field strength profiles by himself (**31**), by Schröter (**23**) and by Mattig (**18**), and of a programme of regular maximum field measures which is now in progress at Potsdam (**17**). Other methods of determining the Zeeman splitting have been suggested, including the accurate photometry of the blended triplet (**31**) and the use of Savart fringes to replace the multiple quarter-wave plate (**19**), but no measurements with these techniques have yet appeared.

The problem of determining the law of variation of the field with depth has been fully discussed by Houtgast and van Sluiters (**10**). Measurements of field strength made from a strong and a weak line in the same spot, or by means of the same line, when the spot is near the centre of the disk, and again when it is near the limb, provide, in principle, means of comparing fields which exist at different optical depths. On reasonable assumptions concerning the physical conditions in the sunspot, Houtgast and van Sluiters determined the mean linear depths at which particular lines are formed, and hence provided two methods for determining the gradient of the field. Yet another method is suggested by them, which assumes knowledge of the direction of the lines of force. If we assume that the lines of force are straight over the observable depths of the sunspot (an assumption already implicit in assigning a unique value to dH/dh), the value of the gradient can be immediately calculated from the divergence of the lines of force.

The classical work on the determination of this law of direction is due to Nicholson (**9**), who used two quite different procedures. The first depended on a comparison of the intensities of the Zeeman components of a triplet, when

observed with the quarter-wave plate and Nicol. According to Seares (**26**), the intensity of these two components is then given by

$$\left.\begin{aligned}\sigma_v &= \tfrac{1}{4}(1-\cos\gamma_0)^2\\ \pi &= \tfrac{1}{2}\sin^2\gamma_0\\ \sigma_r &= \tfrac{1}{4}(1+\cos\gamma_0)^2\end{aligned}\right\} \qquad (2)$$

where γ_0 is the inclination of the magnetic vector to the line of sight. Assuming the validity of this law, if it were possible to measure the intensities, corrected for blending, by accurate microphotometry, the directions of the lines of force could be deduced. Nicholson noticed however that when $\gamma_0 = 90°$, $\sigma_r = \sigma_v$. By observing the point in a spot at which these components were of equal intensity, and repeating the observation as the spot moved towards the limb, he was able to synthesize the directions of the vectors over a considerable part of the spot.

His second method made use of the fact that the π-component is always plane polarized in a plane containing the line of sight and the line of force. Near the limb of the Sun, this implies that the direction of polarization of the π-component coincides with the direction of the lines of force. Nicholson determined this direction at different points in spots near the limb by extinguishing the central component with a Nicol and rotatable half-wave plate, and so extended his observations to near the edge of the penumbra. His pioneer work in this field has not been repeated.

A source of systematic errors which has to be reckoned with in applying the methods developed at Mount Wilson is introduced by the oblique reflections which occur at the coelostat mirrors. The instrumental polarization thus created (**26**) results in a partial reappearance of the unwanted σ-component in the method of determining field strengths, and a consequent displacement in the apparent centre of the measured component. The effect is even more serious however in the methods of determining field direction since these depend directly and critically on the intensity relations of the σ-components, and on the form of their polarization, both of which quantities are distorted in a rather complicated manner by the instrumental polarization.

Summary of results.—The present position of the problem may be seen by placing together the main results of the application of the techniques described above, which constitute the elements of our present picture of sunspot fields. Broxon (**2**) published in 1942 a much-quoted law of field intensity, which is believed (**3**) to represent unpublished results obtained by Nicholson. This is the parabolic law:

$$H(r) = H_0(1-(r^2/b^2)) \qquad (3)$$

where $H(r)$ denotes the field strength at distance r from the spot centre, H_0 is the central field, and b is the penumbral radius (about 2·4 times the umbral radius).

The measures of Mattig yield a somewhat different result; the field was here measured very carefully to the edge of the spot, and was found to disappear more gradually than the parabolic law indicated, being better represented by

$$H(r) = H_0(1-r^4/b^4)\,e^{-2(r/b)^2}. \qquad (4)$$

The normally quoted values of the vertical field gradient are mainly those of Houtgast and van Sluiters (**10**), who discovered the centre-limb variation in field intensity in the Mount Wilson results (**9**), and who applied the measurements made by R. B. King (**14**) on Mount Wilson plates on lines of different strength. They find, from the centre-limb effect $dH/dh = 5{\cdot}7$ oersted/km; from the comparison of weak and strong lines $dH/dh = 2{\cdot}5$ oersted/km, while from the divergence of the lines of force according to Nicholson (**9**) (see equation (5) below) they deduce a field of 0·5 oersted/km. In an independent investigation of lines of different strength Tanaka and Tagaki (**29**) found a barely detectable gradient.

Nicholson's investigation of the directional properties of the lines of force by the study of the positions of equal intensity of the σ-components gave a graph which can fairly be represented by

$$\gamma_0 = 0{\cdot}75\ \tfrac{1}{2}\pi\, r/b \qquad (5)$$

while his determination from the orientation of the plane of polarization of π-components in spots near the limb is well represented by

$$\gamma_0 = \tfrac{1}{2}\pi\, r/b. \qquad (6)$$

Chapman (**3**) suggested this second formula as representing roughly the combined results of Nicholson's measure, which are the only published data on line directions.

It is clear that where independent methods and observations are available, there is considerable disagreement in the resulting values. This fact has given rise to various criticisms and suggestions. Hale shows that the quarter-wave plate method of field strength measurement, in which the assumption is made that the central component is absent, can be used validly, for fields where the value of γ_0 does not exceed 20°. Now it is clear that if Nicholson's law of directions is even a first approximation to the real condition, the method can only be applied without further correction to a region near the centre of the umbra in spots near the centre of the disk. The situation is complicated where the field direction is irregular, or where the third component is provided by scattered light from the photosphere round the spot, a factor always present in observations near the limb. On grounds of this kind Thiessen (**30**) has criticized the Potsdam results, which all suggest the exponential form of equation (4), and believes that a correction for these effects tends to restore the parabolic form. More radical criticism has been made by Stepanov (**28**) who considers that Seares intensity law (equation (2)) is not valid, in the case of a line as broad as $\lambda 6173$, for field strengths below 800 gauss, but must be replaced by a more complicated law derived by detailed consideration of the transfer problem. Recent measures of spot fields by Severny (**27**) using a solar magnetograph, reveal moreover fine structure and irregularities of polarization in spots. It is a little difficult at present to assess the physical meaning of these irregularities, but it seems possible that variations of field direction are involved, a quantity which a magnetograph is better equipped to detect than to analyse. If these irregularities are typical, the conditions under which the quarter-wave plate technique is valid are further delimited. It must however be admitted that the results achieved with this method have provided a fair general picture at least of the umbral field.

The disagreement, amounting to a factor of 10, between the values of the vertical field gradient, is rather disappointing, particularly when we note that the intermediate value is given little weight by Houtgast and van Sluiters on account of the discordant results of Tanaka and Tagaki (**29**) who found large differences between lines of different elements. Since it seems most unlikely that the gradient computed from the law of directions should be too small by an order of magnitude, one is forced to consider that the centre-limb variation is influenced more than was suspected by scattered light and by the presence of the central component.

If this is the case, then we depend on the accuracy of the law of directions for our knowledge of the vertical field gradient. Now it is true that there is broad agreement between the two types of measurement performed at Mount Wilson. But it must be remembered that the measures are extremely difficult ones, involving measures near the limb of the Sun and near the edge of the spot where the components are imperfectly resolved, and that they are subject to systematic errors due to instrumental polarization. The most serious objection to these results lies however in the difficulty of reconciling the law of direction with the results of the Evershed effect. Studies of this effect by Evershed (**4, 5, 6**), Abetti (**1**) and others and notably a recent study by Kinman (**15, 16**) indicate that though irregular transverse components are sometimes present, the velocity-field is mainly radial. Now Jensen (**11**) has pointed out that if, as seems most likely, the motions in sunspots are constrained to the lines of force, these results cannot be reconciled with Nicholson's law of direction.

It appears from this survey of existing methods and results that the basic data of sunspot fields are insecure at almost every point. More observations are required in which the limitations of the various methods are carefully respected and the development of other methods, free from the peculiar systematic limitations of the techniques developed at Mount Wilson, is desirable in order to provide an independent check. In this paper, we now present an account of the development and application of a new method of determining the law of direction.

2. *The Babinet fringe method of field direction determination.*—The principle of the new method is a simple one. Consider the circularly polarized components of a normal Zeeman triplet. Viewed along the field, the path of the amplitude vector is in fact a circle. Viewed normally to the field, one of the orthogonal components of the circularly polarized light is in the line of sight and ineffective, so that the light observed is plane-polarized in the plane of the field (transverse Zeeman effect). It is easy to see, qualitatively, that at any intermediate angle, the light will be elliptically polarized, and that the ratio of the major to minor axes of the ellipse will determine the angle γ_0 between the sight-line and the field, while the orientation of the axes will determine the azimuth of the projection of the field on a plane perpendicular to the sight line. Hence a complete determination of the two constants which describe the shape and orientation of the ellipse also determines the orientation in space of the magnetic field.

In order to express this quantitatively and to devise a method of performing the analysis, we recall some basic relations between equivalent analytic descriptions of polarized light. Consider light whose state of polarization may be described by an ellipse of major and minor axes A and B, the major axis being inclined to arbitrary orthogonal axes at an angle γ. (γ is wrongly indicated in Fig. 1. It

should be measured from the major axis.) It is shown, for example by Schuster (**25**), whose notation we follow, that such light may be represented by perpendicular vectors a_1, a_2 directed along the arbitrary axis of reference, and differing in phase by δ. If we set $B/A = \tan \Psi$, $a_2/a_1 = \tan \psi$, then the following relations hold:

$$\tan \delta = \tan 2\Psi / \sin 2\gamma, \tag{7}$$

$$\cos 2\psi = \cos 2\gamma \cos 2\Psi, \tag{8}$$

$$\sin 2\Psi = \sin 2\psi \sin \delta, \tag{9}$$

$$\tan 2\gamma = \cos \delta \tan 2\psi, \tag{10}$$

$$\cos 2\Psi \sin 2\gamma = \sin 2\psi \cos \delta. \tag{11}$$

Note that in the particular case in which the axes of reference coincide with the axes of the ellipse ($\gamma = 0$), by equation (7), $\delta = \frac{1}{2}\pi$. Schuster (**25**) shows that the sign of δ governs the direction of rotation of the ellipse.

To obtain the quantitative relation between the constants of the ellipse and the direction of the field, consider Fig. 1, in which the circle of polarization is represented in perspective, OE is the sight line, OH the field direction, $E\hat{O}H = \gamma_0$; OH is normal to the plane of the circle. The circular polarization may be defined by a vector $OD = A \sin \omega t$, in the line of intersection of the plane EOH with the circle, and a vector $OF = A \sin(\omega t + \frac{1}{2}\pi)$ in the plane of the circle, perpendicular to OD and therefore to OE. Now since the vector OF has no component along OE, it is observed unchanged for all values of γ_0,

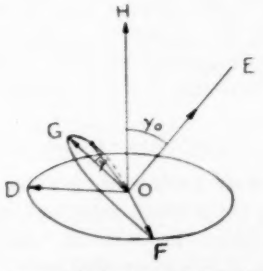

FIG. 1.—*Relation between polarization and direction of the lines of force.*

whereas the effective component of OD in the plane perpendicular to OE (the plane tangential to the celestial sphere) is

$$OG = A \cos \gamma_0 \sin \omega t.$$

These two perpendicular components OF, OG will produce at E light elliptically polarized, in such a way that

$$\cos \gamma_0 = \tan \Psi \tag{12}$$

while the direction of the minor axis OG in the plane perpendicular to OE measured from a suitable origin (the North Point) defines the azimuth of OH with respect to this origin.

2.1. *Determination of the elliptical constants.*—In order to determine the quantities $\tan \Psi$, γ, which describe the shape and orientation of the ellipse, we perform an analysis by means of a Babinet compensator and a polarizer. The

method here described differs somewhat from the conventional application of a Babinet compensator, since it avoids any measurement which involves assessment of intensity or fringe visibility, and yields the quantities $\tan\Psi$, γ, more directly.

The Babinet compensator consists of two similar quartz wedges, of equal angle, cut with their crystal axes normal to the direction of incident light, and respectively parallel and perpendicular to their prism axes. The prisms are cemented together to form a rectangular block (see Fig. 2). We may represent incident elliptically polarized light by vectors in the directions of the crystal axes.

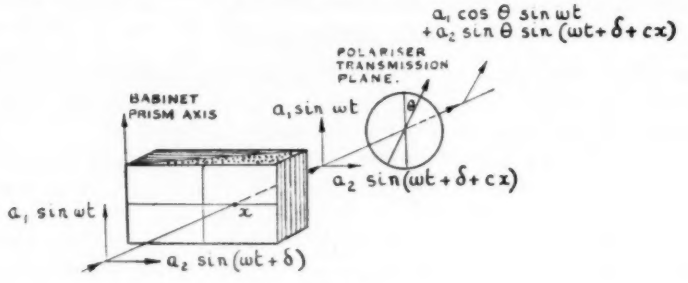

FIG. 2.—*Analysis by Babinet compensator.*

One of these components is the ordinary ray in the first prism and the extraordinary ray in the second; the prisms act the opposite way for the other component. Consequently, the action of a compensator of prism angle α (in radians) on a ray normal to the prisms and distant x from the point of equal prism thickness is to introduce between the two components an additional phase difference

$$\epsilon = (4\pi/\lambda)(\mu_0 - \mu_e)\alpha x = cx \qquad (13)$$

where μ_0, μ_e are the indices of the prism and c is a constant at a given wave-length. Let the vectors representing the incident polarized light, in and perpendicular to the prism axes of the Babinet, be $a_1 \sin\omega t$, $a_2 \sin(\omega t + \delta)$. The emergent vectors at any point x along the Babinet will be

$$a_1 \sin\omega t, \qquad a_2 \sin(\omega t + \delta + cx).$$

A plane-polarizer, whose transmission plane makes an angle θ to the prism axes, will transmit the components of these vibrations in its transmission plane. The resultant plane vibration is

$$a = a_1 \cos\theta \sin\omega t + a_2 \sin\theta \sin(\omega t + \delta + cx). \qquad (14)$$

The intensity a^2 of the resultant vibration will vary periodically as x is increased, having maxima for $(\delta + cx) = 0, 2n\pi$, and minima for $\delta + cx = (2n+1)\pi$. For incident plane polarized light ($\delta = 0$) maxima and minima will occur for $cx = 0, 2n\pi$, and $cx = (2n+1)\pi$. Hence a phase difference δ between the incident components produces a shift $\delta/2\pi$ of the distance between successive fringes.

Now consider the following experiment. Incident elliptically polarized light is transmitted by the Babinet and polarizer, and the phase δ_1 determined (for instance by comparison with plane polarized light). The Babinet and polarizer

are now rotated through an angle τ and the phase δ_2 is determined, corresponding to the vectors in the new axes. Referring now to equation (7) we note that Ψ has remained unaltered in both measurements, but that we have altered γ by τ. Hence by (7)

$$\tan \delta_1 = \tan 2\Psi / \sin 2\gamma; \quad \tan \delta_2 = \tan 2\Psi / \sin 2(\gamma + \tau). \tag{15}$$

Hence we easily derive

$$\tan 2\gamma = \sin 2\tau \Big/ \left(\frac{\tan \delta_1}{\tan \delta_2} - \cos 2\tau \right) \tag{16}$$

and by (7)

$$\tan 2\Psi = \tan \delta_1 \sin 2\gamma.$$

The equations (16) determine the required orientation and axis ratio of the ellipse of polarization in terms of the measured phases δ_1, δ_2. In the particular and most practical case in which by choice $\tau = 45^\circ$, (16) reduces to

$$\left.\begin{aligned} \tan 2\gamma &= \tan \delta_2 / \tan \delta_1, \\ \tan 2\Psi &= \tan \delta_1 \tan \delta_2 / \sqrt{(\tan^2 \delta_1 + \tan^2 \delta_2)}. \end{aligned}\right\} \tag{17}$$

Visibility of the fringe system.—Referring to equation (14) we note that the ratio of minimum to maximum intensity of the fringe system is

$$R = \left(\frac{a_1 \cos\theta - a_2 \sin\theta}{a_1 \cos\theta + a_2 \sin\theta} \right)^2. \tag{18}$$

To obtain maximum visibility a particular value of θ is required for each state of polarization. If however we set $\theta = 45^\circ$, we obtain a system which will show fringes for all configurations except light plane-polarized in or perpendicular to the transmission plane of the polarizer. We note that the value of θ does not enter into our calculation of the phases δ_1, δ_2.

Determination of δ from Zeeman σ-component fringes.—In observing a Zeeman triplet, we obtain by this technique sets of adjacent fringes in both the σ-components, as well as in the π-component of the line observed (see Plate 9). Now we know that the ellipses of polarization of the σ-components are identical except for the direction of rotation of the vector. This provides a very convenient means of determining δ without recourse to standardizing fringes. For under these conditions, the phase difference of the vector-components in and perpendicular to the Babinet prism axes are equal in magnitude but opposite in sign in the two Zeeman σ-components. The phase differences between corresponding fringes in the red and violet components are therefore 2δ, and this may be directly measured. (To satisfy oneself that this is the case, we note that in accordance with the comment following equation (11), we may represent the ellipses by vectors in their principal axes differing in phase by $+\pi/2$ and $-\pi/2$ respectively, and by (7) we see that the value of $\tan 2\Psi$ must also differ only in sign. But since $\tan 2\Psi$ is independent of γ, the phase difference of the red and violet components referred to any axes will by (7) always be equal in magnitude and of opposite sign.)

The advantage of this method of measuring δ lies in the fact that only small differences of adjacent fringes photographed simultaneously and under exactly similar conditions, have to be determined, and the resulting quantity is twice the value required, which reduces accidental error. Another important

advantage is that the differential method much diminishes the effect of instrumental polarization. This may be seen simply by considering the case of a single instrumental metallic reflection, which introduces a spurious phase difference between the vectors in and perpendicular to the plane of reflection. In the case in which this plane coincides with one of the axes of the Babinet, the same systematic error is thereby introduced in the values of δ of both the σ Zeeman components, but their difference remains unaltered. There is a residual effect in the difference when the plane of reflection is not coincident with or normal to the Babinet axes, but this is small in most practical cases.

The proposed method of measuring the inclination of the magnetic lines of force consists, therefore, in setting up before the slit of a large spectrograph, a Babinet compensator followed by a plane-polarizer transmitting in a plane which makes 45° to the axes of the Babinet. The resulting fringe system in a Zeeman triplet is photographed: the Babinet and polarizer are rotated conjointly by 45° and the new fringe system photographed. The double phase difference $2\delta_1$, $2\delta_2$ between corresponding fringes in the σ-components is then measured, and the values of γ, $\tan\Psi$ of the ellipse of polarization is determined from equation (17); from $\tan\Psi$, the inclination to the line of sight γ_0 is calculated from (12). The values γ, γ_0 (respectively the angle measured from the North Point in the image plane along the projected direction of the line of force, and the angle between the magnetic field and the sight line) completely determine the direction of the field at each point in the spot. By a suitable transformation the results may be referred to a coordinate system with axes in and perpendicular to the solar surface.

3. *Experimental arrangements.*—In the summer of 1957 some experiments were made at Oxford to explore the practical possibilities of the Babinet fringe method of field direction measurement. The Oxford 35 m solar telescope (**21**) was used in conjunction with the 12 m Littrow spectrograph, equipped for this purpose with a grating of 20 cm aperture ruled with 600 lines/mm by H. W. Babcock, and used in the fourth order, where the theoretical resolving power, which these gratings closely approach (**20**), is 480 000. The dispersion at λ6173 is 3·83 mm/A. We are much indebted to Dr H. W. Babcock for

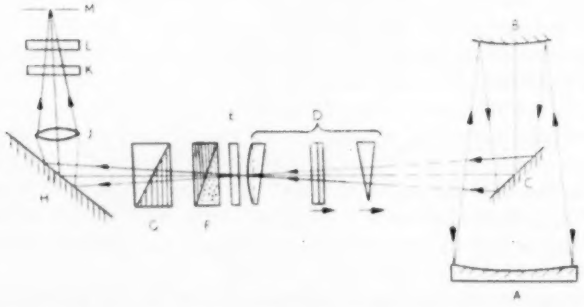

FIG. 3.—*Apparatus for spatial analysis of sunspot fields:* A, *objective;* B, *Cassegrain hyperboloid;* C, *first coudé;* D, *guiding system;* E, *first half-wave plate;* F, *Babinet compensator;* G, *Rochon prism;* H, *second coudé;* J, *re-imaging lens;* K, *second half-wave plate;* L, *interference filter;* M, *spectrograph slit.*

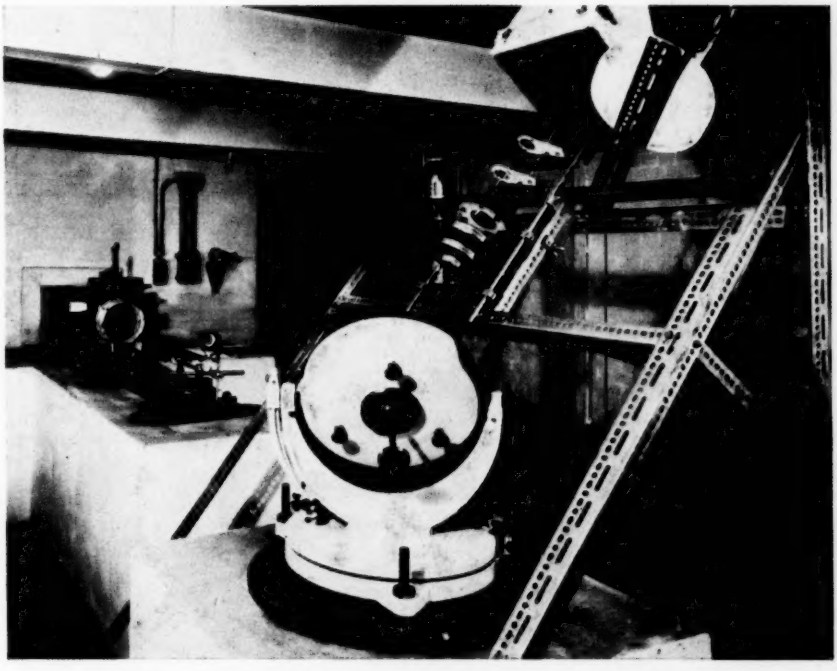

The Oxford 35m solar telescope and spectrograph equipped for the Babinet fringe method of sunspot field analysis.

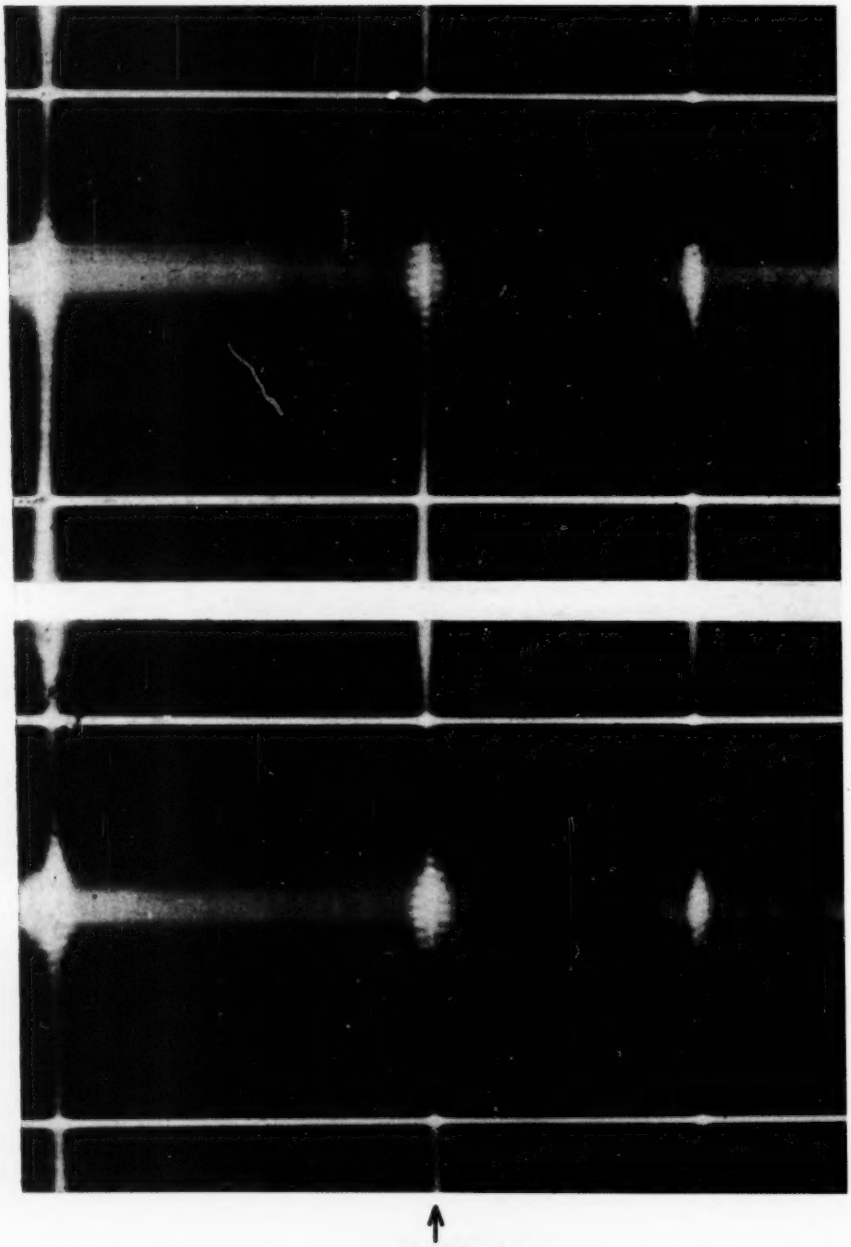

Babinet fringes in the σ and π-components of the Zeeman triplet λ6173, for spots 12580a (*upper photograph*) *and* 12579 (*lower photograph*).

P. J. Treanor, The spatial analysis of magnetic fields in sunspots.

providing this fine grating, which is ideally suited to work of this kind. The arrangement of the accessory equipment is shown in Fig. 3 and Plate 8. The 35·2 m Cassegrain telescope has a hollow polar axis, down which the beam is deflected by a coudé mirror. At the lower end of the polar axis, in the spectrograph basement, the beam is deflected into an east–west direction by a second coudé mirror to the slit of the spectrograph where the image is normally formed. In our observations, the focus was advanced to form the solar image in the polar beam, before the reflection at the second coudé; the analysing apparatus was placed here, so that the polarization produced by the second coudé does not affect the observations. The analysing arrangement consisted of a quartz Babinet compensator, of clear aperture 40 × 25 mm with a prism angle of 7° 30′. The plane polarizer was a Rochon prism 40 × 40 mm, of fluor-crown glass and calcite. This prism produces an undeflected achromatic plane-polarized image, and a chromatic image, polarized orthogonally to the first, which is deflected through several degrees and does not enter the spectrograph. The large aperture, high transmission, and optical quality of the Rochon gives it a considerable advantage over other polarizers. These components were mounted in calibrated rotatable frames on a rigid optical bench supported on a frame of "Dexion" and erected in the polar axis. A lens, placed after the second coudé, re-imaged the spot and fringe system on the slit.

The guiding system.—It is important to be able to guide the spot on the slit accurately during the required exposures, of 5–15 minutes. Since the guiding system must be placed in front of the Babinet, it must be as free as possible from polarizing effects, a condition not well satisfied by tilted-plate guiding devices. The system used consisted of three spectacle prisms. Two of these, with their axes arranged orthogonally, could be moved up and down the polar optical bench by cords controlled by the observer, who watched the image of the spot on the slit through a small telescope. If the powers of the prisms in prism dioptres (deflection in cm/m) are D_1, D_2, and their distances from the image plane z_1, z_2, they produce linear image displacements $x = D_1 z_1$, $y = D_2 z_2$. This provides the guiding requirement, but produces an unwanted angular decollimation of the beam, equal to the vector sum of the angular displacements of the prisms. This is compensated for by a fixed third prism of power $(D_1^2 + D_2^2)^{1/2}$ placed close to the image plane, its direction of deflection being opposed to that of the decollimation. By choosing prism powers in the ratio 3 : 4 : 5 irrational powers were avoided. To avoid vignetting, in re-imaging the Babinet on the slit, a field lens is required in the first image plane. The small positive power required for this was incorporated in the optician's prescription for the third prism.

The remaining components shown in Fig. 3 are the interference filter used to isolate the region round λ6200, and two half-wave plates. The second of these, placed in front of the filter plays a simple but important role. The light received by the slit is always plane-polarized. The polarizing action of the spectrograph is considerable and would nearly extinguish the incident light at certain orientations. The half-wave plate is used to rotate the plane of polarization to the most favourable position. The first half-wave plate represents a slight modification of the experiment as described in the previous section. Instead of rotating the Babinet and polarizer conjointly, with respect to the incident polarized light, one can rotate the incident polarized light in the

opposite direction, the two effects being optically equivalent. A half-wave plate may be used for this purpose, the effective rotation of the light being twice the angle through which the plate is turned. The action of a half-wave plate in connection with the rotation of elliptically polarized light may be understood from Fig. 4. In this OX, OY are incident vectors in the plane of the axes of the Babinet, Q is the advancing axis of the half-wave plate, at an angle $-\beta$ to the OX axis. OX', OY' are the transmitted vectors. If OP is the major axis of the incident ellipse, making an angle γ to the OX axis, the axis of the emergent ellipse will be OP' (the mirror image of OP in the plate axis, as can be seen from the symmetry). The action of the half-wave plate has been to rotate the ellipse through an angle $-2(\beta+\gamma)$. The orientation γ^* of the ellipse OP' which we determine in the experiment in this form is simply related to the orientation of the required ellipse by

$$\gamma = -(2\beta+\gamma^*). \tag{19}$$

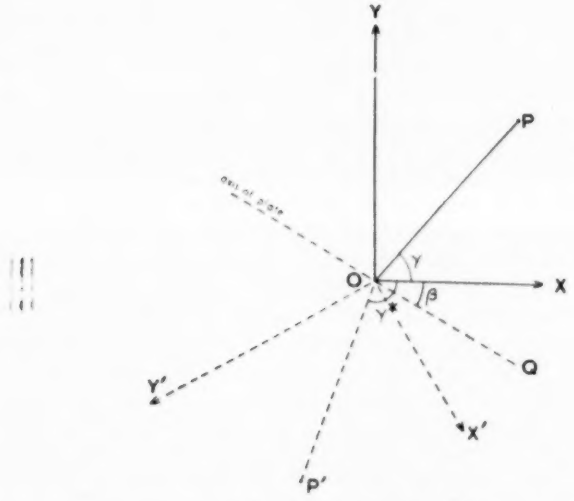

FIG. 4.—*Rotation of elliptically polarized light by a half-wave plate.*

The advantage of this system is that the orientation of the fringes on the slit, and hence their scale in the spectra, remains unchanged.

Subsidiary measurements.—The values of the retardations and the uniformity of the half-wave plates were determined by a method worth mentioning on account of its simplicity. A single-element Lyot filter consisting of a piece of selected mica, about 1 mm thick, placed between crossed polaroids, was set up between a white-light source and the slit of a Hilger direct-reading spectroscope, the axis of the mica being oriented at 45° to the transmission planes. The spectrum shows under these conditions about half a dozen Lyot fringes. The experiment consisted in introducing the wave-plate into the beam between the polaroids, so that its retardation (*a*) supported, (*b*) diminished the retardation of the mica sheet. From the position of the Lyot fringes under these two conditions it is an elementary matter to calculate or obtain graphically the retardation of the plate as a function of wave-length. We found for the first

half-wave plate a retardation of $0{\cdot}485\lambda$ at $\lambda 6173$ (it behaves as a true half-wave plate at $\lambda 6330$). This slight deviation in specified performance leads to quite trivial phase errors never exceeding $5^{\circ}{\cdot}5$.

It was originally intended to determine the polarization produced by the first coudé at the time of observation. Owing to an unavoidable interruption in the observations this was not possible, and a few measures obtained much later using artificial light proved rather uncertain. However the order of magnitude of the effect can be estimated from the theory of metallic reflection and the known optical constants of aluminium. For an angle of incidence of 55°, corresponding to a solar declination $+10^{\circ}$, and using the recent values of ν and κ for evaporated aluminium films derived by Schultz (**24**) we find for rays in and perpendicular to the plane of incidence a phase difference $\epsilon = 20^{\circ}{\cdot}6$ and a ratio of reflectivities $1{\cdot}11$. Drude's much older values for solid aluminium (**4**) give a phase difference $24^{\circ}{\cdot}3$ and ratio of reflectivities $1{\cdot}22$. Seares (**26**) has shown that the effect of the different reflectivity is negligible; this is at least true in the case of good evaporated films. The phase difference is by no means negligible in itself, but its effect enters only slightly into the differential form of the method. It is worth noting for future work however, that when, as happens with us, the only significant source of instrumental polarization is the phase difference produced by a single metallic reflection, this may be accurately compensated by means of a wave-plate of retardation ϵ (or $2\pi \pm \epsilon$, a value more easily realized, since such a plate is a whole-wave plate for a specifiable wave-length $\lambda_1 \neq \lambda$), with its axis in the plane of incidence. An alternative possibility would be to set one Babinet axis parallel to the plane of incidence (the condition for complete independence of instrumental polarization), and to place the first half-wave plate cemented between optical flats, before the reflection at the first coudé. These are alternatives to the procedure of determining the instrumental effect, and applying corrections to the individual measures.

4. *Observations.*—During the months 1957 July–Sept. observations were made by means of the equipment described above on a number of sunspots. For the field direction determination, the well-known normal triplet of Fe I, $\lambda 6173$ was used. Many plates were obtained in which all three components of this line were crossed by the polarization fringe pattern. The normal procedure was to expose in immediate succession on a single plate, at two different settings of the half-wave plate, corresponding to a rotation of the ellipses of 45°. This was followed by a third exposure containing standardizing fringes in plane polarized light (which were used mainly as a convenient means of obtaining the scale of the fringes) and by a fourth exposure in which the Babinet was removed and a normal spectrum of the spot obtained for control purposes. The mounting of the Oxford telescopes endows the image with a rotation at the diurnal rate. By taking the related fringe spectra in immediate succession, it was possible to ensure that the associated spectra related to virtually the same section on the spot. Advantage of the rotation was taken to obtain different sections of the same spot by repeating the observations when possible after a period of some hours. (The image rotates 15°/hr.) On a few plates, an additional fringe spectrum was obtained for an intermediate position of the half-wave plate, corresponding to an angle $\tau = 22\frac{1}{2}^{\circ}$. From the collected material, 18 plates were finally selected referring to spots in four groups, of which some data are assembled in Table I (**33**).

TABLE I

C.M.P. Aug. 1957	Lat.	Mt Wilson No.	Mt Wilson Max H (oer.)
21·9	+16·0	12563	2600
31·1	−30·0	12579	2800
31·9	+25·0	12580	2300
31·9	+25·0	12580 a	2300

All the groups had been observed in previous rotations. The spots studied were the principal spots in groups 12563 and 12579. The principal spot in 12580 was an active elongated object from which attention was eventually transferred to a smaller regular neighbouring spot 12580a in the same group.

The method of determining the field direction was essentially that described in Section 2. The fringe positions in the σ-components were measured on a Hilger measuring machine. Settings on individual fringes were usually consistent to about 0·01 mm, the distance between successive fringes being 0·33 mm. Means of pairs of adjacent fringes were used to reduce the accidental errors. The position of the spot centre, which is required to relate the corresponding σ-values in the pairs of spectra required for each determination of angle, were determined from microphotometer tracings across the nearby continuous spectrum of the spots.

Plate 9 is a reproduction of the fringe systems in λ6173 for the spots 12580a and 12579. The quality of the spectra was fairly uniform for the four selected spots, though these two had a more regular appearance. Two noteworthy features in Plate 9 are the presence of the fringed central component, and the extension of the field beyond the limits of the penumbra. Though this latter effect is somewhat enhanced by the contrast of the reproduction, comparison of the field extent with the penumbral diameters of these spots on copies of the daily photographs provided by the Royal Greenwich Observatory, show that our field diameters exceed the penumbral diameters by a factor of 1·2. This excess may be characteristic of rather small spots in disturbed areas.

Table II gives some typical results of the determination of the inclination of the field to the line of sight, as a function of the distance from the spot centre for the same two spots 12579, 12580a.

Two diametral sections of each of these spots was observed which intersected at about 45° and 75° respectively for 12579 and 12580a, when they were not far from the central meridian (Cols. 1–4). 12579 was again observed when quite close to the limb (Col. 5). In Cols. 1–4 the characteristic increase in the angle of incidence with distance from the centre is evident, and the agreement at the point of intersection near the spot centre is good. The symmetry of the field in the isolated spot 12579 (compare Cols. 3 and 4) is remarkable, and also the change in the direction of the lines of force with respect to the sight line in the limb observations (compare Cols. 4 and 5). The most interesting feature of these values, and one which is common to all our results, is the limited range of angle ω of the observed sections of the cone of lines of force, which in no case approaches the value of 180° embraced by the complete field according to Nicholson's law. Since our measures of direction do not extend to the limit of the penumbra, we

can only arrive at a quantitative estimate of this concentration of the flux by correlating these results with the field strength measurements, which will now be described.

TABLE II

Variation of field direction for spots 12579, 12580*a*

mm	12580a		12579		12579 (limb)
	°	°	°	°	°
−4·0	...	...	...	65·8	...
−3·5	...	...	...	58·3	...
−3·0	...	90·0	45·6	48·7	...
−2·5	64·5	79·9	43·1	44·0	58·0
−2·0	57·7	68·9	39·0	43·1	55·3
−1·5	46·8	61·1	43·1	44·0	64·5
−1·0	33·9	63·0	33·3	35·9	64·5
−0·5	11·0	54·8	27·7	23·1	70·7
0·0	41·3	47·1	27·1	29·4	82·9
+0·5	49·9	31·8	51·7	51·0	90·0
+1·00	46·4	25·9	55·3	44·4	...
+1·5	56·1	43·1	...	53·1	...
+2·0	...	...	...	47·1	...
+2·5	...	...	...	55·3	...
ω	98·6	69·5	46·1	74·9	32·0

Field strengths.—These were determined from the same spectra by direct measurement of the distance between the σ-components. It was found that the grating spectra clearly resolved the Zeeman triplet λ6173 at the centre of the spots where the fields were of the order of 2000 oersted, and the central fields were determined in this way. Attempts to extend the measurements to the edge of the spot were hampered by failing resolution of the components, due almost entirely to their intrinsic width and to the presence of the central component. All the plates however contained the line λ6149 (Fe II), a line of which the physical and magnetic properties mark it out as one of exceptional interest.

TABLE III

	Source	Intensity Disk	Spot	E.P.	Transition	$g\lambda^2$	Pattern
6149·255	Fe II	2	−1	3·873	$b^4D_{1/2}-zP_{1/2}^0$	50·4	Doublet
6173·348	Fe I	5	3	2·213	$a^5P_1-y^5D_0$	95·2	Triplet

Table III compiles data from Rowland (**32**) and Russell and Moore (**22**) relative to this line, and the corresponding comparative data for λ6173. The line λ6149 is weak in spots, it is an ionized line, and has a high excitation potential. These factors all suggest that it is formed in the deeper and therefore hotter part of the spot, at a level not very different from that in which the continuous spectrum of the spot originates, which according to Houtgast and van Sluiters (**10**) is about 120 km lower than the effective depth of λ6173. The Zeeman

splitting factor is lower than that of $\lambda 6173$, but the line has a narrower profile. Its most interesting feature, however, from the point of view of measurement, is that it has no central component. The simple theory of the Zeeman effect predicts a quadruplet in which the σ- and π-components have the same splitting factor and are therefore superimposed. One would not expect this to be exactly verified in the complicated spectrum of Fe II. In fact the line was observed in the spark spectrum by A. S. King (**13**) who found it to be quadruplet, being made up, however, of very close doublets separated by only 1/10 of the main separation. The value of $g\lambda^2$ in the table is theoretical. We may compare this with King's value in various ways. Applying the theoretical value to King's measurements, using the mean separation of his π- and σ-components, we find that the implied field strength is 16 490 oersted. King estimated his field strength in various ways and gives a value of 16 000 ± 160 oersteds. The ratio of splitting of $\lambda 6173$ (which King measured with difficulty) and $\lambda 6149$ is found to be 2·049 which is to be compared with the theoretical value of 1·89. The agreement to within a few percent of the theoretical values with these old and not very consistent values of King justifies our present use of this value, but if the line is to be further used, new laboratory measurements are much to be desired.

It should be pointed out that the complex polarization of $\lambda 6149$ makes it unsuited to the quarter-wave plate technique. This is of no consequence in direct measurements however, and it was found that these could be carried out over a large part of the spot. The partial failure of resolution near the edge of the measurable area produces a systematic error, for which however an order of magnitude correction can be applied, on the assumption that the photographic profiles of the lines may be approximated to a Gaussian form. The correction so deduced rose from about 50 oersteds for a measured field of 1000 oersteds, to 200 oersteds for a field of 700 oersteds, which represented both theoretically and practically the lowest field that could be measured in this simple way. However, it was possible to estimate with a consistency of about 0·1 mm the point at which the field disappeared in both $\lambda 6173$ and $\lambda 6149$. This measurement of the total extent of the field provided two additional points of lower weight, which completed the field variation curves.

Although the observations of the four spots were well scattered over the disk, analysis of the central intensities did not reveal a significant dependence on this quantity, a result to which not much weight can be attached on account of the statistical limitation of the material. However, in view of their homogeneity in this respect, the observations were used to determine the law of variation of field strength over the spots. To do this, standard field profiles were determined by expressing the intensity at given fractions r/r_0 of the field radius r_0 as a fraction I/I_0 of the central intensity. The results are summarized in Table IV, in which they are to be compared with the variation predicted by a parabolic law, differing from Broxon's formula only by the substitution of r_0, the actual field extent, for the penumbral radius b. With this adjustment, the agreement is very good. Our observations tell us little of the exact form of the curve near the edge of the field, and cannot be alleged as positive evidence against Mattig's formula, but they are adequately represented by the simpler parabolic form.

The law of direction.—Using the above determination of the distribution of field strength as a function of distance from the centre of the spot, it is a simple matter to calculate the percentage of total flux contained within the limits of the

TABLE IV

Field-strength distributions in sunspots

Spot	12563	12579	12580	12580a			
No. of spectra	14	9	10	6			
r/r_0	H/H_0	H/H_0	H/H_0	H/H_0	Mean	s.d. of mean.	Parabolic law
−0·8	37·9	39·6	30·5	29·7	34·4	2·2	36·0
−0·6	63·7	64·4	56·0	54·1	59·5	2·2	64·0
−0·4	84·3	84·2	77·0	70·3	78·9	2·9	80·0
−0·2	95·7	97·8	96·6	88·3	94·6	1·9	96·0
0.0	100·0	100·0	100·0	100·0	100·0	...	100·0
+0·2	99·3	96·2	92·1	100·5	97·0	1·7	96·0
+0·4	87·0	81·8	73·7	80·5	80·7	2·4	80·0
+0·6	68·2	60·0	55·4	62·8	61·6	2·3	64·0
+0·8	41·7	31·8	38·3	39·5	37·8	1·7	36·0

field over which we have determined the variation of direction. In this way we find that 40 per cent of the total flux of the spot is funnelled into unit solid angle. We can make a similar computation for Nicholson's measurements by combining Chapman's representation of the latter (equation (6)) with Broxon's law, and in this case find less than 20 per cent of the flux in unit solid angle. It is clear that our results indicate a more strongly radially directed field than those of Nicholson.

A partial funnelling of this kind is not altogether unexpected. Indeed, as was suggested in equation (5), observations by the neutral line method already indicate a degree of concentration intermediate between that implied by equation (6) and our present results, while the interpretation of the observations based on the extinction of the central component is influenced by a single point of low weight near the edge of the penumbra. If the general validity of this phenomenon can be established it may well eliminate the inconsistency already referred to between the magnetic field measurements and the direction of the velocity-fields determined from the Evershed effect.

The variation with depth.—It has already been stated that no statistically significant variation in centre-limb field strengths was found, so that no evidence for a variation of field with depth can be deduced in this way from the present observations. Comparison of the central fields of λ6173 and λ6149, yielded, somewhat unexpectedly, a systematic negative vertical gradient. However, this value is less than the uncertainty of a few per cent in the relative splitting factors of the two lines, a quantity which affects all the relative measures. Even allowing for the effects of these limited systematic uncertainties, and for the accidental errors, it seems however impossible to reconcile the present measures with a large positive gradient. An upper limit of 1 oersted/km is suggested. It will be recalled that this is consistent with the gradient of 0·5 oersted/km calculated from simple geometrical considerations of the divergence required by Nicholson's law of directions. The law of directions indicated by our present observations suggests an even smaller vertical gradient.

It may be recalled that Tanaka and Tagaki also found only slight evidence of a small vertical gradient. Their observations, made with a 14 m solar telescope and a dispersion of 2·5 mm/A, refer to a large number of lines, ranging in intensity from −3 to 28, in a single large spot. The value of their results has been obscured and the interpretation complicated by the large systematic differences of the measured fields in lines of different elements, though the agreement between lines of the same element is good. The differences must surely be due to the use of the splitting values tabulated by Kiess and Meggers (**12**). These are theoretical values derived from Landé's formula which assumes L–S coupling, a condition not strictly applicable to many of the measured lines. The recomputation of the homogeneous data provided by these observations, using accurate laboratory measurements of the Zeeman splitting of these lines is most desirable.

Conclusion.—Although an attempt has been made to use the first fruits of the Babinet method to obtain a pre-view of the complete spatial analysis of a sunspot field, it would be premature to put too much weight on these initial and limited results, obtained from a random collection of spots, in weather far from ideal. The main purpose of the investigation was to demonstrate the practicability of the method, and this much at least we believe has been achieved.

Thanks are due to a number of skilled hands on whom this work has been very dependent: to Messrs Hilger and Watts who produced the Babinet compensator, and to Mr D. S. Brown of Grubb, Parsons, who constructed the Rochon; also to Mr H. P. Wiggins, for several large half- and quarter-wave plates used in these and subsidiary experiments, which satisfied the most searching tests of quality we could devise, and to Mr H. G. East, who constructed various mechanical parts. To Professor Plaskett I owe a special debt of gratitude for his unfailing interest and encouragement. I should also thank Dr Hindmarsh for valuable theoretical discussions. The project was carried out during the tenure of the Skynner Research Fellowship at Balliol College, and the writer wishes finally to record his indebtedness to the College.

University Observatory,
Oxford:
1959 *July* 13.

References

(1) Abetti, G., *Pub. R. Osserv. Arcetri*, **50**, 47, 1932.
(2) Broxon, J. W., *Phys. Rev.*, **62**, 521, 1942.
(3) Chapman, S., *M.N.*, **103**, 117, 1943.
(4) Evershed, J., *Kodaikanal Obs. Bull.*, **2**, 63, 1909.
(5) Evershed, J., *M.N.*, **70**, 217, 1910.
(6) Evershed, J., *Kodaikanal Obs. Bull.*, **51**, 167, 1916.
(7) Hale, G. E., *Ap. J.*, **28**, 315, 1908.
(8) Hale, G. E., *Ap. J.*, **38**, 27, 1913.
(9) Hale, G. E., and Nicholson, S. B., *Magnetic Observations of Sunspots* 1917-1924. (Papers of Mt Wilson Obs., **5**, Part 1, 1938).
(10) Houtgast, J., and van Sluiters, A., *B.A.N.*, **10**, 325, 1948.
(11) Jensen, E., *Symp. I.A.U.* **6**, 258, 1958.
(12) Kiess, C. C., and Meggers, W. F., *Bur. of St. Jn. of Res.* **1**, 641, 1928.
(13) King, A. S., Papers of Mt Wilson Solar Obs., **2**, part 1, 1912.

(14) King, R. B., *Ap. J.*, **80**, 136, 1934.
(15) Kinman, T. D., *M.N.*, **112**, 425, 1952 (Comm. Univ. Obs. Oxford No. 35).
(16) Kinman, T. D., *M.N.*, **113**, 613, 1953 (Comm. Univ. Obs. Oxford No. 41).
(17) Künzel, H., Mattig, W., and Schröter, E. H., *Ast. Nachr.*, **283**, 28, 1956.
(18) Mattig, W., *Zeits. f. Ap.*, **31**, 273, 1953.
(19) Öhman, Y., *Ap. J.*, **111**, 362, 1950.
(20) Pierce, A. K., *J. Opt. Soc. Amer.*, **47**, 6, 1957.
(21) Plaskett, H. H., *M.N.*, **115**, 543, 1953 (Comm. Univ. Obs. Oxford No. 52).
(22) Russell, H. N., and Moore, C. E., *Revised Multiplet Table* (Cont. Princeton Univ. Obs. No. 20, 1945).
(23) Schröter, E. H., *Zeits. f. Ap.*, **33**, 20, 1953.
(24) Schultz, L. G., *J. Opt. Soc. Amer.*, **41**, 1047, 1951.
(25) Schuster, A., *Theory of Optics*, 12–15 and 263, 1904.
(26) Seares, F. H., *Ap. J.*, **38**, 99, 1913.
(27) Severny, A. B., *Russ. Ast. J.*, **36**, Bd. 2, 208, 1959.
(28) Stepanov, V. E., *Isv. Crim. Ast. Obs.*, **19**, 21, 1958.
(29) Tanaka, T., and Tagaki, Y., *Proc. Phys. Math. Soc. Japan*, **21**, 421, 1939.
(30) Thiessen, J., *Naturwiss.*, **40**, 218, 1953.
(31) von Klüber, H., *Zeits. f. Ap.*, **24**, 121, 1947.
(32) *Revision of Rowland's Preliminary Table*, Mount Wilson 1928.
(33) Summary of Mt Wilson Magnetic Observations. *P.A.S.P.*, **69**, 580, 1957.

STELLAR GROUPS, V. LUMINOSITIES, MOTIONS AND MASSES OF THE LATE-TYPE SUBGIANTS

Olin J. Eggen

(Communicated by the Astronomer Royal)

(Received 1959 October 5)

Summary

The available data for 205 subgiants of type G5 and later are listed in Table I. Most of these stars have visual luminosities between +2 and +4·5 as judged by spectroscopic criteria. On the basis of current evolutionary theory this list probably contains some of the oldest stars in the solar neighbourhood.

The stars for which the most reliable trigonometric parallaxes are available, shown in Fig. 1, indicate an (M_V, $B-V$)-distribution similar to that found for the γ Leonis and 61 Cygni groups and the cluster M67. The lower limit to the luminosity observed for the subgiants indicates an upper limit of $\sim 1{\cdot}5 \times 10^{10}$ years for their ages.

The solar motion, derived from the motions of approximately half the subgiants, is near 35 km/sec toward $\alpha = 19^h$, $\delta = +44°$.

The masses derived from the orbits of five visual binaries are discussed. First orbits are derived from three of these binaries including HD 194433 which may contain the oldest stars for which a mass determination is available. The masses of the subgiants probably lie between 1 and 1·5 ⊙.

1. *Introduction.*—A class of objects falling in the H–R diagram intermediate between the G-type giants and dwarfs was first isolated and labelled "subgiants" by Stromberg (1930). The two-dimensional spectral classifications at the Mt Wilson (Adams *et al.* 1935), Victoria (Young and Harper 1924), and Yerkes (Morgan 1938) observatories, as well as trigonometric parallaxes for a few of the brighter members of the class have confirmed the intermediate luminosities of these stars. In current theories of stellar evolution the late-type subgiants have been recognized as representing an intermediate stage in the evolution of stars with near-solar mass. Since evolutionary changes in stars with masses $\sim 1{\cdot}5 \odot$ are not expected in less than $\sim 10^9$ to 10^{10} years, the subgiants are easily recognizable examples of old stars. Therefore it is of some interest to collect the available information for known subgiants (Section 2) for a discussion of their luminosities (Section 3), motions (Section 4) and masses (Section 5). Subgiant components of close eclipsing binaries are not included because both the masses and the evolutionary rates of such stars may be influenced by their close companion.

2. *Catalogue.*—Table I contains a catalogue of all stars classified G5 or later which, on the basis of spectroscopic luminosity criteria, are suspected to lie between $M_V = +2$ and $+4{\cdot}5$ (Adams *et al.* 1935) or classified in luminosity class IV or IV–V (MK) and for which radial velocity determinations are available. Stars of luminosity class III–IV(MK) are not included. A few stars observed at Mt Wilson but not included in the published list of spectroscopic absolute magnitudes

have been subsequently classified as subgiants by Joy and so listed in the radial velocity catalogue (Wilson 1953). Table I contains the following information:

HD: The number in the Henry Draper Catalogue.

Name: The name, BD or CoD number.

V_E, $B-V$, $U-B$: The magnitude and colour. The colours are from various sources and were all determined photoelectrically. The one decimal magnitudes are from a great variety of sources.

Sp, S: The spectral type and luminosity classification and its source; W = Adams *et al.* 1935; DD = Heard 1956; C = Evans, Menzies and Stoy 1957, 1959; MK = Johnson and Morgan 1953; F = Boulon, Duflot and Fehrenbach 1959, R = Roman (1955), MW = M. L. Woods (1955), MP = Moore and Paddock (1950), H = Halliday (1955).

μ_α, μ_δ, S: The components of the proper motion derived from the following sources; GC = Boss General Catalogue; N30 = Morgan N30 catalogue; Y = Yale Zone Catalogues; GAZ = Greenwich astrographic zones; CP = Cape photographic catalogues; CR = relative proper motions from Cape parallax series. A plus sign in the column "S" indicates that modern meridian positions have been used to improve the catalogue proper motion.

ρ, Q: The radial velocity in km/sec from the General Catalogue of Radial Velocities (Wilson 1953) and its quality, Q. A few determinations made since the compilation of that catalogue have been incorporated into the table.

Notes: Additional information for several stars is included in the notes; alternative classifications by KK = Keenan and Keller 1953; absolute magnitude estimates by V = Young and Harper 1924, and WB = Wilson and Bappu 1957.

With only a few exceptions the stars in Table I are of spectral classes G5 to K1, inclusive. Among all stars known from trigonometrical parallaxes to be within 20 parsecs of the Sun and classified as G5 to K1, about 10 per cent have luminosities in the range $M_V + 2$ to $+4{\cdot}5$ as can be seen from the following tabulation:

M_V	No. (G5–K1)
$< +2$	5
$+2$ to $+4{\cdot}5$	13
$> +4{\cdot}5$	93
	111

3. *Luminosity.*—Mean trigonometric parallaxes greater than $0''{\cdot}02$ based on results from at least two observatories are available for 51 of the stars in Table I. These stars are listed in Table II where, in addition to the HD number, the following information is given:

π_t, n: The mean trigonometric parallax (unit = $0''{\cdot}001$) and the number of observatories contributing to it.

$B-V$: The colour; in the few cases where photoelectric observations are not available the colour has been inferred from the spectral type and is followed by a colon.

M_V: The absolute visual magnitude resulting from the mean trigonometric parallax.

M_V(W): The Mt Wilson spectroscopic absolute magnitude (Adams *et al.* 1935) when available.

TABLE I

Subgiants of spectral type later than G5

HD	Name	V_E	$B-V$	$U-B$	Sp	S	μ_α	μ_δ	S	ρ	Q
		m	m	m			″	″			
28	33 Psc	4·56	+1·06	...	sg Ko	W	−0·013	+0·096	GC,Z, N30	− 6·1	a
249	+25°5073	7·2	...	...	K1 IV	DD	+0·121	−0·103	Y	+15·5	b
502	+18°4	7·8	...	...	G4 IV	MP	+0·018	−0·055	G, Y	+ 2.0	c
877	−23°46	6·7	...	...	sg G5	W	+0·005	+0·018	GC, Y	−16·0	c
1037	−15°32	6·9	...	...	sg G8	W	+0·110	−0·029	GC, Y	−29·8	b
1605	+30°43	7·9	...	...	K1 IV	H	+0·051	+0·057	Y	+10·2	b
2589	+76°10	6·21	+0·84	+0·55	sg G9	W	+0·336	−0·020	GC, GAZ	+19·0	b
3141	+41°87	7·7	...	...	Ko IV	MP	−0·189	−0·088	GC	+ 1·0	c
3546	ϵ And	4·37	+0·88	+0·46	sg G3	W	−0·231	−0·251	GC, N30	−83·6	a
4372	+30°113	7·2	...	...	K1 IV	H	+0·012	−0·054	GC, Y	+13·0	b
4398	HR 210	5·6	...	...	sg G6	W	+0·195	−0·004	GC, Y	−14·7	b
4744	+29°141	7·62	+1·07	+0·77	G8 IV	R	+0·214	−0·028	GC, Y	−162·8	b
5286	36 And	5·42	+1·03	...	sg K1	W	+0·128	−0·032	GC, Y	+ 1·5	b
5395	28 Cas	4·80	+1·03	...	sg G4	W	−0·092	−0·042	GC+	−47·0	a
6296	HR 300	6·29	+0·94	...	G5 IV	C	−0·125	−0·015	GC	+56·5	b
6473	HR 312	6·4	...	...	sg G6	W	−0·024	−0·035	GC, GAZ	−27·4	b
6734	29 Cet	6·44	+0·87	+0·48	sg G5	W	+0·133	−0·418	GC, Z	−95·4	b
8375	+33°220	6·3	...	...	G8 IV	H	+0·226	+0·118	GC	+ 2·8	b
8512	θ Cet	3·55	+1·00	...	sg Ko	W	−0·078	−0·216	GC, N30	+17·2	a
10015	+28°271	8·66	+0·83	+0·57	Ko IV–V	R	+0·421	−0·257	Y	− 2·9	b
10486	HR 495	6·5	...	...	sg K2	W	+0·143	−0·015	GC	+12·2	b
11937	x Eri	3·61	+0·85	...	G5 IV	MW	+0·676	+0·300	GC, N30	− 6·3	a
15590	−42°834	7·97	+0·66	...	G5 IV	C	+0·099	−0·065	GC, CP	+36·8	b
16141	79 Cet	6·82	+0·66	+0·21	G5 IV	R	−0·152	−0·430	GC, Y	−53·0	c
16708	+2°412	7·8	...	...	sg G5	W	+0·058	+0·007	Y	+65·3	b
18907	ϵ For	5·88	+0·79	...	G5 IV	C	+0·270	−0·423	GC, Y	+39·9	b
19618	+14°524	9·05	+0·84	+0·51	Ko IV–V	R	−0·069	−0·297	Y	−23·0	d
19743	−61°167	7·06	+0·93	...	G5 IV	C	+0·110	+0·106	GC	− 6·5	b
20277	HR 978	6·0	...	...	sg G8	W	−0·015	−0·107	GC	+19·0	c
20559	95 Cet	5·37	+1·04	+0·81	K1 IV	R	+0·253	−0·050	GC, Y	+27·8	b
20618	59 Ari	5·9	...	...	sg G5	W	−0·021	−0·071	GC, Y	− 0·1	b
20855		7·43	+1·05	...	Ko IV	C	+0·066	+0·102	GC	− 9·5	b
21467	66 Ari	6·1	...	...	sg G6	W	0·000	−0·100	GC, Y	+49·0	c
22849	+29°592	8·6	...	...	K1 IV	DD	−0·041	−0·062	Y	+ 8·1	b
23249	δ Eri	3·50	+0·92	+0·69	Ko IV	MK	−0·093	+0·746	GC, N30	− 6·4	a
23817	β Ret	3·82	+1·16	...	Ko IV	C	+0·312	+0·077	GC, N30	+50·5	a
26766	+29°678	7·3	...	...	K1 IV	DD	+0·120	−0·170	GC, Y	+ 9·0	b
29613	HR 1487	5·43	+1·04	...	sg K1	W	+0·123	−0·124	GC, Y	+56·0	c
31782	+25°766	8·1	...	...	Ko IV	DD	−0·080	−0·074	Z, Y	−67·8	b
32963	+26°789	7·85	+0·66	+0·21	G5 IV	R	−0·078	−0·054	Y	−62·9	b
34538	HR 1737	5·48	+0·91	...	sg G9	W	−0·005	−0·040	GC, Y	+75·3	b
34642	o Col	4·72	+0·93	...	sg Ko	W	+0·080	−0·336	GC, N30	+21·2	b
37160	40 Ori	4·09	+0·95	+0·65	sg G6	W	+0·095	−0·305	GC, Y	+98·7	a
37601	24 Cam	6·2	...	...	sg G9	W	+0·020	+0·030	GC, N30	−28·9	b
37981	+14°991	6·9	...	...	sg K1	W	−0·038	−0·010	GC, Y	+62·7	b
38455	−12°1258	7·6	...	...	G7 IV	MP	+0·009	−0·121	Y	−33·0	c
39169	−1°1038	8·0	...	...	sg Ko	W	+0·012	−0·044	GC, Z	+ 3·0	c
39280	−44°2271	7·74	+0·94	...	G8 IV	C	0·000	+0·030	GC, CP	+29·5	b
39364	δ Lep	3·72	+1·00	...	sg G7	W	+0·231	−0·645	GC	+99·3	a
39861	+81°201	8·9	...	...	sg G5	W	−0·077	−0·375	GC, GAZ	−27·0	b
40409	HR 2102	4·60	+1·07	...	sg K3	W	+0·135	+0·540	GC	+25·1	a
40959	+27°963	8·8	...	...	sg G5	W	+0·005	−0·040	GC, Y	− 2·8	b
44019	−0°1255	7·6	...	...	K2 IV	MP	−0·013	−0·024	Y	+39·0	c
45410	6 Lyn	5·88	+0·94	+0·66	sg G8	W	−0·020	−0·338	GC, N30	+36·0	c
46480	8 Lyn	6·0	...	...	sg G7	W	−0·200	−0·279	GC	−46·4	b
47205	ν CMa	3·87	+1·10	...	K1 IV	R	+0·064	−0·076	GC, Y	+ 2·5	a
50806	HR 2576	6·02	+0·72	...	G5 IV	C	+0·273	−0·437	GC, Y	+71·5	a
52071	+27°1296	7·2	...	...	K2 IV	DD	0·000	0·000	GC, Z	+94·7	b
52711	HR 2643	6·00	+0·59	...	G8 IV	H	+0·162	−0·833	GC, Y	+21·8	b
53590	−0°1587	7·6	...	...	G8 IV	MP	+0·013	−0·031	Y	+15·0	c
55280	18 Lyn	5·10	+1·09	...	sg K2	W	−0·091	−0·260	GC	+23·8	a
58895	−58°1741	6·59	+0·70	...	G5 IV	C	−0·082	+0·136	GC	+19·7	b
59468	−51°2507	6·75	+0·70	...	G5 IV–V	C	−0·291	−0·010	GC, CP	+ 3·4	b
62644	HR 2998	5·06	+0·77	...	G5 IV	C	−0·072	−0·563	GC	+27·0	c
67767	ψ Cnc	5·8	...	...	sg G6	W	−0·065	−0·350	GC, N30	−43·0	b
68978	−31°5719	6·68	+0·61	...	G5 IV–V	C	−0·336	+0·143	GC, CP	+48·5	b
70642	−39°4247	7·17	+0·70	...	G5 IV–V	C	−0·200	+0·240	GC+	+48·1	b
71952	HR 3351	6·5	...	...	sg Ko	W	+0·015	−0·082	GC	+43·6	b

TABLE I—*continued*

Subgiants of spectral type later than G5

HD	Name	V_E	$B-V$	$U-B$	Sp	S	μ_α	μ_δ	S	ρ	Q
		m	m	m							
73593	34 Lyn	5·5	...	...	sg G6	W	+0·029	+0·084	GC	−37·0	b
74543	−73°38	6·82	+1·04	...	Ko IV	C	+0·025	+0·152	GC	+36·1	b
76291	HR 3545	5·74	+1·09	+1·06	K1 IV	R	+0·126	−0·042	GC	+58·5	b
77818	+59°1218	7·65	+1·01	+0·82	sg Ko	W	+0·012	−0·111	Y	−39·1	b
78249	+59°1221	7·09	+0·99	+0·82	sg K2	W	−0·163	−0·033	GC, Y	+46·5	b
79452	HR 3664	5·97	+0·86	+0·37	sg G3	W	−0·147	+0·046	GC	+56·4	b
81265	+31°1978	7·8	...	...	G7 IV	MP	+0·075	−0·183	GC	−0·9	b
82210	24 UMa	4·50	+0·70	...	G5 IV	R	−0·061	+0·075	GC, N30	−27·2	a
84406	+63°861	6·9	...	...	sg Ko	W	−0·116	−0·143	GC	+ 7·9	b
84453	14 LMi	6·82	+0·95	+0·74	sg Ko	W	+0·056	−0·138	GC	−43·7	b
86006	−45°5556	8·16	+0·71	...	G5 IV	C	+0·034	+0·140	GC	+20·4	b
86359	26 Leo	7·6	...	...	sg G7	W	−0·041	−0·019	GC, Z	+17·2	b
87783	−46°5806	5·07	+0·88	...	Ko IV	C	−0·010	−0·056	GC+	+21·5	a
88416	+27°1860	8·5	...	...	Ko IV	DD	−0·086	−0·070	Y	− 0·6	b
88532	+29°2012	8·5	...	...	Ko IV	DD	+0·038	−0·016	Y	−29·0	Var
90572	+4°2333	7·4	...	...	sg Ko	W	−0·116	−0·028	GC, Y	+45·0	c
91011	31 Sex	7·1	...	...	sg Ko	W	+0·063	−0·045	GC, Z	− 0·7	b
92588	33 Sex	6·4	...	...	sg K1	W	−0·141	−0·124	GC, Y	+43·0	a
93636	43 LMi	6·3	...	...	sg K1	W	−0·085	−0·048	GC	+ 9·7	b
94132	HR 4243	6·1	...	...	sg G9	W	−0·394	−0·077	GC, GAZ	+14·7	b
94178	+33°2049	7·6	...	...	sg G7	W	+0·018	−0·053	G	+11·3	b
94264	46 LMi	3·72	+1·04	...	sg K2	W	+0·090	−0·285	GC, N30	+16·1	a
94834	+24°2291	7·7	...	...	K1 IV	DD	−0·058	+0·042	Y	+ 4·7	b
96074	+66°697	7·7	...	...	sg G8	W	+0·010	−0·010	GC, GAZ	−11·0	c
96436	65 Leo	5·7	...	...	sg G7	W	−0·384	−0·088	GC, Z	+55·3	b
97033	+66°704	9·0	...	...	sg G5	W	−0·336	−0·132	GC, GAZ	+27·0	c
97561AB	+20°2572	6·92	+0·75	+0·33	G7 IV	R	−0·382	−0·134	GC+, Y	+45·3	b
98818	−60°3502	7·53	+1·13	...	Ko IV	C	−0·101	+0·037	GC	+36·9	b
100030	+48°1952	6·2	...	...	G8 IV	H	−0·230	−0·079	GC	+38·4	b
100901		6·54	+1·18	...	K1 IV	C	−0·148	+0·022	GC	+ 2·5	b
101408	−45°7180	7·25	+1·04	...	G8 IV	C	−0·026	−0·090	GC, CP	+28·1	b
102326	+77°440	8·75	+0·73	+0·45	G8 IV–V	R	+0·181	−0·090	GC, GAZ	−93·0	c
102928	−4°3152	6·1	...	...	sg Ko	W	+0·002	−0·005	GC, Y	+12·0	c
108309	−48°7426	6·25	+0·67	...	G5 IV–V	C	−0·635	−0·080	GC, N30, CP	+29·3	b
111028	33 Vir	5·67	+0·99	+0·74	sg K1	W	+0·275	−0·452	GC	+51·5	b
111417	−45°8040	8·33	+1·41	...	K3 IV	C	−0·053	−0·043	CP	−16·0	b
113817	−14°3644	7·2	...	...	sg G8	W	−0·042	+0·011	GC, Y	−12·2	b
114174	+6°2697	6·82	+0·66	...	sg G6	W	+0·084	−0·684	GC, N30	+22·2	b
115202	57 Vir	5·1	...	...	sg K1	W	+0·306	−0·121	GC, Y	+34·1	a
115577	−27°9145	6·81	+0·98	...	G8 IV	C	−0·074	−0·084	GC, Y	+152·2	b
117176	70 Vir	4·98	+0·71	...	sg G5	W	−0·238	−0·582	GC, N30	+ 4·2	a
121146	HR 5227	6·4	...	...	sg K2	W	−0·185	−0·060	GC+	−45·4	b
121416	HR 5239	5·82	+1·15	...	Ko IV	C	−0·159	−0·080	GC, CP	− 1·0	b
123409	+29°2943	7·0	...	...	sg G6	W	−0·066	−0·009	GC, Y	−55·1	b
123797	−48°8820	6·63	+0·91	...	G5 IV	C	−0·078	−0·078	GC, CP	−63·2	b
125968	−27°9806	7·75	+0·65	...	G5 IV–V	C	−0·264	−0·252	GC, Y, CR	+25·9	b
128095	+29°2553	8·1	...	...	K1 IV	DD	+0·056	−0·111	Y	+26·3	b
129580A	+58°1523	7·1	...	...	sg Ko	W	+0·131	−0·196	GC	− 9·0	b
B		8·0	...	...	sg G7	W	+0·131	−0·196		−16·1	b
136136	+44°2444	8·6	...	...	sg G8	W	−0·004	−0·009	GC	−45·6	b
138716	37 Lib	4·63	+1·01	...	sg K1	W	+0·305	−0·240	GC, N30	+47·7	a
140301	HR 5847	6·4	...	...	sg Ko	W	−0·005	−0·100	GC, N30	+20·5	b
140687	−24°12275	7·5	...	...	sg Ko	W	−0·089	−0·069	GC, Z	+ 1·7	b
140690	−42°10755	8·10	+0·64	...	G5 IV	C	−0·116	−0·158	GC, NP	+60·5	b
142091	κ CrB	4·60	+1·03	...	sg K1	W	−0·006	−0·355	GC, N30	−24·0	a
142898	+27°2555	8·0	...	...	K1 IV	DD	+0·034	−0·005	Y	−31·5	b
142980	ϕ Ser	5·54	+1·14	+1·16	K1 IV	R	−0·123	−0·087	GC, N30	−68·3	b
143586	+30°2735	8·6	...	...	sg G9	W				−21·2	b
144087A	−11°4057	7·4	...	...	sg G6	W	−0·070	−0·030	GC, Y	−34·0	b
145148	HR 6014	5·98	+1·02	+0·76	Ko IV	R	+0·230	−0·736	GC, N30	− 4·0	b
150275	HR 6191	6·34	+1·00	+0·71	sg Ko	W	−0·101	+0·276	GC, GAZ	−32·0	b
151090	41 Her	6·7	...	...	sg G6	W	−0·213	−0·269	GC	− 5·6	a
151216	+33°2775	9·1	...	...	sg K1	W	...	...	...	−15·5	b
152781	HR 6284	6·5	...	...	sg K2	W	+0·076	+0·034	GC	− 2·7	b
153226	HR 6301	6·5	...	...	Ko IV	H	−0·086	+0·068	GC, N30	−30·7	b
153344	+62°1520	7·06	+0·67	+0·21	G5 IV	R	−0·330	−0·055	GC	−82·1	b
154088	−28°12769	6·57	+0·83	...	G8 IV–V	C	+0·082	−0·262	GC, Z	+14·2	b
158311		7·50	+0·90	...	G8 IV	C	+0·100	−0·006	GC	+24·6	b
158614	HR 6516	5·27	+0·72	...	G8 IV–V	R	−0·123	−0·172	GC, Y	−77·0	a

TABLE 1—*continued*

Subgiants of spectral type later than G5

HD	Name	V_E	$B-V$	$U-B$	Sp	S	μ_α	μ_δ	S	ρ	Q
		m	m	m			″	″			
159809	−45°11742	7·44	+1·02	...	K1 IV	C	−0·072	−0·162	GC, CP	+ 6·8	b
160042	−21°4682	6·7	...	...	sg G7	W	−0·030	−0·019	GC, Z	− 0·3	b
161797	μ Her	3·42	+0·75		G5 IV	MK	−0·308	−0·749	GC, N30	−15·6	a
162076	HR 6638	5·8	...	...	sg G5	W	+0·020	−0·006	GC	−26·3	b
162619	−47°11895	8·75	+1·23	...	K1 IV	C	−0·016	−0·023	CP	−37·0	b
165271	−46°12117	7·65	+0·65	...	G5 IV	C	−0·037	−0·108	GC, CP	−88·1	b
165438	HR 6756	5·9	...	...	sg K1	W	+0·135	−0·036	GC, Y	−18·9	b
165753	−44°12373	7·02	+1·11	...	K0 IV	C	+0·016	−0·037	GC, CP	− 0·7	b
166070	+27°2960	8·4	...	...	K1 IV	DD	+0·018	+0·022	Y	−27·6	b
166867	+29°3198	7·3	...	...	K0 IV	DD	−0·007	−0·034	Y	+173·0	b
167042	HR 6817	5·91	+0·94	+0·72	sg K0	W	+0·113	+0·248	GC	−15·8	a
168723	η Ser	3·26	+0·94	+0·65	G8 IV	R	−0·555	−0·699	GC, N30	+ 8·9	a
170829	HR 6950	6·6	...	...	G8 IV	H	+0·006	−0·263	GC, Y	−59·0	a
171994	HR 6995	6·4	...	...	G8 IV	H	+0·012	+0·031	GC, Y	−46·0	b
173791	HR 7065	5·80	+0·89	...	G6 IV	C	+0·066	+0·053	GC, CP	+ 9·7	b
173949	HR 7075	6·2	...	...	sg G7	W	−0·007	+0·016	GC	−24·7	b
175518	−5°4811	7·47	+0·75	+0·40	K0 IV–V	R	−0·211	−0·391	GC, Y	−77·0	c
176578	−47°12692	6·85	+0·97	...	K0 IV	C	+0·019	−0·124	GC+, CP	− 7·1	b
177565	HR 7232	6·14	+0·70	...	G5 IV	C	−0·193	−0·360	GC, CP	+58·5	b
178395	−42°13943	9·29	+1·09	...	K0 IV	C	−0·024	−0·030	CP	−26·9	b
179094	HR 7275	6·1	...	...	K1 IV	H	−0·104	−0·062	GC	+ 4·2	a
181391	26 Aql	5·1	...	...	sg K0	W	+0·113	+0·046	GC, N30	−18·5	b
182156	−31°16655	7·63	+1·17	...	K0 IV	C	+0·044	−0·122	GC, CP	+14·8	b
182572	31 Aql	5·15	+0·79	+0·40	sg G7	W	+0·721	+0·638	GC, N30	−99·8	a
183877	−28°15936	7·14	+0·68	...	G5 IV	C	+0·068	−0·748	GC, Y	−40·0	b
184010	+26°3573	...	...	...	sg G8	W	+0·020	+0·029	GC, Y	− 2·0	c
...	+15°4061	8·5	...	...	K0 IV	F	+0·037	+0·005	Y	−88·0	F
185351	HR 7468	5·10	+0·97	...	sg K0	W	−0·107	−0·104	GC	− 5·2	b
186975	−46°13237	7·25	+1·10	...	K0 IV	C	−0·075	−0·028	GC, CP	−24·4	b
188326	+38°3891	7·56	+0·78	+0·35	G8 IV	R	−0·039	+0·340	GC	−71·1	b
188376	ω Sgr	5·1	...	...	sg G5	W	+0·206	+0·080	GC, Z	−21·0	a
188512	β Aql	3·70	+0·86	+0·49	sg G8	W	+0·039	−0·481	GC, N30	−39·8	a
190248	δ Pav	3·64	+0·76	...	G5 IV	MW	+1·196	−1·145	GC, N30	−21·8	a
190360	HR 7670	5·70	+0·72	+0·38	sg G8	W	+0·672	−0·530	GC, Y	−46·2	b
191026	27 Cyg	5·33	+0·85	+0·54	sg G6	W	−0·234	−0·437	GC, N30	−33·6	b
191190	−47°13275	6·81	+1·16	...	K1 IV	C	+0·042	−0·064	GC, CP	−50·6	b
191615	+25°4124	7·80	+0·94	+0·83	G8 IV	R	+0·005	+0·037	Y	−94·0	b
194433	HR 7808	6·23	+0·98	...	sg K1	W	−0·240	−0·118	GC, CP	+25·2	b
196755	κ Del	5·02	+0·74	+0·19	G5 IV	R	+0·316	+0·016	GC, N30	−52·0	a
196925	74 Dra	5·9	...	...	sg G8	W	+0·071	+0·218	GC, GAZ	−14·0	c
197900	−44°14143	6·46	+1·18	...	K1 IV	C	+0·086	−0·060	GC+, CP	−14·8	b
198149	η Cep	3·40	+0·91	+0·42	sg G7	W	+0·090	+0·820	GC, N30	−87·3	a
198896	+42°3746	8·5	...	...	sg G8	W	...	...	...	+ 4·0	d
199190	−70°1800	6·87	+0·61	...	G5 IV	C	+0·447	−0·280	GC	−34·1	b
199223	HR 8010	6·0	...	...	sg G9	W	+0·064	+0·012	GC	−30·6	a
199580	+42°3915	7·18	+0·97	+0·73	sg G9	W	+0·225	+0·220	GC	−19·4	b
199976	−8°5544	8·2	...	...	sg G7	W	+0·243	+0·025	Y	−37·9	b
200026B	−43°14327	6·89	+0·97	...	K0 IV	C	+0·068	−0·113	GC, CP	−31·5	a
200553		7·20	+0·93	...	G8 IV	C	−0·034	−0·074	GC, CP	−14·7	b
206341	−28°17407	7·68	+1·08	...	K0 IV	C	−0·065	−0·110	GC, Y	−21·3	b
208627	−44°14717	6·54	+0·89	...	G8 IV	C	−0·005	−0·060	GC+, CP	+13·4	b
210441	−44°14805	6·60	+1·00	...	G8 IV	C	+0·050	+0·014	GC, CP	−13·3	b
...	+15°4622	9·3	...	...	sg K3	W	+0·017	−0·008	Y	−21·6	b
212943	35 Peg	4·81	+1·05	+0·89	sg K0	W	+0·080	−0·309	GC, Y	+53·8	a
215549	+29°4753	6·37	+0·92	+0·68	sg K0	W	−0·266	−0·352	GC	− 0·6	b
218101	HR 8784	6·44	+0·83	+0·55	G8 IV	R	+0·186	−0·198	GC, Y	−27·4	b
218935	60 Peg	6·4	...	...	sg K0	W	−0·192	−0·116	GC, Y	−10·2	b
219834	94 Aqr	5·2	...	...	G5 IV	R	+0·293	−0·098	GC	+ 9·1	b
220167	+59°2703	7·4	...	...	K1 IV	F	−0·067	−0·006	GC	−76·0	F
221148	HR 8924	6·26	+1·08	+1·14	sg K3	W	+0·178	−0·225	GC, Y	−25·0	b
221585	+62°2244	7·42	+0·74	+0·38	G8 IV	R	+0·434	+0·043	G	+ 8·5	b
221639	+59°2744	7·3	...	...	sg G9	W	+0·094	+0·010	Y	+ 0·1	b
222107	λ And	3·88	+1·02	+0·68	sg G7	W	+0·158	−0·422	GC, N30	+ 6·8	a
222404	γ Cep	3·22	+1·03	+0·92	sg K1	W	−0·065	+0·153	GC, N30	−42·4	a
222480	−32°17623	7·13	+0·66	...	G5 IV	C	+0·109	+0·040	GC, CP	+21·5	b
222803	HR 8993	6·11	+0·99	...	G8 IV	C	+0·299	+0·014	GC, CP	−30·8	b
223524	HR 9027	6·1	...	...	sg K0	W	+0·134	+0·078	GC	−17·7	b

Notes to Table I

HD	
28	K1 III (4550) R, Sp. B. P=73^d, V (+1·7)
3546	G8 III R, V (+1·4)
5286	ADS755, WB (+4·0)
5395	G8 III–IV (wk lines), R, V (+0·4)
6734	Ko IV R
10015	dG8 (+5·0) W
11937	11^m 6″
16141	dG2W
20559	ADS2459, gKo (+0·9) W
23249	dKo (+4·6) W, WB (+5·1)
32963	G2 V DD
37160	Ko III R, G6 III–IV KK
39169	ADS4442
39364	G8$^+$ III KK
40959	Optical comp. to ADS4629
45410	Ko IV R
50806	dG3 W
52711	dG3 (+4·2) W
76291	gK2 (+0·8) W
77818	K1 IV R
78249	K1 IV R
79452	G6 III R
82210	dF9 (+3·7) W
84453	Ko IV R
86006	The values from CP are $\mu_\alpha = +0''·057$, $\mu_\delta = +0''·030$; these are supported by relative values determined from parallax plates.
87783	SDS, 0″·5
90572	ADS7779
94264	K1 III R, WB (+2·1)
96436	ADS8060, $\Delta m \sim 6^m$
97561	dG4 W; ADS8094, $\Delta m \sim 0^m$
102326	dG7 W
102928	Sp. B., range 28 km/sec.
108309	$V = 10^m·4$, $B-V = +1^m·28$, common proper motion
111028	K1 IV R, K1, III–IV KK, WB (+3·7)
115202	K1 IV (4550) R
117176	G5 IV–V MKK
129580	ADS9346
136136	ADS9573, optical
138716	WB (+3·0), K1 III R
140690	SDS 0″·3
142091	Ko III–IV R
142980	gK4 (−0·1) W, WB (+2·0)
144087	ADS9910
145148	dK2 (+5·6) W, WB (+3·7), K1 III–IV KK
151090	10^m·7 K3, 164″ common motion
150275	K1 III R, WB (+2·0)
153344	dG4 W
158614	dG6 (+4·8) W, ADS10598
159809	SDS
161797	dG4 (+4·2) W
162076	WB (+2·1)
165438	WB (+3·6)
167042	WB (+4·1), K1 III R
168723	Ko III–IV MKK
170829	Sp. B.
173949	ADS11661
175518	dG8 (+5·3) W
179094	Sp. B. P=29^d
181391	Sp. B. P=266^d, G8 III–IV R, WB (+1·3)
182572	G8 IV R
+19°4061	Vel. by Fehrenbach
185351	Ko III R, WB (+2·3)
188326	dG4 (+4·6) W
188512	G8 IV MKK, ADS13110
190360	G6 IV R, 14^m·8 M6 2′·5
191026	Ko IV R
191615	Ko III DD
194433	K2 IV–V C, SDS
196755	dG2 (+3·8) W
196925	9^m Go 3′, Sp. B range 16 km/sec
198149	Ko IV MKK, WB (+2·9)
189223	ADS14430
198896	Sp. B with range of 36 km/sec, optical companion
199580	K1 IV R
199976	ADS14528
200026	SDS
212943	Ko III R, WB (+3·2)
215549	Ko III–IV R, ADS16248
219834	ADS16672, dG4 (+3·6) W
220167	Vel. by Fehrenbach
221148	K3 III R
221585	dG3 (+4·4) W
222107	Sp. B. period=21^d, G8 III–IV MK
222404	K1 IV MKK, WB (+2·6)

U, *V*, *W*: The vectors of the space motion directed, respectively, away from the galactic centre in the direction of galactic rotation and toward the north galactic pole. The trigonometric parallaxes together with the proper motions and radial velocities in Table I were used in computing these motions.

The colours and absolute visual magnitudes from the trigonometric parallaxes are plotted in Fig. 1 where stars with (1) $\pi \geqslant 0''·05$ are indicated by filled circles (2) $\pi < 0''·05$ as determined at more than 2 observatories are indicated by open circles and (3) $\pi < 0''·05$ from observations at only two observatories are indicated by crosses. The standard main sequence shown in the figure is that of the Hyades cluster (Sandage and Eggen 1959).

Also shown in Fig. 1 are the subgiant sequences of a globular cluster (M13), two high velocity groups (γ Leonis and 61 Cygni) and one galactic cluster (M67). The only available photometric results for M67 are those of Johnson and Sandage (1955). From photoelectric (*U*, *B*, *V*)-photometry of about 50 stars in the cluster Johnson and Sandage found an ultra-violet excess which they interpreted as due

TABLE II

Stars in Table I with trigonometric parallaxes at least as large as 0".02 from determinations at 2 or more observatories

HD	π_t	n	$B-V$	M_V	$M_V(W)$	U	V	W
			m	m	m			
3546	31	4	+0·88	+1·8	+2·6	− 78	− 59	+ 15
5395	40	3	+1·03	+2·6	+2·8	− 36	− 33	− 3
8512	34	4	+1·00	+1·2	+2·1	− 18	− 15	− 28
11937	52	2	+0·85	+2·1	...	+ 64	− 18	+ 11
16141	33	2	+0·66	+4·4	+4·1	− 78	− 36	+ 9
18907	35	2	+0·79	+3·6	...	− 6	− 76	− 20
23249	109	4	+0·92	+3·7	+4·6	+ 13	+ 28	+ 13
23817	42	2	+1·16	+1·9	...	+ 18	− 57	− 16
37160	24	4	+0·95	+1·0	+2·5	+ 75	− 84	− 33
39364	22	3	+1·00	+0·4	+3·1	− 36	−118	−129
40409	40	2	+1·07	+2·6	...	− 49	+ 23	+ 28
45410	23	2	+0·94	+2·7	+2·5	+ 66	− 40	− 11
47205	52	2	+1·00	+2·4	+0·7	− 6	− 7	− 2
50806	35	2	+0·72	+3·7	+4·5	− 22	− 97	− 6
62644	50	2	+0·77	+3·6	...	− 39	− 26	− 35
67767	29	2	+0·7:	+3·2	+4·2	− 37	− 41	− 45
94132	24	2	+0·8:	+3·0	+4·4	+ 75	− 22	− 22
96436	33	3	+0·7:	+3·3	+2·6	+ 8	− 38	+ 27
108309	36	3	+0·67	+4·0	...	+ 59	− 70	− 11
111028	21	4	+0·99	+2·3	+2·4	−101	− 68	+ 18
114174	42	2	+0·66	+5·0	+4·2	− 54	− 64	− 10
115202	41	2	+1·0:	+3·2	+2·1	− 49	− 8	+ 9
117176	41	2	+0·71	+3·1	+4·4	− 17	− 74	− 8
138716	24	3	+1·01	+1·5	+2·1	− 83	0	− 35
142091	36	2	+1·03	+2·4	+2·0	− 31	− 39	− 18
144087	39	3	+0·74	+5·5	+4·3	+ 32	− 9	− 13
145148	26	5	+1·02	+3·1	+5·6	− 86	− 70	− 88
151090	27	3	+0·7:	+3·9	+4·5	− 12	− 62	+ 6
*158614	50	6	+0·72	+4·5	+4·8	+ 62	− 47	− 19
161797	117	2	+0·75	+3·6	+4·2	− 16	− 32	− 5
167042	20	2	+0·94	+2·4	+2·2	+ 62	− 3	− 22
168723	54	4	+0·94	+1·9	+1·4	− 42	− 67	+ 15
170829	28	2	+0·8:	+3·8	+3·9	+ 4	− 66	− 32
175518	31	3	+0·75	+4·9	+5·3	+ 35	− 98	+ 8
177565	66	2	+0·70	+5·2	...	− 55	− 29	− 17
181391	27	2	+0·9:	+2·3	+2·3	+ 25	+ 5	− 12
182572	59	3	+0·79	+4·0	+4·5	+124	− 28	− 21
183877	24	2	+0·68	+4·0	+4·7	+ 36	−142	− 46
188512	67	5	+0·86	+2·8	+4·0	− 2	− 31	+ 2
190248	170	2	+0·76	+4·8	...	+ 48	− 13	− 13
190360	46	2	+0·72	+4·0	+4·6	+ 13	− 47	− 89
191026	32	4	+0·85	+2·9	+4·5	− 98	− 34	− 2
194433	33	2	+0·98	+3·9	+2·5	− 26	− 18	+ 10
196755	22	4	+0·74	+1·7	+3·8	+ 63	− 38	− 4
198149	71	4	+0·91	+2·7	+2·6	+ 34	− 97	+ 12
199190	30	2	+0·61	+4·3	...	+ 85	− 19	− 19
212943	21	3	+1·05	+1·4	+2·3	− 32	− 16	− 82
215549	25	4	+0·92	+3·4	+4·8	− 76	− 10	− 31
219834	33	2	+0·7:	+2·8	+3·6	+ 45	0	− 10
222107	43	3	+1·02	+2·0	+2·3	− 7	− 49	− 9
222404	64	4	+1·03	+2·2	+2·1	− 22	− 38	+ 1

*158614 Luminosity corrected for equal components before plotting in Fig. 1.

to a reddening of $E_{B-V}=+0^{m}\cdot06$. After correcting for this reddening, they fitted the main sequence of M67 to that of nearby stars and found a corrected modulus of $V_E-M=9^{m}.5$. From a more refined analysis of the data, Sandage (1957) later altered the modulus to $9^{m}\cdot2$.

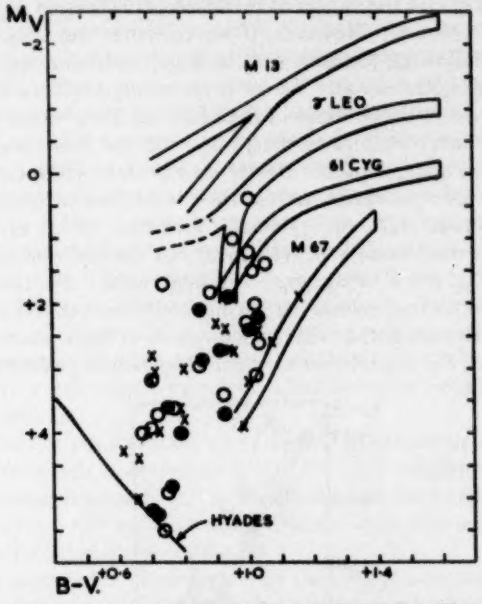

FIG. 1.—*The $(M_V, B-V)$-diagram for the stars in Table II. The subgiant sequences of the disk-population groups, γ Leo and 61 Cyg, and cluster M67 and the halo population globular cluster M13, are shown schematically.*

The unevolved main sequence of M67 begins at apparent magnitude $V_E\approx14^{m}$. Photoelectric observations are available for the following 11 cluster members fainter than $V_E=14^{m}$ (Johnson and Sandage 1955, Table I):

Star	V_E	$(B-V_{obs})$	$(B-V)^1$	Mod(1)	$(B-V)^2$	Mod(2)
	m	m	m	m		
a	14·95	+0·69	+0·75	9·35	+0·63	10·03
149a	14·91	0·78	0·84	8·86	0·72	9·48
i	15·23	0·84	0·90	8·89	0·78	9·48
m	14·83	0·69	0·75	9·23	0·63	9·91
s	16·19	0·66	0·72	(10·76)	0·60	(11·41)
t	14·05	0·64	0·70	8·73	0·58	9·39
v	15·78	0·84	0·90	9·44	0·78	10·03
w	15·64	0·89	0·95	9·06	0·83	9·64
aa	16·05	1·07	1·13	8·68	1·01	9·25
132a	15·83	1·08	1·14	8·35	1·02	8·94
149b	14·76	+0·48	+0·54	(10·28)	+0·42	(11·20)
				$9\cdot0\pm0^{m}\cdot3$ (AD)		$9\cdot6\pm0\cdot3$ (AD)

The photoelectric (U, B, V)-photometry of 34 cluster stars with $(B-V)_{obs}>+0^{m}\cdot4$ indicates a mean ultra-violet excess of $\delta(U-B)=+0^{m}\cdot06$ from the standard $(U-B, B-V)$-relation for the Hyades main sequence stars

(Sandage and Eggen 1959). The $\Delta(B-V)=F[\delta(U-B)]$ relation previously derived then indicates that if the excess is due to line-blanketing, the observed values of $B-V$ must be corrected by $+0{\cdot}06$ before the main sequence stars can be fitted to the Hyades main sequence. The values of $(B-V)^1$ listed above result from this correction and the values of modulus (1) represent V_B-M_V (Hyades) for the corrected colours. However, if we interpret the observed excess as a reddening effect, following Johnson and Sandage, we obtain the corrected values of $(B-V)^2$ and of modulus (2). There is no strong evidence to support either of these two extreme interpretations of the observed ultra-violet excess. Two or three early-type cluster stars have been observed but these are either (1) field stars, (2) unevolved main-sequence cluster members, in which case their presence is unexplained by current theory unless they were formed much later than the majority of the cluster stars, or (3) cluster members which originated as F–G dwarfs and whose evolutionary development has carried them to their present position in the $(M_V, B-V)$-diagram. Although either alternative (2) or (3) is probably the true situation, neither carries any confidence that the colours of these stars can be directly compared with unevolved A–B stars, even if we knew the appropriate $(U-B, B-V)$-relation to which they should be referred.

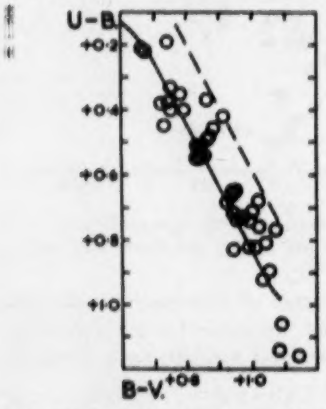

FIG. 2.—*The $(U-B, B-V)$-relation for the few stars in Table I with available (U, B, V)-photometry. The full curve represents the standard relation (Hyades) and the broken line that for M13.*

The sub-giant sequence of M67, obtained from modulus (1) is indicated in Fig. 1 together with the subgiant sequence for the high velocity groups γ Leonis (Eggen 1959a, d) and 61 Cygni (Eggen 1959b) and the globular cluster M13 (Eggen and Sandage 1959). If we used modulus (2) for M67 the tip of the subgiant sequence in Fig. 1 would join the 61 Cygni sequence. It should be emphasized that all the subgiant sequences shown in Fig. 1 are highly schematic.

The $(U-B, B-V)$-diagram for the stars in Table I for which three-colour photoelectric observations are available is shown in Fig. 2 where the standard relation for the Hyades (Sandage and Eggen 1959) is shown as the continuous curve and that for M13 and the very high velocity group, Groombridge 1830, as a broken line. If we accept the interpretation that the observed excesses of stars are caused by line-blanketing and if the stars in Fig. 2 are representative of those in Table I, then the subgiants represent (1) a few stars with ultra-violet deficiency

and therefore stronger metal lines than the Hyades standards, (2) a large number (more than 50 per cent of the total) with an observed excess between 0 and $0^m.1$, similar to the excesses observed in the γ Leonis and 61 Cygni groups and in M67, and (3) a few stars with excesses as large ($\sim +0.2$) as those observed in some globular clusters. Because the number of stars with available (U, B, V)-photometry is small, and because there exists the possibility of contamination by unknown companions, it can not now be determined whether there is a continuous variation from $\delta(U-B)=0$ to the observed extreme of $+0^m.25$. That is to say, if we adopt the nomenclature proposed by the Vatican conference on stellar populations (O'Connell 1958), it can not now be decided whether or not the subgiants in the solar neighbourhood represent a continuum from "disk"-population stars with high or moderately high metal abundances, represented by M67 and the high-velocity groups, to "halo"-population stars with very low metal abundances, represented by globular clusters such as M13 and the very high velocity groups (Groombridge 1830). This is a question of some importance that might be answerable when (U, B, V)-photometry is available for more of the stars in Table I. However, because of the very high dwarf/subgiant ratio in globular clusters and the relatively few globular cluster dwarfs in the vicinity of the Sun (Eggen and Sandage 1959) we would expect very few globular cluster (halo) subgiants among the objects in Table I.

The lower limit to the luminosities of the subgiants seems to be well defined in Fig. 1 and corresponds to the luminosity of the M67 subgiants if modulus (1) is correct. This lower boundary to the luminosity of the subgiants indicates an upper limit of $\sim 1.5 \times 10^{10}$ years as the age of the disk-population near the Sun, using Hoyle's (1959) dating procedure.

The marked variation in slope shown by the subgiant sequences illustrated in Fig. 1 seems to be unrelated to the ultra-violet excesses which range from $+0^m.25$ for M13 through $+0^m.04$ for γ Leonis, $+0^m.07$ for 61 Cygni group and -0.02 for the very similar ζ Hercules group, (Section 4, Table III) to 0 or $+0^m.06$, depending upon the amount of reddening, for M67. At present no group of disk-population stars with a mean ultra-violet excess between $0^m.1$ and $0^m.2$ is known.

4. *Motion.*—The components of the space motions listed in Table II are plotted in Figs. 3 (U, V) and 4 (V, W). The ellipse shown in Fig. 3 is that found previously (Eggen 1959c) to contain all the known Ap and Am stars brighter than $V_B = 6^m$ and probably represents the (U, V)-limits for the "older population I" stars (O'Connell 1958). The lack of subgiants falling within this ellipse in Fig. 3 is at least partly caused by observational selection because parallax programmes mainly contain stars with appreciable proper motion. Space motions have also been computed for an additional 63 stars not in Table II but for which values of $M_v(W)$ determined at Mt Wilson (Adams *et al.* 1935) are available. Six, or ten per cent, of these stars have values of (U, V) that fall within the ellipse drawn in Fig. 3. The (1) median and (2) mean values of U, V and W for the 51 stars in Table II plus the 63 additional stars for which values of $M_v(W)$ determined at Mt Wilson are available, together with the (3) median and (4) mean values previously found for the Ap and Am stars are as follows:

	U	V	W
(1)	+8	−28	−8 km/sec
(2)	+9·3	−33·9	−9·4 "
(3)	+7	− 6	−8 "
(4)	+7·8	− 7·7	−7·3 "

The median and mean values for the subgiants give the same apex for the solar motion ($\alpha = 19^h$, $\delta = +44°$) but the total solar motion from the median values is 30 whereas the mean values give 36 km/sec. The average motions of the subgiants, which are largely a disk population, differ from that of the older population I stars only in the value of V. This merely means that the disk-population contains stars whose galactic orbits have a larger range in semi-major axes (a) than the stars contained in the older population I, but both populations have the same upper limit, near $a = 1{\cdot}1\ R_\odot$, where $R_\odot$ is the Sun's distance from the galactic centre.

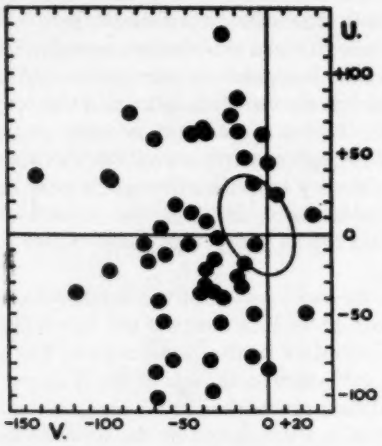

FIG. 3.—*The (U, V)-vectors for stars in Table II. The ellipse encloses the (U, V)-vectors of all the known Ap and Am stars (older population I) brighter than* $V_B = 6^m$.

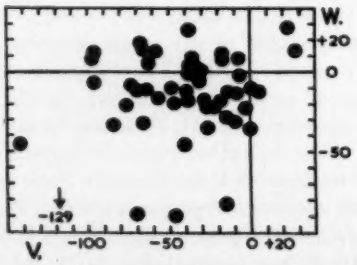

FIG. 4.—*The (V, W)-vectors for the stars in Fig. 3.*

Several groups of high velocity stars, which contain some of the subgiants in Table I, have previously been discussed. The largest are the 61 Cygni group (Eggen 1959b) the γ Leonis group (Eggen 1959a, d) and the ζ Herculis group (Eggen 1958). The stars now considered to be probable members of the later group are listed in Table III and the motions of the stars are in Table IV. The subgiant sequence of the ζ Herculis group is nearly identical to that of the 61 Cygni group in Fig. 1.

There are undoubtedly additional groups among the stars in Table I. However, if the very large ratio of dwarfs to subgiants that is observed in M67 also holds in the groups, it is more profitable to search for moving groups among the dwarfs, and observational programmes are now being carried out to increase the material available for such a search. An example of a possible group of subgiants in Table I which, if the dwarf/subgiant ratio is as high as that in M67, should contain very many dwarfs, is the following:

HD		M_V	U	V	W	Remarks
	"	m				
23817	0·034	+1·48	+22	−62	−11	β Ret; π_t=32Y(16), 67C(7)
26766	0·015	+3·2:	+20	−63	−12	π_t=12A(20)
52711	0·0645	+5·05	+17	−64	− 6	π_t=56A(16), 61M(7)
121146	0·016	+2·3:	+17	−67	−11	π_t=22G(8)
159809	0·012	+2·84	+16	−68	− 9	

TABLE III

Probable members of the ζ Herculis group

HD	Name	V_B	$B-V$	$U-B$	$\delta(U-B)$	Sp.	π_g	M_V
		m	m	m	m		"	m
2151	β Hyi	2·77	+0·61	...	...	G2 IV	0·1485	+3·63
4075	+75° 36	7·4:	+0·7:	...	...	dG4	0·0255	+4·4:
9166	+67° 133	6·76	+1·23	+1·39	...	K3 III	0·0095	+1·14
19058	ρ Per	3·5 var	+1·70	...	...	M4 II–III	0·0115	−1·3 var
25728	ι Ret	4·92	+1·45	...	...	gK5	0·010	−0·08
43899	HR 2263	5·4:	+1·1:	...	...	gKo	0·0145	+1·2:
68788	+73° 407	8·38	+0·84	+0·53	−0·01	K1 V	0·0355	+6·13
70523	−17° 2464	5·77	+1·05	+0·89	−0·05	K1 III	0·0105	+0·82
71377	−12° 2524	5·54	+1·19	+1·14	...	K2 III	0·009	+0·31
83425	+5° 2207	4·66	+1·30	+1·46	...	K3 III	0·0125	+0·14
89668	−0° 2726	9·41	+1·09	+1·00	−0·02	K3 V	0·0455	+7·70
90250	29L Mi	6·49	+1·09	+0·99	−0·01	K1 III	0·0085	+1·14
98824	71 Leo	7·04	+1·05	+0·96	−0·02	K1 III	0·0075	+1·42
100733	HR 4463	5·7 var	+1·66	...	...	M3 III	0·0055	−0·56
119425	84 Vir	5·37	+1·10	+1·05	−0·06	K1 III–IV	0·0215	+2·03
129245	+80° 448	6·26	+1·30	+1·46	...	K3 III	0·009	+1·03
136422	ϕ Lup	3·59	+1·55	...	...	gMo	0·009	−1·71
*150680	ζ Her	2·82	+0·64	+0·21	−0·03	Go IV	0·103	+2·89
166207	+50° 2525	6·1:	+1·0:	...	...	Ko IV	0·010	+1·1:
210967	ϵ Oct	4·8 var	+1·6:			M6	0·0055	−1·5 var
217166	+8° 4973	6·64	+0·65	...	...	dG1	0·027	+4·55
*219829	+4° 4994	8·03	+0·80	+0·43	0·00	Ko V	0·0305	+5·44
221354	+56° 2605	6·75	+0·83	+0·50	0·00	Ko V	0·068	+5·91
				mean=	−0·02			

*150680 ADS 10157
219829 ADS 16645, $\Delta m = 1^m$, $P = 108$ yrs.

The individual values of the absolute trigonometric parallax listed under "Remarks" are in units of 0".001 and are followed by the observatory abbreviation and, in parenthesis, the weight. If these stars belong to a moving group they are among the faintest, and therefore oldest, subgiants known since they indicate a subgiant sequence similar to that obtained for M67 from modulus (1) in Section 3

TABLE IV

Motions of the probable members of the ζ Herculis group

HD	ρ	μ_α	μ_δ	S	U	V	W
	km/sec	″	″			km/sec	
2151	+23·0 a	+2·228	+0·324	GC, N30	+55	−44	−28
4075	− 8·4 b	+0·380	−0·095	GC+	+59	−42	−20
9166	−13·9 b	+0·104	−0·052	GC+	+53	−48	−30
19058	+28·2 b	+0·131	−0·106	GC, N30	+57	−47	−16
25728	+60·5 a	+0·067	+0·092	GC, N30	+51	−52	−30
43899	+70 d	−0·007	+0·085	GC, CP	+54	−50	−20
68788	− 3·4 b	−0·300	−0·483	GC+	+56	−50	−22
70523	+67·7 b	−0·100	−0·010	GC, Y	+56	−53	−25
71377	+65 c	−0·085	−0·024	GC, Y	+54	−53	−25
83425	+45·2 a	−0·164	−0·056	GC, N30	+60	−48	−20
89668	+35 c	−0·655	−0·165	Y, CR, Ci	+59	−49	−18
90250	+11·4 b	−0·110	−0·071	GC	+50	−50	−21
98824	+ 5·3 b	−0·120	−0·020	GC+	+59	−43	−20
100733	+18·4 b	−0·087	−0·015	GC, CP	+54	−54	−16
119425	−42·4 b	−0·293	−0·077	GC	+59	−44	−28
129245	−22·6 b	−0·100	+0·095	GC+	+59	−41	−25
136422	−29·4 a	−0·093	−0·086	GC, N30	+53	−48	−18
150680	−69·9 a	−0·471	+0·390	GC, N30	+54	−47	−24
166207	−57·1 b	−0·006	+0·100	GC, N30	+56	−44	−17
210967	+11·7 a	+0·073	−0·040	GC, N30	+56	−47	−19
217166	−26·5 b	+0·392	−0·142	GC+	+50	−54	−23
219829	−14·3 b	+0·466	−0·108	GC+	+57	−47	−21
221354	−25·1 b	+1·095	+0·111	GC	+59	−51	−12

and shown in Fig. 1. Also, it is of interest to note that the short period ($0^d·06$) variable CY Aqr may also be a member:

CY Aqr; $\mu_\alpha = 0''·059$, $\mu_\delta = -0''·065$, $\rho = -32$ km/sec.

π	M_V	U	V	W
″	m			
0·005	4·5	+26	−81	−30 km/sec
0·006	4·8	+24	−71	−21 ,,
0·007	5·1	+21	−64	−14 ,,
0·008	5·4	+20	−54	− 9 ,,

There is no direct determination of the distance of CY Aqr but the value $M_V \approx 5^m$ derived from the assumption that it shares the space motion of β Ret is about a magnitude fainter than that derived from the trigonometric parallaxes of two similar stars, SX Phe ($0^d·06$) and AI Vel ($0^d·11$), for which $M_V \approx +4^m$.

5. *Masses.*—The incidence of binaries among the stars in Table I is not high. Only 5 per cent of the stars are known spectroscopic binaries and an additional 10 per cent have known visual, mostly widely separated, companions. Orbits have been published for only two of the visual binaries, ADS 755 (36 And) and 10598 (HD 158614). Preliminary orbits have now been computed for an additional three stars, 95 Cet (ADS 2459), HD 87783 (SDS), and HD 194433 (SDS). The five binaries are discussed below.

(i) 36 And (ADS 755). The period is 166·5 years (Baize 1946) and the semi-major axis, adjusted to the "standard observers" (Eggen 1956) is $a = 0''·965$. The magnitudes are nearly equal with the mean component having $V_E = 6·2$, $B-V = +1^m·03$. The spectral type is sgK1. The system was discussed

previously (Eggen 1957) when it was shown that the parallax is probably in the following range:

	$M_V(\overline{AB})$	$m(\overline{AB})$
"	m	
0·020	+2·7	2·0 ⊙
0·023	+3·0	1·3
0·025	+3·2	1·0

where $\overline{AB}$ indicates the mean component. There is no trigonometric parallax available but the spectroscopic absolute magnitude is $M_V = +2^m{\cdot}3$ (Adams *et al.* 1935). Wilson and Bappu (1957) found $M_V = +4^m{\cdot}0$ from the widths of the emission H- and K-lines; this value would give $\pi = 0''{\cdot}036$ and the improbably low mean mass of 0·35 ⊙. The most likely values are $\pi = 0{\cdot}023$ and $m(\overline{AB}) = 1{\cdot}3$ ⊙.

(ii) 95 Cet (ADS 2459). I have derived the following preliminary orbit:

$P = 200$ yrs.	$A = +0''{\cdot}393$
$a = 1''{\cdot}030$	$B = +0{\cdot}410$
$e = 0{\cdot}48$	$F = +0{\cdot}162$
$T = 1841.1$	$G = +0{\cdot}887$

The comparison with the more reliable observations is as follows:

t	PA	Sep	n	Obs		O−C
1854.81	73°	0"·70 ±	2	Da	0°	+0"·03 ±
1888.77	118	0·45	2	β	0	+0·02
1898.15	137	0·51	2	A	−4	+0·14
1899.81	157	0·35	2	See	+5	−0·04
1900.78	155 ±	...	1	A	0 ±	...
1907.14	172	0·40	4	A	−4	+0·02
1916.78	198	0·50	4	A, VB	−4	+0·01
1921.69	211	0·52	2	A	+3	−0·05
1929.79	218	0·72	7	B	+1	+0·04
1935.34	220	0·76	9	V, B	−2	−0·01
1942.15	224	0·80	7	B, VB	−3	−0·06
1948.99	233	0·92	4	B	+4	+0·01
1956.11	236	0·96	4	Bz	+2	−0·07
1957.73	237	1·08	3	B	+2	+0·04

The total magnitude and colour are $V_B = 5^m{\cdot}37$, $B-V = +1^m{\cdot}04$ and the spectral type is K1 IV. The components differ visually by $2^m{\cdot}0$. Values of the absolute magnitudes of the individual components, the total mass of the system, Σm, and the mass of the secondary component computed from the mass-luminosity relation (Eggen 1956) on the assumption that it is a main sequence star, $m(B)_e$, are listed for four values of the parallax; the difference $\Sigma m - m(B)_e$ is taken to be the mass of the subgiant, $m(A)$.

	$M_V(A)$	$M_V(B)$	Σm	$m(B)_e$	$m(A)$
"	m	m			
0·015	1·3	3·3	8·1 ⊙	1·6 ⊙	6·5 ⊙
0·018	1·7	3·7	4·7	1·4	3·3
0·020	1·9	3·9	3·4	1·3	2·1
0·022	2·1	4·1	2·6	1·2	1·4

If the subgiant has a mass of 1·4 ⊙, the second component is ~ F6 and the parallax is 0"·022; these seem to be the most probable values. The trigonometric parallax determinations, in units of 0"·001, are 16A(20), 2M(10) and −17Y(10).

(iii) HD 87783 (SDS). The following preliminary orbit has been computed by D. Jones (1959):

$P = 232$ years	$A = -0''.607$
$a = 0''.64$	$B = -0.211$
$e = 0.72$	$F = 0.165$
$T = 1932.8$	$G = -0.495$

The comparison with the observations is as follows:

t	PA	Sep	n Obs	O − C	
	°	″		°	″
1897.10	45 ±	0.6 ±	1 I	− 9 ±	0.0 ±
1901.70	57	0.53	1 I	− 1	−0.05
11.27	70	0.5 ±	1 I	0	+0.1 ±
14.24	100 ±	...	1 I	+21 ±	...
26.40	144	0.20	1 B	+ 3	−0.02
30.34	282 ?	0.15 ?	3 B	112 ?	−0.03 ?
30.43	153	0.14	2 φ	−18	−0.04
35.97	227	0.14	4 V	− 1	−0.06
45.29	298	0.30	1 B	+ 3	0.00
47.33	305	0.30	2 B	0	−0.03
48.54	317	0.31	4 B	+ 7	−0.04
51.30	312	0.41	2 B	− 7	+0.02
56.25	330	0.47	1 B	+ 1	+0.01

The total magnitude and colour are $V_E = 5^m.07$, $B - V = +0^m.88$ and the spectral type is Ko IV. The components differ visually by $1^m.5$. Three assumed values of the parallax give the following results:

	$M_V(A)$	$M_V(B)$	Σm	$m(B)_c$	$m(A)$
″	m	m			
0.010	0.3	1.8	4.9 ⊙	2.5 ⊙	2.4 ⊙
0.011	0.5	2.0	3.7	2.4	1.3
0.012	0.7	2.2	2.8	2.2	0.4

If the preliminary elements are nearly correct, the parallax is almost certainly in the range shown above and the luminosity of the bright component is rather high for a subgiant. It is possible that the parallax is $0''.012$ and both components are subgiants with equal mass, $1.4\odot$.

(iv) HD 158614 (ADS 10598). The period is 46.1 years (Ashbrook and Duncombe 1951) and the semi-major axis, adjusted to the standard observers, is $a = 0''.92$. The mean magnitude and colour of the nearly equal components are $V_E = 6^m.0$, $B - V = +0^m.72$. The absolute magnitudes and masses of the mean component for three values of the parallax are as follows:

	$M_V(\overline{AB})$	$m(AB)$	$m(\overline{AB})_c$
″	m		
0.050	+4.5	1.4 ⊙	1.1 ⊙
0.055	+4.7	1.1	1.0
0.060	+4.9	0.85	0.95

where $m(\overline{AB})_c$ is computed from the mass-luminosity relation for main sequence stars. The trigonometric parallax determinations are 55A(20), 31M(8), 58Y(10), 67Yk(4), 49S(7), 39C(8), mean = 50. The stars are probably only $\sim 0^m.5$ above the main sequence with $\pi \approx 0''.05$.

(v) HD 194433 (SDS). The following orbital elements have been derived by D. Jones (1959); we are indebted to W. H. van den Bos for the 1959 observations:

$P=135$ years	$A=+0''.214$
$a=0''.79$	$B=-0.665$
$e=0.59$	$F=-0.750$
$T=1949.8$	$G=-0.125$

The comparison with the observations is as follows:

t	PA	Sep	n	Obs	O−C	
	°	"			°	"
1880.86	97	1.07	1	R	−12	−0.03
90.73	96	1.08	1	Slr	− 4	0.00
96.67	100	0.78	3	See	+ 6	−0.23
98.68	93	1.44	1	Slr	+ 2	+0.31
1902.53	83	1.31	2	I	− 3	+0.35
13.62	71	0.93	2	I	− 2	+0.04
16.69	71	1.02	2	V	+ 2	0.17
25.53	54	1.00	8	V	+ 2	+0.26
27.22	50	0.66	2	B	− 1	−0.05
28.68	43	0.72	2	ϕ	− 3	+0.04
29.42	44	0.71	4	B	0	+0.04
30.62	40	0.66	8	B	− 1	+0.01
33.70	32	0.67	4	B	0	+0.06
33.88	33	0.61	8	V	+ 1	0.00
36.40	23	0.50	5	ϕ	− 1	−0.05
36.69	23	0.50	4	B	0	−0.04
41.07	3	0.42	3	B	0	−0.05
42.36	358	0.44	3	V	+ 3	0.00
43.48	338	0.37	4	V	−12	−0.05
44.75	340	0.34	2	B	0	−0.05
45.46	330	0.36	3	V	− 5	+0.03
45.75	330	0.38	2	B	+ 1	+0.04
47.70	317	0.34	2	B	+ 3	+0.02
49.79	292	0.28	4	B	+ 3	−0.01
52.70	245	0.25	1	B	− 2	−0.05
59.57	188	0.52	7	B	− 3	+0.02

The total magnitude and colour are $V_E=6^m.23$, $B-V=+0^m.98$ and the spectral type is sg K1, Mt Wilson or K1 IV–V, Cape. The components differ visually by $1^m.17$. Four assumed values of the parallax give the following results:

	$M_V(A)$	$M_V(B)$	Σm	$m(B)_e$	$m(A)$
"	m	m			
0.020	+3.1	+4.2	3.7 ⊙	1.2 ⊙	2.2 ⊙
0.021	+3.2	+4.3	2.9	1.2	1.7
0.022	+3.3	+4.4	2.5	1.1	1.4
0.023	+3.4	+4.5	2.2	1.1	1.1

If the orbital elements are correct the mass of the brighter component can be quite accurately determined. If $M_V(A)\leqslant+3^m.2$ the derived mass is greater than that of a main sequence star of the same luminosity. Although this result depends on the assumption that the fainter star is a main sequence object, the fact that the magnitude difference between the components is $1^m.2$ makes the assumption almost certainly true. On the other hand, if the luminosity of the subgiant is as faint as $M_V(A)=+3.6$ the mass is rather lower than expected for an evolved main sequence star. We will adopt $\pi=0.023$, $m(A)=1.1\odot$. The

trigonometric parallax determinations are 25C(10) and 43Y(8). This important system deserves further study since it may contain the oldest stars for which a mass is now obtainable.

It seems well established from the binaries discussed above as well as from a few others outside the range of luminosity and spectral type discussed here (ζ Her, γ Leo) that the masses of the late-type subgiants are in the range 1 to 1·5 ⊙.

In addition to the 5 pairs discussed above there are only two others in Table I that may offer an opportunity for a mass determination in the near future. These stars are the following:

HD 90572 (ADS 7779)

t	PA	Sep	n	Obs
	°	″		
1843.28	58	0·82	2	Ma
55.12	63	1·21	6	OΣ
70.13	66	1·06	7	Da
98.67	71	1·15	5	Hu
1909.30	75	1·07	9	...
16.60	80	0·78	14	...
24.52	82	0·72	6	...
43.24	91	0·91	3	V
54.27	100	0·73	3	Cou

HD 97561 (ADS 8094)

t	PA	Sep	n	Obs
	°	″		
1829.70	288	1·05	5	OΣ
45.32	287	0·87	2	OΣ
75.39	284	0·68	3	Sp
88.30	277	0·54	8	..
95.00	276	0·42	7	Com
1903.60	275	0·40	5	...
08.31	266	0·39	19	...
13.34	262	0·35	26	...
22.00	254	0·34	11	...
24.10	249	0·25	10	...
32.26	241	0·22	9	VB
43.12	203	0·21	12	VB
49.65	189	0·22	5	VB

Royal Greenwich Observatory,
Herstmonceux Castle,
Hailsham, Sussex:
1959 *September.*

References

Adams, W. S., Joy, A. H., Humason, M. L., and Brayton, A. M., 1935, *Ap. J.*, **81**, 187.
Ashbrook, J., and Duncombe, R. L., 1951, *A.J.*, **56**, 57.
Baize, P., 1946, *A.J.*, **51**, 221.
Boulon, J., Duflot, M., and Fehrenbach, C., 1959, *J.O.*, **42**, 1.
Eggen, O. J., 1956, *A.J.*, **61**, 361.
—— 1957, *A.J.*, **62**, 45.
—— 1958, *M.N.*, **118**, 165. *Note.*—Most of the data listed in this reference for HD 119425 is nonsense and the star should be removed from the list of group members.
—— 1959 a, *Obs.*, **79**, 88. *Note.*—Some of the data listed in this reference for HD 31782 is erroneous and the star should be dropped as a member of the group.
—— 1959 b, *Obs.*, **79**, 135.
—— 1959 c, *Obs.*, **79**, 197.
—— 1959 d, *Obs.*, **79**, 182.
Eggen, O. J., and Sandage, A. R., 1959, *M.N.*, **119**, 255.
Evans, D. S., Menzies, A., and Stoy, R. H., 1957, *M.N.*, **117**, 534.
—— —— —— 1959, *M.N.*, **119**, 638.
Halliday, I., 1955, *Ap. J.*, **122**, 222.
Heard, J. F., 1956, *Pub. David Dunlap Obs.*, **II**, No. 4.
Hoyle, F., 1959, *M.N.*, **119**, 124.
Johnson, H. L., and Morgan, W. W., 1953, *Ap. J.*, **118**, 513.
Johnson, H. L., and Sandage, A. R., 1955, *Ap. J.*, **121**, 616.
Jones, D., 1959, private communication.

Keenan, P. C., and Keller, J., 1953, *Ap. J.*, **117**, 241.
Morgan, W. W., 1938, *Ap. J.*, **87**, 460.
Moore, J. H., and Paddock, G. F., 1950, *Ap. J.*, **112**, 48.
O'Connell, D. J. K., 1958, *Ricerche Astron. Specola Vaticana*, **5**.
Roman, N. G., 1955, *Ap. J. Sup.*, **II**, No. 18.
Sandage, A. R., 1957, *Ap. J.*, **125**, 422.
Sandage, A. R., and Eggen, O. J., 1959, *M.N.*, **119**, 278.
Stromberg, G., 1930, *Ap. J.*, **71**, 175.
Wilson, O. C., and Vainu Bappu, M. K., 1957, *Ap. J.*, **124**, 661.
Wilson, R. E., 1953, *Papers of the Mt Wilson Obs.*, **VIII**.
Woods, M. L., 1955, *Memoirs Commonwealtn Obs.*, No. 12.
Young, R. K., and Harper, W. E., 1924, *Pub. Dom. Astroph. Obs.*, **3**, No. 1.

STELLAR GROUPS, VI.
SPACE MOTIONS OF THE DWARF A-TYPE AND GIANT M-TYPE STARS IN THE SOLAR NEIGHBOURHOOD

Olin J. Eggen

(Communicated by the Astronomer Royal)

(Received 1959 October 9)

Summary

The A-type dwarfs and M-type giants fall in restricted regions of the $(M_V, B-V)$-diagram permitting the derivation of homogeneously accurate parallaxes and, therefore, space motions for objects in these two classes that are brighter than visual magnitude 5 and for which accurate radial velocities are available. The space motion vectors, (U, V), of the A-type stars, which are a pure sample of the older population I, are not randomly distributed and indicate the possibility that the majority of this population may exist in isoperiodic groups similar to the Hyades and Sirius groups. The restricted region of the (U, V)-plane defined by the A-type dwarfs is used to isolate the disk population among the M-type giants. The M-type giants are almost equally divided between disk population and older population I stars.

---

1. *A-type dwarfs.*—In a discussion of the luminosities of the stars brighter than visual magnitude 5 (Eggen 1957) the following two features of the distribution of the A-type stars in the $(M_V, B-V)$-diagram were noted:

(*a*) The so-called peculiar (Ap) and metallic-line (Am) stars in galactic clusters or with well-determined trigonometric parallaxes lie in a well-defined region and their luminosities show an average deviation of about $0^m.1$ from the expression (Eggen 1959c)

$$M_V = 7.0(B-V) + 0^m.4. \qquad (1)$$

(*b*) The stars placed in luminosity class V of the MK-system occupy a region of the $(M_V, B-V)$-diagram bounded by the Ap and Am stars (eqn. (1)) and the Pleiades main sequence.

The Pleiades main sequence and equation (1) are represented in Fig. 1. Since the region in the $(M_V, B-V)$-diagram occupied by the Ap, Am and AV stars is quite restricted, relatively accurate luminosities, and therefore distances, of these stars can be obtained from the spectroscopic classification alone. This is important since these stars are defining members of what has been called "older population I" (Oort: see O'Connell 1958) and, at least for the brighter examples, the distance is all that is lacking of the data needed for computing space motions.

All the stars brighter than visual (HR) magnitude $5^m.0$ and which satisfy the following conditions are listed in Table I:

(i) Classified (MK) as Ap, Am or B9–F0V. The authorities for the Ap and Am classifications are listed by Bertaud (1959) and those for the dwarfs are mainly by Slettebak (1954, 1955), Johnson and Morgan (1953) and de Vaucouleurs (1957); one or two are by Woods (1955). In a few cases stars were omitted

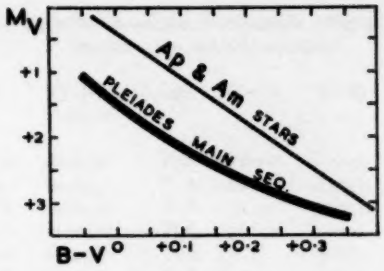

FIG. 1.—*Schematic representation of the Pleiades main sequence and equation* (1). *The luminosities of the A-type dwarfs are bracketed by these features.*

because of disagreement among the classifiers as to the luminosity class and there are undoubtedly one or two mis-classified stars, which therefore fall outside the region defined in Fig. 1, remaining in Table I.

(ii) Colours between $B-V=-0^{m}\cdot05$ and $+0^{m}\cdot35$. The main sources of the photometric data are Eggen (1955), Johnson and Morgan (1953), Hogg (1958), Stoy (1953), Johnson and Knuckles (1957), Naur (1955) and Osawa (1959). A few colours transformed from the values of C_2/T listed by Hertzsprung (1940), are identified by colons.

(iii) Proper motion listed in at least one of the fundamental catalogues given in the column labelled "S" as 1 = GC, 2 = N30 and 3 = FK3.

(iv) Radial velocity of quality "a" or "b" in the general catalogue (Wilson 1953). A few recent determinations have also been incorporated into the means.

TABLE I

A-type dwarfs brighter than visual magnitude $5^{m}\cdot0$ *for which accurate radial velocities are available*

HR	Name	V_E	$B-V$	$U-B$	Sp	ρ Q km/sec.	μ_α	μ_δ	S
63	θ And	4·60	+0·06	+0·02	A2V	+ 1·4b	−0·055	−0·017	12
68	σ And	4·53	+0·05	+0·06	A2V	− 8·0b	−0·067	−0·038	12
100	κ Phe	3·93	+0·18	...	A3V	+ 8·8b	+0·102	+0·030	1
269	μ And	3·88:	+0·12:	...	A5V	+ 7·6b	+0·151	+0·035	123
343	θ Cas	4·32	+0·17	+0·11	A7V	+ 9·4b	+0·228	−0·019	1
403	δ Cas	2·67	+0·14	+0·10	A5V	+ 6·7b	+0·297	−0·047	123
553	β Ari	2·65	+0·13	+0·10	A5V	− 1·9a	+0·100	−0·108	123
580	50 Cas	4·00:	+0·05:	...	A1V	−14·3b	−0·044	+0·027	123
620	58 And	4·70:	+0·12:	...	A5V	+ 7·6b	+0·157	−0·035	123
707	ι Cas	4·53	+0·13	...	Ap	+ 1·2b	−0·013	+0·016	12
804	σ Cet	3·47	+0·10	+0·06	A2V	− 5·1b	−0·141	−0·147	123
879	π Per	4·58:	0·00:	...	A0V	+14·2b	+0·031	−0·038	123
1046		5·06	+0·05	+0·04	A1V	+ 0·3b	−0·043	−0·007	1
1251	38 Tau	3·90	+0·05	...	A1V	− 5·7a	+0·003	−0·001	123
1329	ω Tau	4·75	+0·27	...	Am	+15·7a	−0·041	−0·059	1
1338	γ Dor	4·23	+0·34	...	F0V	+27·0b	+0·101	+0·189	123
1380	64 Tau	4·80	+0·16	+0·12	A7V	+37·5b	+0·114	−0·036	12
1387	κ Tau	4·22	+0·13	+0·12	A7V	+40·1b	+0·099	−0·047	12
1427		4·78	+0·17	+0·13	A7V	+37·5a	+0·105	−0·028	12
1444	ρ Tau	4·66	+0·24	+0·09	F0V	+37·5b	+0·101	−0·025	123
1458	88 Tau	4·30	+0·18	...	Am	+29·0a	+0·056	−0·045	1

TABLE I—*continued*

A-type dwarfs brighter than visual magnitude 5^{m}.0 for which accurate radial velocities are available

HR	Name	V_E	$B-V$	$U-B$	Sp	ρ Q km/sec.	μ_α	μ_δ	S
1479	92 Tau	4·68	+0·16	+0·12	A5V	+36·9b	+0″·084	−0″·021	12
1567	7 Cam	4·47	−0·02	0·00	A1V	− 7·9a	−0·019	+0·006	1
1592	4 Aur	4·95:	+0·09:	...	AoV	+ 6·9a	+0·048	−0·104	12
1620	ι Tau	4·64	+0·14	+0·14	A7V	+42·2a	+0·063	−0·042	123
1621		4·91	−0·04	...	B9V	+24·2b	+0·035	−0·013	1
1762		4·70	−0·03	...	AoV	+29·6b	+0·006	+0·002	1
2085	η Lep	3·72	+0·32	0·00	FoV	− 1·6b	−0·041	+0·138	123
2238	2 Lyn	4·38:	0·00:	...	A2V	− 3·6a	−0·007	+0·022	123
2491	α CMa	−1·46	−0·01	−0·06	A1V	− 7·6a	−0·537	−1·210	123
2550	α Pic	3·28	+0·21	+0·03	A5V	+20·6b	−0·071	+0·265	123
2564	38 Gem	4·60:	+0·36:	...	FoV	+25·9b	+0·075	−0·084	12
2740		4·46	+0·33	...	FoV	− 0·8a	−0·137	+0·102	123
2763	λ Gem	3·57	+0·10	+0·09	A3V	− 9·2b	−0·045	−0·040	123
2852	ρ Gem	4·16	+0·31	−0·04	FoV	− 5·7b	+0·151	+0·171	123
2890/1	α Gem	1·8:	...	...	A1V, Am	+ 3·0a	−0·165	−0·110	1
3067	φ Gem	4·95	+0·10	+0·08	A3V	+ 8·0b	−0·036	−0·035	123
3314		3·89	−0·01	0·00	AoV	+10·0b	−0·068	−0·026	123
3449	γ Cnc	4·73	0·00	+0·03	A1V	+28·7b	−0·106	−0·044	123
3485	δ Vel	1·99	0·00	+0·02	AoV	+ 2·2b	+0·018	−0·080	12
3492	ρ Hya	4·38:	+0·02:	...	AoV	+32·8b	−0·019	−0·037	1
3569	ι UMa	3·12	+0·18	+0·06	A7V	+12·2a	−0·442	−0·240	123
3572	α Cnc	4·22	+0·18	...	Am	−13·8b	+0·034	−0·035	123
3619	15 UMa	4·46	+0·27	+0·11	Am	− 0·1a	−0·137	−0·040	13
3624	τ UMa	4·66	+0·35	+0·14	Am	− 9·0a	+0·100	−0·060	13
3662	18 UMa	4·82	+0·20	+0·09	A5V	−15·1b	+0·054	+0·057	123
3690	38 Lyn	3·82	+0·06	+0·05	A3V	+ 1·6b	−0·030	−0·130	13
3799	26 UMa	4·60:	+0·01:	...	A2V	+23·1b	−0·064	−0·042	12
3856		4·51	−0·05	...	B9V	+24·4b	−0·041	+0·014	1
3974	21 LMi	4·48	+0·17	+0·08	A7V	−17·8b	+0·054	−0·001	13
4090	30 LMi	4·74	+0·25	+0·17	FoV	+13·4a	−0·068	−0·069	1
4248	ω UMa	4·80:	+0·03:	...	A1V	−17·4a	+0·048	−0·029	123
4300	60 Leo	4·42	+0·07	+0·05	Am	−10·2b	−0·008	+0·033	13
4357	δ Leo	2·55	+0·13	+0·12	A4V	−20·6b	+0·144	−0·137	123
4359	θ Leo	3·41	+0·02	+0·02	A2V	+ 7·8a	−0·059	−0·083	123
4386	σ Leo	4·00:	−0·02	...	B9V	− 5·3b	−0·094	−0·015	123
4534	β Leo	2·18	+0·09	+0·05	A3V	− 0·1b	−0·496	−0·120	123
4554	γ UMa	2·44	0·00	+0·01	AoV	−12·9a	+0·094	+0·005	123
4660	δ UMa	3·30	+0·08	+0·07	A3V	−12·9b	+0·104	+0·003	123
4689	η Vir	3·92	+0·02	...	A2V	+ 2·3b	−0·063	−0·023	123
4825/6	γ Vir	2·75	+0·35	−0·04	FoV	−19·7a	−0·574	+0·006	123
4828	ρ Vir	4·95	+0·07	+0·04	AoV	+ 1·6b	+0·084	−0·093	123
4963	θ Vir	4·38	−0·01	...	A1V	− 2·9b	−0·035	−0·037	123
5028	ι Cen	2·68	+0·04	...	A2V	+ 0·1a	−0·337	−0·090	123
5062	80 UMa	4·01	+0·16	+0·08	A5V	− 7·5a	+0·119	−0·024	1
5105	78 Vir	4·94	+0·04	0·00	Ap	− 8·0a	+0·041	−0·030	12
5107	ζ Vir	3·37	+0·10	...	A3V	−13·2b	−0·286	+0·036	123
5359	λ Vir	4·55	+0·14	...	Am	−10·9b	−0·016	+0·025	12
5463	α Cir	3·20	+0·24	...	Ap	+ 7·4a	−0·190	−0·240	123
5511	109 Vir	3·74	0·00	−0·03	AoV	− 6·1b	−0·114	−0·032	123
5733	μ Boo	4·30	+0·30	+0·08	FoV	− 8·8a	−0·148	+0·083	123
5881	μ Ser	3·55	−0·05	...	AoV	− 9·4b	−0·088	−0·028	123

TABLE I—*continued*

A-type dwarfs brighter than visual magnitude 5^{m}·0 for which accurate radial velocities are available

HR	Name	V_E	$B-V$	$U-B$	Sp	ρ Q km/sec.	μ_α	μ_δ	S
5892	ϵ Ser	3·70	+0·17	...	Am	− 9·4a	+0·125	+0·061	123
5980	δ Nor	4·78	+0·24	...	Am	−15·5b	+0·002	+0·028	123
6031	ψ Sco	4·98	+0·10	...	Am	− 5·7b	−0·010	−0·020	1
6117	ω Her	4·60	+0·01	−0·03	Ap	− 6·6a	+0·042	−0·061	123
6129	3 Oph	4·69	+0·18	...	Am	−30·6b	−0·079	+0·004	1
6153	ω Oph	4·48	+0·13	...	Ap	+ 2·5a	+0·013	+0·030	1
6168	σ Her	4·20:	+0·02:	...	B9V	−10·9b	−0·014	+0·042	123
6254	52 Her	4·80	+0·09	+0·04	Ap	0·0a	+0·023	−0·062	1
6324	ϵ Her	3·92	−0·03	−0·09	AoV	−25·1b	−0·050	+0·025	123
6436	69 Her	4·80	+0·04	−0·01	A2V	− 9·9b	−0·041	+0·058	12
6446	53 Ser	4·33	+0·05	...	A1V	+ 4·8b	+0·041	+0·001	1
6554/5	υ Dra	4·85	+0·265	+0·08	Am	−15·6a	+0·143	+0·053	123
6581	o Ser	4·27	+0·08	...	A2V	−30·0b	−0·074	−0·058	12
6771	72 Oph	3·73	+0·15	...	A4V	−23·9a	−0·064	+0·081	123
6789	δ UMi	4·41	+0·01	...	A1V	− 7·6b	+0·010	+0·054	123
7001	α Lyr	0·00	0·00	−0·01	AoV	−13·9a	+0·199	+0·282	123
7056	ζ LyrA	4·37	+0·18	+0·17	Am	−26·0a	+0·023	+0·021	1
7069	111 Her	4·30:	+0·11:	...	A3V	−44·6b	+0·069	+0·117	123
7141	θ SerA	4·59	+0·15	+0·09	A5V	−44·0b	+0·042	+0·032	123
7235	ζ Aql	2·98	+0·01	...	B9V	−26·3b	−0·010	−0·097	123
7420	ι Cyg	3·90	+0·16	...	A5V	−19·5b	+0·018	+0·130	123
7590	ϵ Pav	3·96	−0·02	−0·02	AoV	+ 0·1b	+0·083	−0·133	123
7653	15 Vul	4·68	+0·16	...	Am	−20·9b	+0·054	+0·006	12
7724	ρ Aql	4·90:	+0·06:	...	A2V	−23·0b	+0·052	+0·056	123
7871	ζ Del	4·63:	+0·15:	...	A3V	−25·0a	+0·041	+0·011	12
7950	ϵ Aqr	3·75	+0·03	+0·01	A1V	−16·0b	+0·030	−0·032	123
7990	μ Aqr	4·80	+0·32	...	Am	− 9·1b	+0·041	−0·028	123
8075	θ Cap	4·12	−0·03	...	AoV	−10·9b	+0·082	−0·058	123
8140	θ Ind	4·43	+0·17	...	A5V	−14·5b	+0·105	−0·065	12
8151	θ Mic	4·85	+0·02	...	Ap	+ 2·3b	+0·071	+0·001	123
8322	δ Cap	2·94	+0·29	...	Am	− 6·3a	+0·261	−0·293	123
8576	β PsA	4·31	+0·02	...	AoV	+ 6·3a	+0·064	−0·012	123
8585	α Lac	3·80	+0·03:	...	A2V	− 4·0b	+0·134	+0·020	123
8709	δ Aqr	3·29	+0·05	+0·06	A3V	+18·0b	−0·041	−0·022	123
8717	ρ Peg	4·89	+0·01	0·00	A1V	−10·1b	+0·073	+0·017	1
8728	α PsA	1·16	+0·09	+0·08	A3V	+ 6·5a	+0·232	−0·162	123
8830	7 And	4·55	+0·18	...	FoV	+12·5b	+0·089	+0·098	1
8949	ι Phe	4·75	+0·09	...	Ap	+19·4b	+0·039	+0·004	13
8984	λ Psc	4·52	+0·19	+0·07	A7V	+12·4b	−0·133	−0·148	123

Parallaxes of the 23 Ap and Am stars were obtained by the use of equation (1). The luminosity of each of the 88 dwarfs was assumed to be half-way between that given by equation (1) and that of a star on the Pleiades main sequence with the appropriate colour. The resulting parallaxes are listed in Table II together with the computed space motion vectors. These vectors are directed as follows: U (away from the galactic centre), V (in the direction of galactic rotation) and W (toward the north galactic pole). Ninety per cent of the 111 stars in Table I are within 50 parsecs of the Sun. The (U, V)- and (V, W)-vectors in Table II are plotted in Figs. 2 and 3, respectively.

TABLE II

Space motion vectors for the stars in Table I

HR	π	U	V	W	HR	π	U	V	W
			km/sec					km/sec	
63	21	−11	+ 5	− 2	4386	23	+15	− 7	−12
68	23	−16	− 2	− 3	4534	76	+24	−19	− 8
100	44	+10	− 5	−10	4554	50	−12	0	−11
269	38	+21	− 2	+ 2	4660	44	−14	0	− 9
343	36	+30	−10	0	4689	26	+ 8	− 7	− 3
403	70	+20	− 7	+ 1	4825/6	80	+33	− 8	−17
553	69	+ 1	−10	− 3	4828	20	−28	− 9	− 5
580	30	−16	− 9	− 2	4963	20	+ 4	− 9	− 7
620	26	+24	−17	+ 1	5028	52	+22	−21	− 3
707	23	− 3	+ 4	0	5062	40	−14	+ 2	− 8
804	43	−18	− 3	−11	5105	14	−13	+ 2	−13
879	19	+18	− 3	− 8	5107	45	+31	−12	− 3
1046	18	+ 4	+ 7	− 8	5359	16	+12	+ 5	− 1
1251	30	− 4	+ 1	+ 2	5463	60	+11	−21	−11
1329	32	+11	− 1	−15	5511	27	+13	−19	+ 1
1338	57	+21	−19	−14	5733	50	+16	− 9	0
1380	27	+40	−17	− 3	5881	25	+12	−17	+ 2
1387	31	+42	−13	− 5	5892	38	+ 5	+14	−13
1427	28	+39	−17	− 6	5980	28	− 4	+14	+15
1444	30	+39	−14	− 4	6031	17	+ 4	− 7	− 4
1458	30	+26	−15	− 9	6117	15	−13	− 7	−20
1479	29	+37	−13	− 4	6129	24	+32	−12	− 2
1568	18	− 9	+ 2	− 4	6153	23	− 2	+ 5	+ 1
1592	22	+11	−21	− 7	6168	23	+12	− 6	− 4
1620	28	+42	−13	− 3	6254	18	−16	− 1	− 5
1621	14	+14	−23	− 5	6324	23	+19	−20	− 6
1762	16	+18	−20	−12	6436	19	+17	− 7	+ 4
2685	69	+ 5	+ 8	+ 2	6446	25	− 4	+ 5	− 5
2238	21	− 5	+ 3	− 1	6554/5	30	+ 9	+ 1	−27
2491	(375)	−14	0	−12	6581	28	+26	−20	+ 2
2550	63	+20	−19	− 8	6771	44	+23	−10	+ 4
2564	50	+20	−19	+ 6	6789	21	+ 8	− 9	− 7
2740	50	+15	+ 6	− 7	7001	150	+15	− 8	− 8
2763	41	− 6	+ 1	− 9	7056	29	+14	−20	−10
2852	55	−10	+12	+14	7069	30	+44	−19	− 9
2890/1	(72)	+ 7	− 4	−10	7141	30	+41	−19	− 3
3067	22	+10	− 7	− 5	7235	40	+10	−26	− 6
3314	25	+10	− 9	− 9	7420	41	+16	−19	− 1
3449	17	+37	−18	− 7	7590	23	+23	−19	−11
3485	62	− 7	− 3	− 3	7653	23	+15	−17	− 8
3492	23	+20	−25	+11	7724	20	+29	− 9	0
3569	63	+34	−15	−15	7871	29	+17	−18	+ 3
3572	31	−15	+ 2	− 5	7950	30	+12	−11	+ 1
3619	39	+13	− 5	−10	7990	37	+ 8	− 7	− 1
3624	43	−12	− 4	+ 9	8075	21	+15	−18	−11
3662	31	−17	+ 6	− 6	8140	33	+22	− 6	+ 1
3690	32	+ 2	−19	− 3	8151	14	+18	0	−20
3799	20	+28	− 7	+ 9	8322	80	+ 9	−20	−10
3856	16	+ 7	−26	− 7	8576	22	+ 9	− 5	−12
3974	33	−16	+ 2	−11	8585	30	+19	− 9	− 7
4090	37	+12	−10	+ 8	8709	40	−10	+ 6	−15
4248	19	−20	− 5	− 9	8717	17	+22	− 9	+ 2
4300	20	+ 3	+ 8	− 9	8728	120	+ 3	− 9	− 9
4357	72	−17	+ 2	−17	8830	33	+19	+ 8	+ 6
4359	32	+ 4	−17	+ 1	8849	18	+ 2	− 7	−20
					8984	35	−25	− 1	−15

The distribution of the (U, V)-vectors in Fig. 2 confirms two previous conclusions obtained from a preliminary discussion of the known Ap and Am stars brighter than $V_g = 6^m$:

(i) The (U, V)-vectors lie in a very restricted region of the (U, V)-plane—the limiting ellipse shown in the figure is that found previously for the Ap and Am stars (Eggen 1959b).

(ii) The vectors are not randomly distributed within this ellipse.

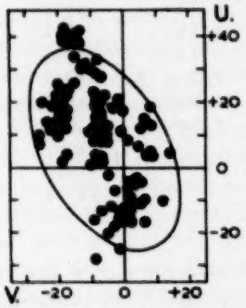

FIG. 2.—*The distribution of the (U, V)-vectors for the dwarf A-type stars.*

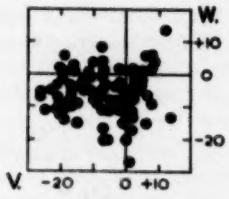

FIG. 3.—*The distribution of the (V, W)-vectors of the dwarf A-type stars.*

The (U, V)-limits in Fig. 2 are indicated by an ellipse because of the analogy with the velocity (dispersion) ellipsoid usually derived from statistical discussions of stellar motions. In fact, however, the distribution of the (U, V)-vectors of the dwarf A-type stars appears to be only roughly elliptical and the scarcity of stars with negative values of both U and V—that is, stars inbound toward the galactic centre on orbits with semi-major axes less than the Sun's distance from the galactic centre—seems to be real. Moreover, the tilt, or deviation of the vertex, of the velocity (dispersion) ellipse from parallelism with the U-axis, usually found for A-type stars (cf. Alexander 1958), is clearly reflected in the tilt of the limiting ellipse and seems to arise partly from the concentration of vectors near $(U, V) = (-16, 0)$ which represent the Sirius group (Eggen 1958, Paper I).

It is also apparent from Fig. 2 why the Sirius and the Hyades, $(U, V) = (+40, -17)$, groups could be detected by the "convergent-point" type of analysis described in Paper I since they lie at the extremes of the

(U, V)-distribution of the older population I stars. The objects that represent these two groups in Fig. 2 are the following (Hyades *cluster* members are identified by an asterisk) :

Hyades					Sirius				
HR	U	V	W	Name	HR	U	V	W	Name
1380*	+40	−17	− 3	64 Tau	68	−16	− 2	− 3	σ And
1387*	+42	−13	− 5	κ Tau	804	−18	− 3	−11	γ Cet
1427*	+39	−17	− 6	...	2491	−14	0	−12	α CMa
1444*	+39	−14	− 4	ρ Tau	3572	−15	+ 2	− 5	α Cnc
1479*	+37	−13	− 4	92 Tau	3662	−17	+ 6	− 6	18 UMa
1620*	+42	−13	− 3	ι Tau	3974	−16	+ 2	−11	21 LMi
3449	+37	−18	− 7	γ Cnc	4357	−17	+ 2	−17	δ Leo
7069	+44	−19	− 9	111 Her	4554	−12	0	−11	γ UMa
7141	+41	−19	− 3	θ Ser A	4660	−14	0	− 9	δ UMa
					5062	−14	+ 2	− 8	80 UMa
					5105	−13	+ 2	−13	78 Vir
					6524	−16	− 1	− 5	52 Her

The non-randomness of the distribution of the rest of the (U, V)-vectors in Fig. 2 is undoubtedly real and is confirmed by the space motions of the early-type visual binaries (Eggen 1959c). Since lines of constant $V \approx -7$ and -19 km/sec represent, over the small range of U in the figure, lines of constant semi-major axis (a) for galactic orbits with $a \approx 0{\cdot}93 R_\odot$ and $0{\cdot}98 R_\odot$, where $R_\odot$ is the Sun–galactic centre distance, the concentrations of (U, V)-vectors in Fig. 2 would seem to indicate that these values of V represent two preferred values of a for the older population I other than the Hyades and Sirius groups. Older

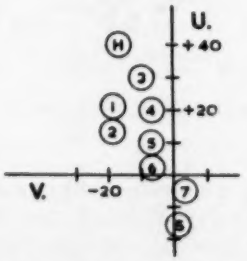

FIG. 4.—*Suggested interpretation of the distribution of the (U, V)-vectors of dwarf A-type stars shown in Fig. 3. The circles marked "S" and "H" contain the members of the Sirius and Hyades groups, respectively.*

population I therefore consists mainly of stars outbound from the galactic centre on orbits with these values of a and with eccentricities varying uniformly between about 0 and 0·05. However, by analogy with the known Hyades and Sirius groups, the interpretation of Fig. 2 that is shown in Fig. 4 seems more likely. Here seventy-five per cent of the stars in Table I are assigned to seven groups, other than the Hyades and Sirius groups. Some of the groups have so nearly a common orbital period and eccentricity that the slight blurring of the

(U, V)-vectors caused by the $\sim 0^m.5$ uncertainty in the assumed luminosities of the stars taken from Fig. 1, and the uncertainties in the motions of even these well-observed bright objects, is enough to merge one group with another. It is obvious from Fig. 2 that the convergent-point method of assigning stars to groups is impracticable for these low velocity groups. In fact, it was previously found (Eggen 1959a) that the Hyades and Sirius groups are at the limit of detectability by this method. The matter is also further complicated by the fact that the motion in W, although generally small, may be independent of that in U and V for these low velocity stars and the "convergent-point" of the group motion is consequently difficult to assign with accuracy.

The possible groups of older population I stars, other than the Hyades and Sirius groups, which are indicated in Fig. 4 will be more fully discussed in a later paper of this series concerning the motions of the G–K giants. However, whatever interpretation is placed on Fig. 2, the obvious non-randomness in the (U, V)-distribution makes the classical, statistical treatment of the motions of these stars, for such constants as those of the solar motion, of dubious significance and it will not, therefore, be applied to the material in Table I.

The obvious absence of a "solar group" with $(U, V) = (0, 0)$ in Fig. 2 should be noted. Since the stars in Table I are probably all younger than about 5×10^8 years and the Sun is nearly 5×10^9 years old, members of a solar group would not be expected in this material.

2. *M-type giants.*—On the basis of current evolutionary theory we can expect the M-type stars that are classified as giants on the Mount Wilson system or as of luminosity class III on the MK system to be a mixture of three populations; the older population I, typified by the A-type dwarfs discussed above, the disk population, typified by the subgiants (Paper V, Eggen 1960) and a relatively small number of representatives of the halo population. Furthermore these stars probably fall in a rather restricted region of the $(M_V, B-V)$-diagram. The older population I, with ages up to about 5×10^8 years, will mainly lie between $M_V = 0^m$ and -1^m (cf. Hyades and Sirius groups, Paper I) and the disk population, with ages up to about 10^{10} years, will cover the same luminosity range (cf. 61 Cygni and γ Leonis groups, Paper V). Because of the very large dwarf/giant ratio in the halo population globular clusters, and the relatively few halo dwarfs in the solar neighbourhood (Eggen and Sandage 1959, Paper IV), very few halo population giants, which have $M_V \approx -2^m$, will be found among the bright stars. Therefore, if we confine ourselves to the stars for which accurate proper motions and radial velocity material are available and that are redder than about $B-V = 1^m.5$ (that is, spectral type later than $\sim$K5), the true space motions can be reliably bracketed between those computed for assumed luminosities of $M_V = 0^m$ and -1^m.

The stars brighter than visual (HR) magnitude $5^m.0$ and with $B-V \geqslant 1^m.5$ are listed in Table III. The arrangement and source of the material in Table III are similar to that in Table I. Known supergiants of Class I have been omitted although a few stars recognized as of luminosity Class II are included and there are undoubtedly several others of that class not recognized. The spectral types are mainly by the Mount Wilson observers (Wilson 1953) and by Hoffleit (1942); very few M-giants have been classified on the MK system. Most of the stars whose magnitudes are followed by a "v" in the table were discovered to be small-amplitude variables by the Cape observers (Stoy 1953).

TABLE III

M-type giants brighter than visual magnitude $5^{m}.0$

HR	Name	V_E	$B-V$	Sp	ρ Q km/sec	μ_α	μ_δ	S
		m	m			s	s	
45	χ Peg	4·80	+1·58	M2 III	−45·8b	+0·091	+0·005	123
48	7 Cet	4·45	+1·66	gM1	−22·5a	−0·028	−0·063	1
105	η Scl	4·85	+1·66	gM4	+12·2b	−0·022	−0·043	12
224	δ Psc	4·27	+1·55	K5 III	+32·3a	+0·083	−0·046	123
248	20 Cet	4·78	+1·58	gMo	+15·8a	+0·006	−0·012	123
337	β And	2·06	+1·58	Mo III	+ 0·3a	+0·178	−0·111	123
555	ψ Phe	4·40v	+1·60	gM5	+ 1 c	−0·090	−0·080	123
585	59 Cet	4·05	+1·58	gM1	+18·0a	+0·130	−0·018	123
602	χ Phe	5·00	+1·50	gMo	−30·6a	−0·032	−0·043	12
911	α Cet	2·48	+1·65	M2 III	−25·9a	−0·009	−0·075	123
921	ρ Per	3·2v	+1·69	M4 III	+28·2b	+0·131	−0·106	123
1003		3·70v	+1·58	gM3	+41·7a	+0·053	+0·036	12
1162	π Eri	4·43	+1·65	gM2	+45·7a	+0·047	+0·061	1
1208	γ Hyi	3·35	+1·64	M2 III	+15·5a	+0·051	+0·114	123
1231	γ Eri	3·43	+1·60	Mo III	+61·7a	+0·063	−0·109	123
1247	δ Ret	4·56	+1·64	gM1	− 1·4b	+0·009	−0·013	123
1264	γ Ret	4·49	+1·63	gM6	− 7·0b	−0·002	+0·026	1
1393	43 Eri	3·97	+1·50	gK5	+24·1a	+0·058	+0·052	123
1457	α Tau	0·80	+1·52	K5 III	+54·1a	+0·067	−0·189	123
1496	54 Eri	4·34	+1·60	gM4	−33·6a	+0·021	−0·093	12
1654	ϵ Lep	3·19	+1·50	K5 III	+ 1·0a	+0·025	−0·071	123
1663		5·00v	+1·52	gK5	+36·0a	+0·062	−0·001	123
2011	31 Aur	4·70	+1·60	gM1	+37·7a	+0·036	−0·048	13
2091	π Aur	4·30	+1·65	M3 II	+ 0·9a	+0·003	−0·009	1
2216	η Gem	3·0v	+1·66	M3 III	+19·0a	−0·065	−0·014	123
2245		5·00	+1·59	gM3	+34·5a	−0·024	+0·116	12
2286	μ Gem	2·97	+1·67	M3 III	+54·8a	+0·059	−0·113	123
2608		4·93	+1·69	gM1	+22·1a	−0·002	+0·007	12
2748	L^2 Pup	2·9v	+1·6	gM5	+53·0a	+0·104	+0·326	1
2878	σ Pup	3·29	+1·51	K5 III	+88·1a	−0·064	+0·184	12
2905	69 Gem	4·09	+1·60	Mo III	−20·6a	−0·033	−0·110	123
2993		4·67	+1·62	gK5	+32·7a	−0·017	+0·028	12
3017		3·61	+1·74	gM2	+17·1a	−0·009	−0·002	12
3141	28 Mon	4·72	+1·51	K4 III	+26·7a	+0·060	−0·075	13
3187		5·00v	+1·52	gMo	+25·3a	−0·011	−0·002	12
3225		4·49v	+1·65	gMo	+15·9a	−0·008	−0·006	1
3275	31 Lyn	4·13	+1·60	K5 III	+24·4a	−0·017	−0·103	123
3576	ρ UMa	4·71	+1·56	gM3	+ 4·6a	−0·021	+0·015	123
3628	κ Pyx	4·66	+1·62	gK5	−44·7b	+0·039	+0·004	1
3705	α Lyn	3·13	+1·55	gMo	+37·6a	−0·220	+0·013	123
3718	θ Pyx	4·54	+1·68	gMo	+20·0b	−0·012	−0·011	123
3773	λ Leo	4·18	+1·60	K5 III	+26·7b	−0·026	−0·042	13
3803		3·19	+1·58	gK5	−13·9a	−0·033	−0·011	12
3950	π Leo	4·59	+1·67	M2 III	+23·4a	−0·032	−0·027	123
3980	31 Leo	4·28	+1·55	K4 III	+41·1a	−0·081	−0·066	1
4050		3·41v	+1·57	gMo	+ 8·6a	−0·023	+0·003	123
4063		4·55v	+1·63	gMo	+12·9a	−0·009	−0·013	1
4069	μ UMa	3·00v	+1·55	Mo III	−20·5b	−0·081	+0·029	123
4094	μ Hya	3·84	+1·51	K5 III	+34·6a	−0·128	−0·081	12
4142		4·91	+1·69	gMo	+11·2a	−0·011	−0·008	1
4159		4·43	+1·66	gMo	+ 9·9a	−0·019	−0·010	1
4174	γ Cha	4·15	+1·60	gK6	−22·4a	−0·037	+0·013	123

TABLE III—*continued*

M-type giants brighter than visual magnitude $5^{m}.0$

HR	Name	V_E	$B-V$	Sp	ρ Q km/sec	μ_x	μ_y	S
		m	m			"	"	
4200		4·57v	+1·73	gK5	+ 9·3a	−0·028	−0·003	1
4299	61 Leo	4·73	+1·63	K5 III	−13·5a	+0·015	−0·037	123
4362	72 Leo	4·62	+1·66	gM2	+15·6a	−0·021	−0·008	123
4434	λ Dra	3·76	+1·68	Mo III	+ 7·2a	−0·040	−0·021	123
4517	3 Vir	4·00	+1·51	Mo III	+50·7a	−0·020	−0·188	123
4530	μ Mus	4·78v	+1·56	gM2	+37·4b	+0·023	−0·026	1
4605	κ Cha	5·00	+1·50	gMo	− 2·4b	−0·071	+0·039	1
4671	ϵ Mus	4·16v	+1·56	gM5	+ 7·1a	−0·234	−0·036	1
4682		4·97	+1·61	gMo	− 7·1b	−0·078	−0·028	1
4763	γ Cru	1·68	+1·60	M3 III	+21·3a	+0·028	−0·269	123
4902	ψ Vir	4·76	+1·60	gM3	+17·6a	−0·025	−0·020	123
4910	δ Vir	3·32	+1·57	M3 III	−17·8a	−0·469	−0·058	123
4920	36 Com	4·66	+1·66	gMo	− 1·6a	−0·038	+0·028	13
5002		4·83	+1·53	gK5	−10·3a	−0·011	−0·027	1
5015	σ Vir	4·80	+1·71	gM2	−26·9a	−0·008	+0·011	123
5095	74 Vir	4·70	+1·66	gM3	+18·2a	−0·102	−0·050	13
5154	83 UMa	4·45	+1·70	M2 III	−17·1a	−0·024	−0·014	123
5192	2 Cen	4·16v	+1·48	M1 III	+40·7a	−0·047	−0·064	1
5200	5 Boo	4·00	+1·60	K5 III	− 5·6a	−0·095	+0·034	1
5219		4·70	+1·56	gM2	−43·6a	−0·024	−0·038	13
5226	10 Dra	4·00	+1·50	gM3	−10·7a	−0·001	−0·008	123
5490	34 Boo	4·65	+1·57	gM3	+ 5·6a	−0·017	−0·020	12
5603	σ Lib	3·35	+1·65	gM4	− 4·3a	−0·073	−0·048	123
5705	ϕ Lup	3·59	+1·55	gK5	−29·4a	−0·094	−0·086	123
5838	κ Lib	4·74	+1·62	K5 III	− 3·8b	−0·039	−0·109	12
5879	κ Ser	4·00	+1·68	gM1	−38·7a	−0·050	−0·092	123
6020	δ Aps	4·78	+1·65	M4 III	−12·0a	−0·004	−0·042	13
6056	δ Oph	2·72	+1·60	gMo	−19·9a	−0·046	−0·147	123
6146	30 Her	4·2v	+1·6	gM6	+ 3·4a	+0·027	−0·008	12
6159	29 Her	4·85	+1·50	K5 III	+ 3·1a	−0·180	−0·081	1
6166		4·20	+1·60	gM2	− 2·1a	+0·020	−0·004	1
6229	η Ara	3·75	+1·61	gMo	+ 9·0a	+0·040	−0·030	123
6285	ζ Ara	3·16	+1·63	gM1	− 6·0a	−0·014	−0·034	123
6318	30 Oph	4·86	+1·50	K4 III	− 6·7a	−0·047	−0·080	12
6337		4·98	+1·63	M3 III	+43·4a	+0·019	−0·070	1
6682		4·90	+1·67	gM1	+ 4·4b	−0·010	−0·009	12
6705	γ Dra	2·20	+1·52	K5 III	−27·6a	−0·011	−0·022	123
6815	104 Her	4·74	+1·52	gM3	− 0·3b	−0·015	+0·025	13
6832	η Sgr	3·15	+1·58	M3 II	+ 0·5a	−0·130	−0·163	12
6868	106 Her	4·70	+1·52	gMo	−32·8b	+0·013	−0·059	1
6855	ζ Pav	4·35	+1·48	gM1	+12·2a	0·000	+0·001	123
7157	R Lyr	4·0v	+1·60	M5 III	−28·3a	+0·019	+0·082	3
7405	α Vul	4·45	+1·51	Mo III	−85·5	−0·130	−0·104	123
7635	γ Sge	4·00	+1·52	K5 III	−32·8a	+0·060	+0·025	123
7650	62 Sgr	4·48v	+1·64	gM4	+ 9·9a	+0·034	+0·018	123
7673	ξ Tel	4·95	+1·66	gK6	+36·0a	−0·009	+0·004	123
7951	3 Aqr	4·50v	+1·65	gM3	−22·0a	−0·005	−0·039	123
7952	ζ Ind	4·88	+1·55	gM1	− 5·2b	+0·043	+0·028	12
7980	ω Cap	4·13	+1·65	K5 III	+ 9·0b	−0·006	−0·003	123
8080	24 Cap	4·57	+1·61	gM1	+31·9a	−0·026	−0·044	123
8225	2 Peg	4·49	+1·65	M1 III	−18·9a	+0·018	+0·006	12
8582		4·85	+1·61	gM4	− 3·4a	+0·041	−0·022	12

TABLE III—*continued*

M-type giants brighter than visual magnitude $5^{m}.0$

HR	Name	V_B	$B-V$	Sp	ρ Q km/sec	μ_α	μ_δ	S
		m	m			s	"	
8636	β Gru	2·20v	+1·61	M3 II	+ 1·6a	+0·135	−0·005	123
8679	τ Aqr	4·07	+1·59	gMo	+ 1·0a	−0·015	−0·032	123
8698	λ Aqr	3·78	+1·64	gM2	− 8·8a	+0·006	+0·040	123
8775	β Peg	2·30	+1·66	M2 III	+ 8·7a	+0·187	+0·142	13
8795	55 Peg	4·50	+1·56	M2 III	− 5·4a	+0·007	−0·010	123
8834	ϕ Aqr	4·34	+1·58	gM2	− 0·4a	+0·036	−0·191	123
8860	8 And	4·70	+1·60	gM2	− 8·0a	+0·034	+0·009	1
9064	ψ Peg	4·67	+1·58	gM3	− 4·2a	−0·040	−0·028	123
9089	30 Psc	4·43	+1·64	gM2	−11·8a	+0·050	−0·033	123

TABLE IV

Space motion vectors for the stars in Table III

HR	π_1	U	V	W	π_2	U	V	W
		km/sec				km/sec		
45	11	+22	− 48	+28	7	+ 43	− 58	+26
48	13	−19	− 20	+19	8	− 32	− 29	+19
105	11	−19	− 13	−10	7	− 27	− 18	− 8
224	14	+27	− 10	−35	9	+ 36	− 25	−40
248	11	+ 4	0	−16	7	+ 4	− 3	−18
337	39	+15	− 18	−10	25	+ 24	− 28	−16
555	13	−45	+ 1	− 1	8	− 73	+ 1	− 1
585	15·5	+32	− 31	− 6	10	+ 45	− 47	− 1
602	10	−27	+ 8	+30	6	− 43	+ 5	+29
911	32	−20	− 9	+10	20	− 28	− 14	+ 7
921	23	+39	− 14	−13	14	+ 50	− 36	−14
1003	18	+34	− 15	−25	11·5	+ 42	− 17	−19
1162	13	+51	− 7	−14	8	+ 64	− 5	− 3
1208	21	+24	− 17	−14	13·5	+ 39	− 19	−17
1231	20·5	+30	− 45	−41	13	+ 24	− 63	−40
1247	12	− 3	− 3	+ 5	8	− 4	− 5	+ 7
1264	13	+ 9	+ 8	+ 1	8	+ 14	+ 9	− 1
1393	16	+29	− 18	− 1	10	+ 39	− 20	+ 6
1457	69	+50	− 15	−20	44	+ 49	− 23	−22
1496	13·5	−41	− 8	+16	8	− 59	− 26	+15
1654	23	−10	− 12	− 1	14·5	− 16	− 19	− 1
1663	10	+11	− 45	+ 2	6	+ 13	− 57	+18
2011	11·5	+40	− 20	+ 7	7	+ 41	− 36	+ 9
2091	14	+ 2	− 3	0	9	+ 2	− 5	− 1
2216	25	+21	0	−11	16	+ 22	+ 3	−18
2245	10	+54	− 32	−22	6	+ 91	− 33	−26
2286	26	+50	− 33	+ 5	16	+ 43	− 51	+ 2
2608	10	+ 8	− 20	− 7	6·5	+ 1	− 20	− 7
2748	26	+65	− 49	+31	17	+ 87	− 48	+58
2878	22	+65	− 76	−11	14	+ 88	− 70	− 7
2905	16	−16	− 24	−27	10	− 15	− 41	−39
2993	12	+26	− 24	− 1	7	+ 34	− 21	0
3017	19	+ 6	− 16	− 4	12	+ 6	− 6	− 5
3141	11	−10	− 46	+14	7	− 27	− 63	+16
3187	10	+ 6	− 24	− 8	6	+ 8	− 23	−11
3225	12	+ 2	− 16	− 4	8	+ 4	− 17	− 6

TABLE IV—*continued*

Space motion vectors for the stars in Table III

HR	π_1	U	V	W	π_2	U	V	W
			km/sec				km/sec	
3275	15	+27	− 30	+ 7	9·5	+ 35	− 40	+ 7
3576	11	+ 8	+ 5	− 4	7	+ 10	+ 9	− 9
3628	12	−22	+ 43	− 1	7	− 29	+ 43	+ 8
3705	23	+58	− 2	− 4	14	+ 79	− 1	−24
3718	12	+ 6	− 21	0	8	+ 6	− 22	− 4
3773	15	+19	− 21	+11	9	+ 21	− 30	+ 6
3803	23	+ 6	+ 13	− 5	14·5	+ 8	+ 14	− 8
3950	12	+17	− 23	+ 6	7·5	+ 18	− 29	− 1
3980	14	+31	− 44	+ 8	9	+ 38	− 57	− 5
4050	21	+ 2	− 8	− 3	13	+ 5	− 10	− 7
4063	12	− 2	− 13	− 6	8	− 2	− 15	−10
4069	25	+ 1	+ 2	−27	16	+ 10	+ 3	−31
4094	17	+23	− 52	−10	11	+ 33	− 63	−28
4142	10	− 1	− 10	− 8	6·5	0	− 10	−11
4159	13	+ 2	− 11	− 6	8	+ 4	− 12	−10
4174	15	+19	+ 18	0	9	+ 24	+ 19	− 5
4200	12	+ 6	− 11	− 6	8	+ 10	− 13	− 9
4299	11	−14	− 3	−16	7	− 22	− 9	−19
4362	12	+10	− 10	+11	7	+ 14	− 14	+ 9
4434	18	+12	− 6	+10	11	+ 18	− 13	+11
4517	16	−19	− 68	+22	10	− 31	− 95	+ 8
4530	11	−27	− 27	−12	7	− 33	− 24	−17
4605	10	+31	− 19	+13	6	+ 51	− 39	+21
4671	15	+30	− 94	−26	9·5	+ 67	−114	−37
4682	10	+34	− 12	−18	6	+ 54	− 25	−29
4763	46	−16	− 18	−25	29	− 19	− 18	−41
4902	11	0	− 20	+ 9	7	+ 3	− 15	+ 7
4910	21	+87	− 62	−17	14·5	+123	− 93	−17
4920	12	+16	− 1	+ 4	7	+ 28	− 1	+ 5
5002	11	+11	+ 6	−10	7	+ 14	+ 4	−17
5015	11	+14	+ 8	−23	7	+ 16	+ 8	−22
5095	12	+14	− 45	+11	7	+ 31	− 71	+ 9
5154	13	+ 2	− 12	−19	8	+ 4	− 15	−20
5192	14	−17	− 46	+ 4	9·5	− 13	− 54	− 2
5200	16	+29	− 5	+ 3	10	+ 46	− 14	+10
5219	11	+ 2	− 29	−38	7	0	− 39	−36
5226	16	− 2	− 6	−10	10	− 2	− 6	−10
5490	12	− 3	− 8	+ 8	7	− 3	− 16	+10
5603	21	+10	− 17	− 2	14	+ 15	− 25	− 1
5705	19	+38	− 17	−11	12	+ 46	− 34	−13
5838	11	+ 2	− 44	−22	7	+ 1	− 71	−34
5879	16	+11	− 41	−25	10	+ 3	− 60	−23
6020	11	+10	− 16	−18	7	+ 17	− 19	−23
6056	28	+ 9	− 27	−17	18	+ 5	− 40	−21
6146	14	− 6	+ 7	− 4	9	− 9	+ 10	− 8
6159	12	− 4	− 65	+43	7	− 5	−112	+72
6166	14	0	+ 4	− 6	9	0	+ 6	−10
6229	18	− 6	− 2	−15	11	− 5	0	−25
6285	23·5	+ 9	− 4	− 1	15	+ 11	− 7	− 2
6318	11	− 5	− 40	− 3	7	− 11	− 62	− 4
6337	10	−55	+ 5	+ 1	6	− 70	− 6	−11
6682	10	− 4	− 7	+ 1	6·5	− 3	− 10	+ 2
6705	36	+ 2	− 25	−12	23	0	− 25	−12

TABLE IV—*continued*

Space motion vectors for the stars in Table III

HR	π_1	U	V	W	π_2	U	V	W
			km/sec				km/sec	
6815	11	+ 9	+ 1	+ 9	7	+ 13	+ 2	+14
6832	23	+ 3	− 42	+ 7	15	+ 4	− 65	+12
6855	13·5	0	− 11	− 4	8·5	− 10	− 10	− 4
6868	11	+ 2	− 34	−24	7	− 8	− 41	−32
7157	16	+32	− 21	− 4	10	+ 45	− 17	− 2
7405	13	− 3	−103	+19	8	− 34	−122	+33
7635	16	+31	− 20	− 7	10	+ 40	− 16	−14
7650	13	− 2	+ 11	−13	8	+ 3	+ 16	−18
7673	10	−32	− 7	−16	6	− 34	− 6	−14
7951	12·5	+ 6	− 25	+ 6	8	+ 2	− 32	+ 4
7952	10·5	+15	+ 14	−11	7	+ 20	+ 21	−18
7980	15	− 8	+ 1	− 5	9·5	− 9	0	− 4
8080	12	−33	− 8	−17	8	− 38	− 16	−16
8225	13	+11	− 8	+ 4	8	+ 15	− 16	+ 8
8582	11	+14	− 10	− 2	7	+ 21	− 16	− 4
8636	36	+14	− 5	− 9	23	+ 23	− 8	−14
8679	15	−11	− 9	− 3	10	− 14	− 10	− 2
8698	17·5	+ 9	+ 4	+10	11	+ 13	+ 9	+12
8775	33	+34	+ 7	+ 2	21	+ 53	+ 7	+ 5
8795	12·5	+ 1	− 8	+ 1	8	+ 2	− 10	0
8834	14	−24	− 54	−27	9	− 36	− 85	−42
8860	11·5	+11	− 12	0	7·5	+ 18	− 14	0
9064	11·5	−21	− 1	− 4	7	− 34	0	− 8
9089	13	+ 8	− 24	+ 3	8	+ 14	− 36	+ 3

The space motion vectors of the stars in Table III are given in Table IV where the first set of values for (U, V, W) were computed on the basis of an assumed luminosity of 0^m and the second set on the basis of -1^m. The values of (U, V) and (V, W) based on the assumption that $M_V = -1^m$ are plotted in Figs. 5 and 6, respectively. If the true values of the luminosities lie between 0^m and -1^m, then the (U, V) and (V, W) distributions seen in Figs. 5 and 6 represent the most "expanded" form of these distributions for the stars in Table III; the use of the assumption $M_V = 0^m$ makes all the space motions smaller and the distributions in the (U, V)- and (V, W)-planes somewhat more compact. The ellipse drawn in Fig. 5 is the limiting ellipse of the (U, V)-distribution of the dwarf A-type stars in Fig. 2. The M-type giants that fall within this ellipse are indicated by open circles; the crossed circles indicate the additional stars that would fall within the ellipse if the assumption that $M_V = 0^m$ was used. The six stars falling near $(U, V) = (+40, -17)$ and indicated by filled circles are probably members of the Hyades group. Such members would be expected to have $M_V \approx -1^m$.

The remaining stars of Table III are represented by crosses in Fig. 5. The majority of these stars are undoubtedly members of the disk population. It is of interest to note that the 113 stars of Table III are evenly divided between stars falling within and those falling outside the limiting ellipse for the A-type dwarfs. Therefore, since we can identify the stars marked as crosses in Fig. 5 with the disk population, it appears that at least 50 per cent of the M-type giants in Table III originated as main sequence stars of spectral type F2–G0 and with masses $\sim 1{\cdot}5\odot$.

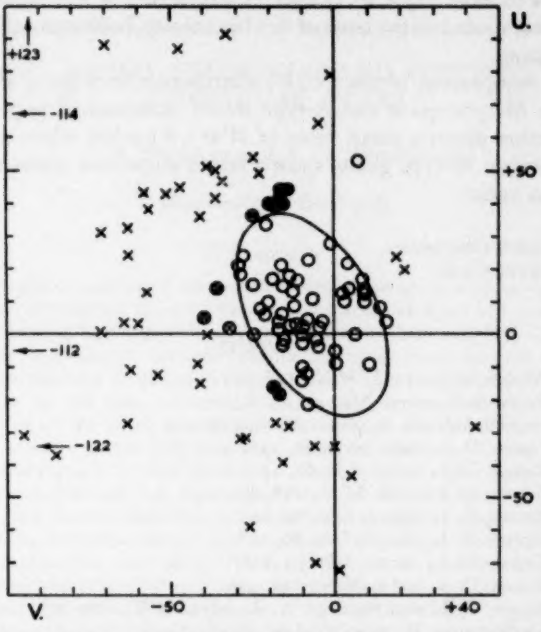

FIG. 5.—*The distribution of the (U, V)-vectors of the M-type giants computed on the basis of the assumption that the absolute magnitudes are* -1^m. *The six stars shown as filled circles are probably members of the Hyades group and the crosses indicate probable members of the disk population.*

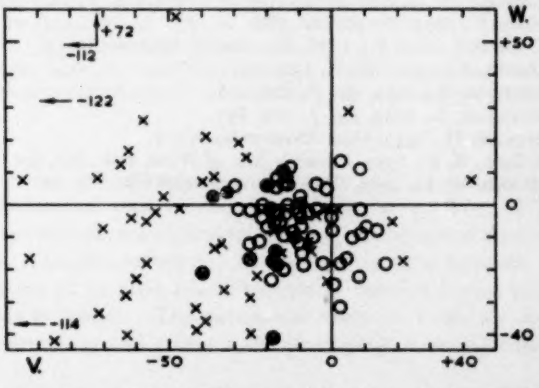

FIG. 6.—*The distribution of the (V, W)-vectors of the M-type giants computed on the basis of the assumption that the absolute magnitudes are* -1^m. *The symbols are as in Fig. 5.*

Although the assumption that $M_V = -1^m$ will only be correct for a fraction of the stars involved, the distribution of the (U, V)-vectors within the limiting ellipse in Fig. 5 bears some resemblance to that of the same vectors for the dwarf A-type stars in Fig. 2. This is especially striking in the marked, apparent scarcity of stars with negative values of both U and V. There are also, apparently, very few M-type giant members of the Sirius group. Although we would expect

such members to have $M_V \approx 0^m$ (Paper I), inspection of the vectors in Table V of that paper, computed on the basis of this luminosity, indicates only one member: 61 Leo, HR 4299.

Finally, a comparison of the (U, V)-distribution in Figs. 3 and 6 indicates that both the M-type giant and A-type dwarf members of population I show a small dispersion about a mean value of $W \approx -8$ km/sec whereas, as expected, the disk population M-type giants show a larger dispersion about approximately the same mean value.

Royal Greenwich Observatory,
Herstmonceux Castle:
1959 *October.*

References

Alexander, J., 1958, *M.N.*, **118**, 161.
Bertaud, C., 1959, *J.O.*, **42**, 45.
de Vaucouleurs, A., 1957, *M.N.*, **117**, 449.
Eggen, O. J., 1955, *A.J.*, **60**, 131.
Eggen, O. J., 1957, *A.J.*, **62**, 45.
Eggen, O. J., 1958, *M.N.*, **118**, 65.
Eggen, O. J., 1959 a, *Obs.* **79**, 143.
Eggen, O. J., 1959 b, *Obs.* **79**, 197.
Eggen, O. J., 1959 c, *Obs.* **79**, 206.
Eggen, O. J., 1960, *M.N.*, **120**, 430.
Eggen, O. J., and Sandage, A. R., 1959, *M.N.*, **119**, 278.
Hertzsprung, E., 1940, *B.A.N.*, **9**, 101.
Hoffleit, D., 1942, *Harvard College Obs. Cir.* No. 448.
Hogg, A., 1958, Mt. Stromlo mimeogram.
Johnson, H. L., and Knuckles, C. F., 1957, *Ap. J.*, **126**, 113.
Johnson, H. L., and Morgan, W. W., 1953, *Ap. J.*, **117**, 313.
Naur, P., 1955, *Ap. J.*, **122**, 182.
O'Connell, D. J. K., 1958, *Ric. Astron. Specola Vat.*, **5**.
Osawa, K., 1959, *Ap. J.*, **130**, 159.
Slettebak, A., 1954, *Ap. J.*, **119**, 146.
Slettebak, A., 1955, *Ap. J.*, **121**, 653.
Stoy, R. H., 1953, *Cape Mimeogram*, No. 1.
Wilson, R. E., 1953, *Carnegie Inst. of Wash. Pub.*, No. 601.
Woods, M. L., 1955, *Mem. Commonwealth Obs.* No. 12.

47 TUCANAE: RADIAL VELOCITIES AND SPECTRAL TYPES OF INDIVIDUAL STARS

M. W. Feast and A. D. Thackeray

(Received 1959 October 9)

Summary

A discussion is given of the radial velocities and spectral types of 32 stars in 47 Tuc determined from 64 plates. The spectral types of 23 red giants lie in the range of MK types G8–M2 and luminosity classes II–III. There is a slight CN discrepancy, but the spectra are much more normal than the extreme population II globular cluster stars. The metal/hydrogen ratio is unlikely to be less than 1/4 normal. The spectroscopic evidence suggests that the top of the giant branch lies below and to the red of that of other globular clusters in the HR diagram. One red giant, not known to be a variable star shows a variable spectrum. A mean velocity of $-14{\cdot}2$ km/sec for the cluster is deduced. A dependence of radial velocity on spectral type is found. It is unlikely that this is due to the wavelength system employed. From the velocity dispersion of the red giants it is found that under almost any assumption the mass of 47 Tuc is unlikely to be greater than $6{\cdot}0 \times 10^5$ solar masses and taking into account the dependence of velocity on type may well be less than $2{\cdot}5 \times 10^5$ solar masses. The mass/light ratio (0·3 solar units) is much less than in intermediate spirals and elliptical galaxies. The membership and spectrum of a bright B8 III star is discussed. Two irregular and one semi-regular red variables have spectral types in the range M2–3 II–III; three regular (200d) red variables have types in the range M2–3 II–Ib, and are normal Me variables. The velocities of these stars are discussed. The distance modulus of 47 Tuc is deduced from the RR Lyrae member (HV 814). It is shown that a distance of 4·4 kpc, which follows if HV 814 has a median absolute visual magnitude of $+0{\cdot}5$, fits best with the spectroscopic absolute magnitudes of the red giants, the red variables and the B-type member.

Introduction and observations.—Between 1951 and 1959 a considerable number of spectra of individual stars in the globular cluster 47 Tuc (NGC 104) were obtained. They were taken with the two-prism spectrograph at the Cassegrain focus of the 74-inch Radcliffe reflector. Altogether we now have for discussion 64 acceptable spectra of 32 stars (three spectra of two RR Lyrae variables are not included in this number). The details are listed in Table I. Exposure times were usually between 3 and 5 hours, the photographic magnitudes being mostly near $13^{m}{\cdot}0$.

In the present paper we discuss the radial velocities and spectral types derived from these spectra. The programme was initially planned in conjunction with a photometric programme being carried out by Dr A. J. Wesselink which will be published separately. A preliminary condensed account of the spectral types and the photometry has already been given (**1**) and another paper (**2**) has discussed the membership of two RR Lyrae variables in the cluster and their spectra. This investigation has been restricted to the brightest stars in the cluster. These include a selection of the red giants, the long period and irregular variables and a bright blue cluster member.

TABLE I

Spectra of individual stars in 47 Tuc

Camera	Dispersion at $H\gamma$ (A/mm)	No. of spectra	Usual slit-width (microns)	Projected slit-width (km/s)	Width of spectrum (mm)
b	29	1	60	48	0·10
c	49	39	90	72	0·20:
d	86	24	175–200	140–160	0·23

The stars studied are identified by number or letter in Plates 10 and 11(i)*a* (which are reproduced from a 74 inch Newtonian plate of the cluster in blue light). Three 'stars' are noted in Table II as blends of more than one star. All others observed were well resolved on the slit.

The adopted velocities and spectral types are listed in Table II.

TABLE II

Radial velocities and spectral types in 47 Tuc

Member Stars

Star	Sp.	Date (U.T.)	Velocity km/sec	Camera	Obs.
No. 1	B8 III:	1952 VII 29.077	−14·7	c	T
		1954 VI 29.118	−18·5	c	T
		VII 26.103	− 9·5	b	T
			−14·2		
No. 3	K3 III (−?)	1952 VIII 17.028	−13·4	c	T
		1953 IX 23·931	−18·1	c	F
			−15·8		
No. 4	G8 III: (II?)	1952 VIII 1.077	**−10·2**	c	F (B)
No. 6	G8 III	1953 IX 22.996	+ 2·4	c	T
		1954 XI 16.810	−17·3	d	T
			− 7·4		
No. 7	Ko III	1953 XII 22.800	**−13·2**	d	T
No. 8	Ko II or III	1953 X 15.947	−17·2	c	F
		1955 VII 25.091	+ 0·4	d	F
			− 8·4		
No. 10	K3 II	1952 VIII 6.046	−14·0	c	T
		1953 IX 27.074	−22·3	c	F
		IX 29.926	−24·2	d	F
		1955 IX 29.983	−22·4	c	F
			−20·7		
No. 11	K4 II–III	1951 IX 18.889	−25·8	d	T
		1953 IX 26.922	−25·2	c	F
		1955 VII 28.085	−14·8	c	F
		IX 4.036	−20·4	d	F
			−21·6		
No. 12	M1 II (or II–III)	1952 X 9.894	−12·8	c	T
		1955 VIII 31.045	− 5·9	d	F
			− 9·4		

TABLE II—*continued*

Member Stars—continued

Star	Sp.	Date (U.T.)	Velocity km/sec	Camera	Obs.
No. 13	G8: (III:)	1954 VIII 17.036	− 4·5	d	F
No. 14	M1 II	1952 X 7.927	−23·3	c	F (B)
No. 15	G8 III	1952 VIII 12.042	− 6·0	c	T (B)
No. 16	G8 II–III	1954 IX 21.000	−10·8	c	F
		X 11.936	+ 6·8	d	T
			− 2·0		
No. 18	M	1954 IX 16.996	− 5·8	c	F
No. 19	K	1953 XI 23.774	−31·1	d	F
No. 21	Ko (III:)	1952 X 25.879	−15·4	c	F
		1955 VII 31.090	−17·3	d	F
			−16·4		
No. 23	M1–2 III	1953 X 2.911	−14·0	c	T
No. 24	M1 II	1953 IX 27.933	−29·0	c	T
No. 26	M2 II (or II–III)	1953 IX 19.999	−13·1	c	T
		1954 VIII 9.068	−29·6	d	F
			−21·4		
No. 36	M2		(no velocity)		F
No. 51	K2 II	1957 VII 19.093	−18·1	d	T
No. 52	Ko III	1957 VI 22.127	− 1·8	d	F
No. 58	Ko III	1957 VII 13.095	−11·0	d	T
No. 79	K2 II	1957 VII 16.095	−20·4	d	T

Red Variables

Star	Sp.	Date (U.T.)	Velocity km/sec Emission	Absorption	Camera	Obs.
V1	M2–3 Ib (II–Ib?)	1952 VII 2.118	−19·0	− 2·9	c	T
		VII 14.090	−17·8		c	T
		1953 IX 3.119	−17·3		c	T
		IX 4.047	−21·5	− 7·0	c	F
		IX 12.944	−18·4	− 6·8	c	F
		X 24.840	−12·7		d	T
		X 30.859	−15·7	− 8·9	c	F
		XI 20.853		−13·6	d	F
		1954 XI 19·729	−17·1		d	T
		1955 VII 12.118	−14·0		c	F
			−17·0	− 7·8		
V2	M2–3 II–Ib	1952 VII 7.124	− 5·0	− 2·8	c	F
		VII 15.115	−12·2	− 3·5	c	F
		VIII 3.106	−14·5	− 7·7	c	F
		1957 VIII 2.075	− 4·8	− 6·8	c	F
			− 9·1	− 5·2		
V3	M2–3 II–Ib	1952 XI 9.809	−40·1	−37·0	c	F
		XII 5.799	−46·0	−47·2	c	T
		1953 XI 28.840	−44·1	−43·0	c	F
		XII 1.797	−41·8		d	F
		1959 VIII 15.052	−34·9	−23·7	c	F
			−41·4	−37·7		

TABLE II—*continued*

Red Variables—continued

Star	Sp.	Date (U.T.)	Velocity km/sec Emission	Absorption	Camera	Obs.
V5	M2 II or III (?III)	1953 XII 13.785		−14·6	d	T
		1955 VI 25.125		−15·3	d	T
				−15·0		
V7	M2:	1953 IX 2.991		− 7·7	c	T
V8	M2–3 II:	1953 X 26.862	−37·8	−23·1	c	F

Non-Members

Star	Sp.	Date (U.T.)	Velocity km/sec	Camera	Obs.
Comp b	G8 V:	1953 IX 28.061	+ 1·3	c	T
		XI 23.919	+27·3	d	T
			+14·3		
No. 22	F8 V	1953 X 23.915	−13·5	d	F

Notes on Table II.—The table gives the star number, the spectral type, the time of mid-exposure (U.T.), the velocity (km/sec), the camera used (cf. Table I) and the initial of the observer. (B) in the last column indicates that the ' star ' observed is a blend of more than one star.

These results will be discussed in the following sections; it is convenient, however, at this stage to draw attention to stars No. 22 and *b* (a Harvard comparison star). These two stars are classified as late type dwarfs and their types leave no doubt that they are foreground stars. The magnitude of No. 22 is about the same as that of the red giant members and that of *b* is rather brighter than this. The velocity of *b* is definitely discordant from the adopted cluster velocity of −14·2 km/sec (see below). Though the velocity of No. 22 agrees rather well with the cluster velocity this agreement must be fortuitous. These two stars are omitted from further discussion.

Spectral types of the red giants.—Spectral types of the red giants were obtained on the MK system by comparison with standard stars. The 23 stars in the category are a selection of the brightest non-variable stars, distributed fairly uniformly about the centre of the cluster and fairly close to the centre compared with the distance to which the cluster can be traced (26′·8).

It should be emphasized that the photograph reproduced in Plates 10 and 11(i)*a* is a light exposure to show the stars studied and does not give a correct impression of the size of the cluster. The stars range from the brightest non-variable stars to stars about a magnitude fainter. The spectral types in Table II show a continuous range of types from G8 to M2 with luminosity class between II and III. There are 5 stars of type G, 11 of type K and 7 of type M. It is well known (cf. (3)) that some globular clusters show marked spectral peculiarities. Weakening of the metal lines with respect to hydrogen has been particularly noted (e.g. in M92) and this is usually interpreted as a real metal deficiency in these stars. The giants in 47 Tuc were therefore examined for any sign of this effect. In particular, following Deutsch (3) we have studied line ratios involving hydrogen and the metals (e.g. CH or Fe I 4325/Hγ) and ratios involving metals alone (e.g. Cr I 4254/Fe I 4250). Whilst it is found that in a cluster such as M92 much earlier

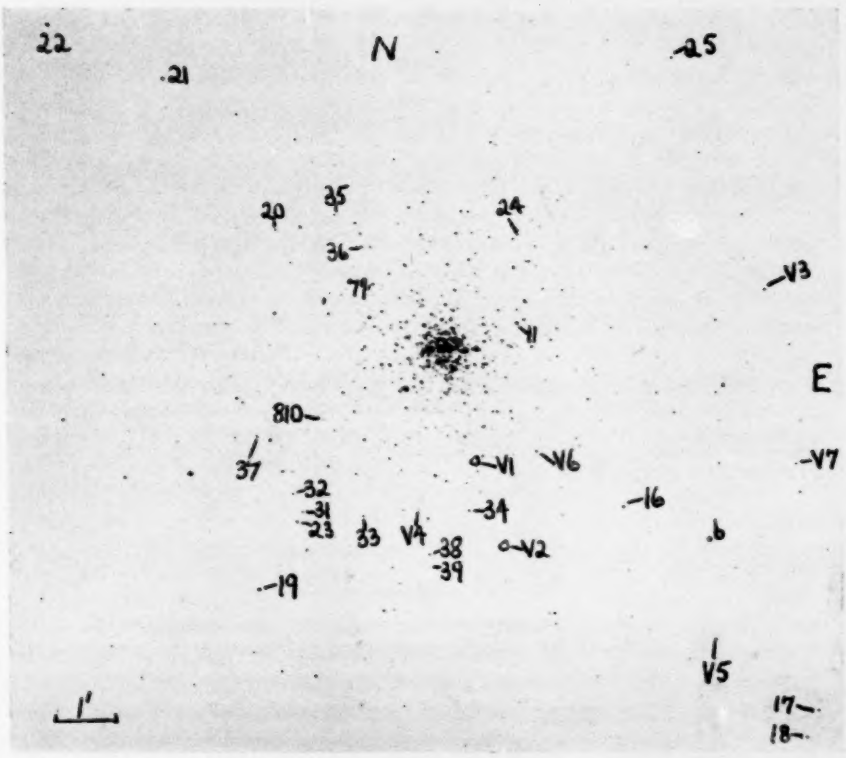

74-inch Newtonian photograph of 47 Tuc (blue light) identifying stars discussed in text. Some stars not discussed are given Radcliffe numbers. The Bailey variables are marked " V " and HV 810 (RR Lyrae type) is also marked.

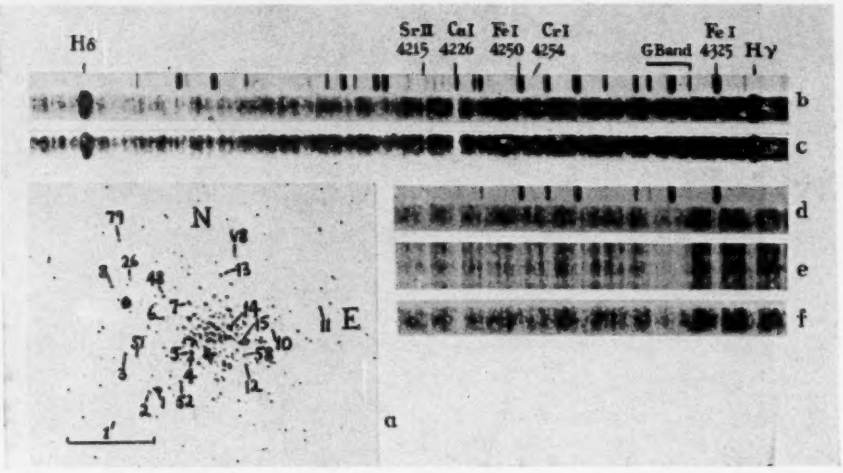

(i)

(a) Enlargement of central region of 47 Tuc (blue light); (b)–(f) Spectra in the violet region (approx. 4100–4350A) of stars in 47 Tuc and comparison stars. All spectra are enlargements from c camera plates; (b) 47 Tuc V.1 (212d Me variable) with Iron Arc comparison; (c) RV Pup 190d galactic Me variable; (d) 47 Tuc No. 6 G8 III (with Iron Arc comparison); (e) δ Boo standard G8 III+CN–1; (f) 47 Tuc No. 14 M1 II.

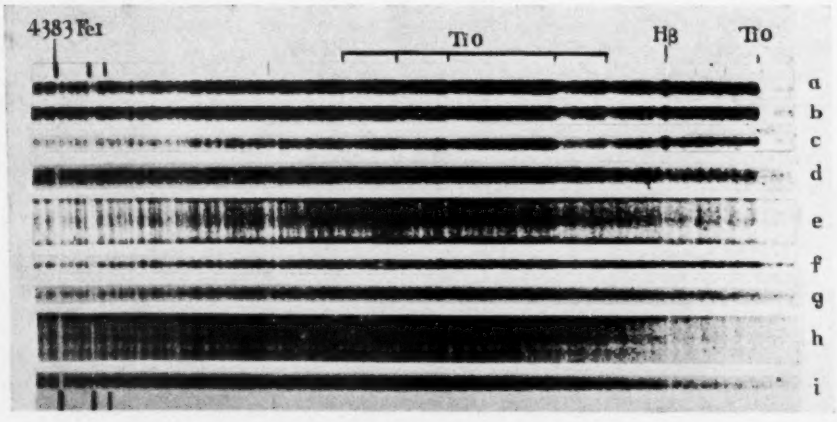

(ii)

Spectra in the blue region (approx. 4380–4980A) of stars in 47 Tuc and comparison stars. All spectra are enlargements from c camera plates.

(a) 47 Tuc V1 (212d Me variable) with Iron Arc comparison; (b) RV Pup 190d galactic Me variable; (c) 47 Tuc V3 (192d Me variable); (d) 47 Tuc No. 14 M1 II; (e) κ Ser standard M1 III; (f) 47 Tuc No. 26 M2 II (or II–III); (g) 47 Tuc No. 3 K3 III (–); (h) δ Boo standard G8 III+CN–1; (i) 47 Tuc No. 6 G8 III with iron arc comparison.

M. W. Feast and A. D. Thackeray, 47 Tucanae.

types are indicated by the former ratios than the latter, in the case of 47 Tuc the two methods agree well. Thus 47 Tuc is much closer to the "normal" population I giants than to the extreme population II giants of some globular clusters. Examination of the 47 Tuc G–K spectra in the light of the criteria established by Keenan and Keller (**4**) for high velocity stars shows that whilst the 47 Tuc spectra are much more like the normal giants of the MK system than the metal weak globular cluster giants, there is a slight weakening of CN in the 47 Tuc stars of a comparable amount to that found in the high velocity stars. In the M type stars the types were determined in the usual way from the strength of the TiO bands. These types were found to agree well with those determined from atomic line ratios (line criteria for M types being taken from Keenan's work (**5**)). In Plate II (i) and (ii) some typical spectra of stars in 47 Tuc are reproduced. The spectra shown were all taken at an original dispersion of 49 A/mm at Hγ. Some standard stars are also shown for comparison including δ Boo which is a high velocity star with a slight CN weakening (G8 III + CN − 1) (see Keenan (**6**)).

The fact that the giants in 47 Tuc appear from their spectra to be nearer to "normal" population I giants than to the extreme population II stars lends great interest to the HR diagram for this cluster. Whilst a full discussion must naturally await the publication of the photometric results certain facts can be ascertained from the spectra themselves:

(1) 47 Tuc contains non-variable M giants, that is, the stars at the tip of the giant branch are later in type than those found in any other globular cluster so far;

(2) the luminosity classes assigned to the giants in 47 Tuc (II–III) are fainter than those generally assigned in other clusters (II–Ib) (cf. (**7**)).

We may deduce from these spectroscopic results that:

(3) the giant branch in the HR diagram in 47 Tuc lies below and to the red of those of other globular clusters thus far studied. The preliminary photometric results (**1**) bear out these deductions.

These observations appear to fit well with presently held ideas as to the interpretation of the HR diagram of globular clusters. The spectral peculiarities of globular cluster giants is attributed to a low metal/hydrogen ratio, and Hoyle and Schwarzschild (**8**) showed that the position of the giant branch in the HR diagram is sensitive to this ratio. The giant branch is depressed and extends farther to the red for the clusters with a more normal (population I) ratio. The exact position of the giant branch computed theoretically is critically dependent on the mixing length in the stellar model (**9**) and has not yet been fixed completely satisfactorily. Kinman (**7**) has investigated in a semi-quantitative manner the spectral types of stars in globular clusters and their relation to the metal/hydrogen abundance ratio. He finds no peculiarities in the *integrated* spectrum of 47 Tuc and deduces that the metal/hydrogen ratio is unlikely to be less than 1/10 normal. Our observed CN weakening in the giants is near the limit of detection on our plates and places the 47 Tuc stars in the same category as the high velocity stars showing this abnormality. The work of Schwarzschild *et al.* (**10**) and the discussion by Keenan (**11**) indicate that in the giants showing extreme high velocity characteristics the metal/hydrogen ratio does not drop below that of ordinary giants by a factor of more than 3 or 4. Until a proper curve of growth analysis of 47 Tuc can be carried out, we may tentatively adopt a metal/hydrogen ratio of not less than about 1/4 normal, since the CN weakening in the 47 Tuc stars is not particularly marked. It should be noted that the above remarks apply only to the G and early K stars in

47 Tuc. For stars of later type additional sources of opacity other than hydrogen are undoubtedly present and an analysis such as that given by Kinman breaks down. It may be recalled that the spectra of the RR Lyrae stars in 47 Tuc (**2**) show evidence of a moderate abundance anomaly. We may conclude that the cluster shows some metal deficiency compared with normal population I stars but to a less extreme degree than any other globular cluster so far studied.

It should be mentioned that star No. 10 appears on at least one spectrogram to have exceedingly weak hydrogen lines whilst on other spectrograms these appear to be normal for the type. The most probable explanation is that there is weak H emission occuring from time to time. Perhaps the star is variable and it would be interesting to examine it photometrically.

The distance modulus of 47 Tuc.—In later sections we shall require a value for the distance of 47 Tuc. Shapley (**12**) deduced a modulus of 14·7. This distance modulus would make 47 Tuc extremely bright with an integrated photographic absolute magnitude of $-10{\cdot}0$ (**13**) compared with an average value of about $-8{\cdot}2$ (**6**). It would also make the Me variable members much brighter than similar stars in the general field (see below). Shapley's estimate was based on the magnitude of the brightest stars, assuming this to be the same in all clusters. The dependence of the position of the giant branch on chemical composition discussed above renders this assumption invalid. In particular the giants in 47 Tuc will be absolutely fainter than those in other clusters so that Shapley's modulus will have been overestimated. Preliminary consideration (**1**) of the luminosity classes of the 47 Tuc giants and of the colour magnitude diagram led to a modulus in the range $13^{m}{\cdot}5$ to $14^{m}{\cdot}0$. Since that time it has been shown (**2**) that two RR Lyrae stars are cluster members. The *c*-type variable which has been studied photoelectrically has a median magnitude (V) of $13^{m}{\cdot}9$. Provided we adopt a value for the absolute magnitude of the RR Lyrae stars (M_v) this star then gives a distance modulus. Unfortunately the absolute magnitude of the RR Lyrae stars at median light remains in some doubt. A value of $0^{m}{\cdot}0$ was adopted for many years but recently values near $+0^{m}{\cdot}5$ have found favour ((**14**), (**15**); see also (**16**) and (**7**)). In the following we shall derive quantities based on both assumptions and it will appear that in general the results are best interpreted if the absolute magnitude of the RR Lyrae stars in 47 Tuc is $+0^{m}{\cdot}5$.

It is not known exactly how much correction for absorption is necessary. However studies of foreground stars in the direction of the Small Magellanic Cloud (i.e. in the same region of the sky) indicate (**17**) a probable absorption correction of about $0^{m}{\cdot}2$. The distances deduced from these data are given in Table III.

TABLE III

Distance of 47 Tuc and absolute magnitudes

Assumed M_v of RR Lyrae Stars	$0^{m}{\cdot}0$	$+0^{m}{\cdot}5$
Uncorrected distance modulus	$13^{m}{\cdot}9$	$13^{m}{\cdot}4$
Corrected distance modulus	$13^{m}{\cdot}7$	$13^{m}{\cdot}2$
Distance	5·5 kpc	4·4 kpc
Mean m_v for red giants studied	$11^{m}{\cdot}3$	
Mean M_v of red giants	$-2^{m}{\cdot}6$	$-2^{m}{\cdot}1$
Mean M_v of red giants from spectra (II–III)	$-1^{m}{\cdot}4$	
Integrated photographic apparent magnitude of cluster (**13**)	$4^{m}{\cdot}7$	
Integrated photographic absolute magnitude of cluster	$-9^{m}{\cdot}2$	$-8^{m}{\cdot}7$

Since the preliminary photometric results (Wesselink, unpublished) indicate that the red giants studied spectroscopically have an average visual magnitude (m_v) of near $11^m{\cdot}3$, the absolute magnitudes for these stars on the two hypotheses are shown in Table III. An absolute magnitude of $-2^m{\cdot}6$ would place the stars in luminosity class II according to the calibration of the MK system by Keenan and Morgan (**18**). But an absolute magnitude of $-2^m{\cdot}1$ would be in good agreement with the assigned luminosity class (III–II) as discussed above.

Arp (**19**) finds the integrated absolute magnitudes of 7 clusters ranging from $-7{\cdot}6$ to $-8{\cdot}9$. Since they depend on an absolute magnitude for the RR Lyrae stars of $0^m{\cdot}0$ these figures must be compared with the value derived for 47 Tuc on our first assumption, *viz.* $-9^m{\cdot}2$ (assuming the absolute magnitude of the RR Lyrae stars does not change from cluster to cluster, as is possible). The integrated magnitude of 47 Tuc is, then, greater than that of the clusters in Arp's list but not surprisingly so if account is taken of the considerable spread amongst these 7 clusters.

The radial velocities of the red giants

(*a*) *c camera velocities* (49*A*/*mm*).—All the plates (19 plates of 15 stars) were measured on the Observatory's projection measuring machine (**20**) by MWF and 16 of these plates on a Hilger machine by ADT. The measurements were reduced in both cases using wavelengths deduced from α Boo (**21**). In many cases weighted means of lines seen multiple at high dispersion had to be used. Using the 16 spectra in common between the two measurers we deduce the following means from these spectra:

ADT	$-17{\cdot}6$ km/sec
MWF	$-13{\cdot}9$ km/sec.

When, however, the measurements were reduced, using for each spectrum only lines measured by both measurers, we find for the means:

ADT	$-15{\cdot}3$ km/sec
MWF	$-15{\cdot}5$ km/sec.

This improvement in the agreement of the two sets of measures is probably due to the rejection of spurious lines, lines at the margin of visibility, misidentified lines, etc. It has, therefore, appeared best for the c camera results to adopt the velocities derived in this second manner and to take a straight mean of the results of the two measurers. A list of the wavelengths used is given in Table IV.

Where possible velocities were also derived from wavelengths for G and K stars at this dispersion used at Victoria (**22**). Unfortunately, sufficient Victoria lines to give a significant velocity could not be measured in a good many of the spectra, so that the results obtained in this way were not used in deriving the mean velocities of the stars. However the "Victoria" velocities will be needed in the later discussion.

(*b*) *d camera velocities* (86*A*/*mm*).—The 16 plates of 15 stars were measured on the projection micrometer. The wavelengths adopted for the reductions were those used at this dispersion by Kinman (**23**) in his globular cluster work. These wavelengths are provided with corrections according to spectral type to Ko but not later. The Ko corrections have therefore been used for all the later type stars.

TABLE IV

Wavelengths used for the reduction of the c camera plates (with principal contributors in the case of α Boo)

4667·84	Fe+Ti	4430·62	Fe
46·80	Fe+Cr	29·83	Ca II
05·77	Ni+V	22·01	Fe+V
4586·14	Ca+V+⊙	18·04	Ti II+Fe
71·32	Mg+Ti II	15·11	Fe
64·67	Cr+Fe+Ti II.	08·47	Fe+V
49·35	Ti II+Ti	04·74	Ti+Fe
45·32	Ti II+Cr+V	00·49	Sc II+SiF
22·78	Ti	4395·15	Ti II+V
18·04	Ti	83·50	Fe
12·75	Ti	75·98	Fe
01·29	Ti II	67·86	Several
4496·53	Ti+Cr	51·49	Cr
94·56	Fe	40·48	Hγ
88·61	Several	37·50	Fe+Ti II
68·52	Ti II	25·55	Fe+Sc II
62·05	Fe+V	20·85	Sc II+Ti II
54·76	Ca	4314·78	Ti
43·82	Ti	4254·36	Cr
35·64	Several	50·46	Fe

(*c*) *Discussion.*—The mean velocities of the cluster derived from c and d plates appear to be significantly different. We find a mean difference between the results of the two cameras of $c-d=+10{\cdot}0\pm3{\cdot}5$ (s.e.) km/sec. A difference of about 10 km/sec between c and d camera plates of the same star has also been found in the case of early type stars in the Magellanic Clouds (i.e. at the same zenith distance) (unpublished material) whereas the standard B star τ Sco which passes near the zenith in Pretoria shows very good agreement between c and d camera velocities. We may infer from this that the effect depends on zenith distance. (The considerable amount of earlier work with the c camera shows that the effect is not in the velocities from that camera.) It may be that atmospheric dispersion affects the guiding at the wide slit used with the d camera. Atmospheric dispersion might be expected to give an effect of the right sign and magnitude. However Kinman (**23**) has argued from the agreement of the velocities derived from integrated spectra of clusters and from the spectra of individual members that any effect due to atmospheric dispersion is unimportant. If such is the case the effect must have some other cause. In view of these findings we have applied a correction of + 10 km/sec to all the d camera velocities. The final means (Table II) are derived giving equal weight to the c and d camera velocities.

The mean velocity of 47 Tuc derived from 22 red giants (35 spectra) giving unit weight to each star is −14·2 km/sec. Kinman (**23**) gives a velocity of −24 km/sec from 5 accordant integrated spectra of 47 Tuc obtained with the d camera. It will be noted that if our correction of + 10 km/sec is applied to this mean it agrees exactly with ours.

Velocity dispersion of the red giants.—One of the aims of the present investigation was to attempt to obtain an estimate of the mass of 47 Tuc from the velocity dispersion in the cluster. Before proceeding to this attempt we investigate the velocities for a dependence on spectral type.

Plots of the velocities of the individual red giants against spectral type are shown in Fig. 1. This figure appears to show, and statistical tests indicate, a significant variation of the mean velocity with spectral type. As will be seen from Figs. 1 to 4, this variation is shown not only by the adopted velocities but also (i) by the c camera velocities alone derived as discussed above from the α Boo wavelengths (ii) by the d camera velocities alone derived from Kinman's globular cluster wavelengths; and (iii) by the c camera velocities reduced according to the Victoria wavelengths. The fact that the different dispersions and different wavelength systems all show the same effect indicates that it is unlikely to be due to erroneous wavelengths. The c camera line residuals were examined to see if any residuals showed large dependence on spectral type but that was not found to be the case.

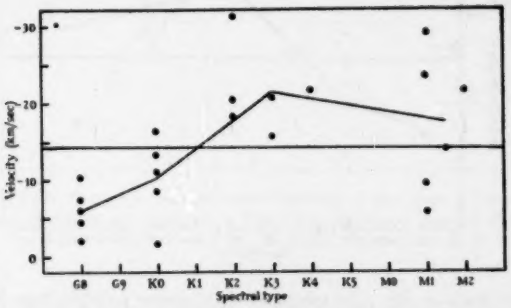

FIG. 1.—*Plot of the adopted velocities of individual red giants in 47 Tuc against spectral type. The mean velocity of the stars is indicated by the horizontal line and a line joins the means for the groups G8, K0, K2–K4 and M1–M2.*

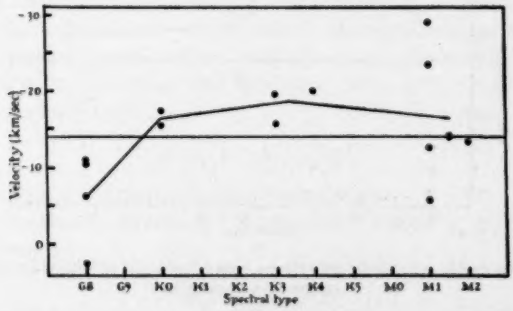

FIG. 2.—*Same as Fig. 1 but using only the c camera velocities from Table II (α Boo wavelengths).*

In M92 (**24**), the only other cluster for which radial velocities of an appreciable number of stars have been determined, the spectral types of these stars have not been given so a test for this effect cannot be made. In Fig. 5 the velocities are shown on the plane of the sky. There appears to be no significant variation of velocity with position in the cluster. In particular, the cluster does not exhibit significant rotation.

Although an instrumental origin for the dependence of radial velocity on spectral type cannot be completely disproved, it is of interest to note that a physical

origin can be suggested which is in line with modern ideas concerning atmospheres of red giants. It is known that late type giants of comparable absolute magnitudes to those in 47 Tuc are suffering mass loss with velocities of the order of 10 km/sec ((**25**) etc). In the case of the globular cluster giants studied, these lie at the tip of the giant branch where helium burning accompanied by a considerable change in stellar structure is believed to occur (**8**). The details of stellar evolution at this point are only qualitatively defined but the possibility of considerable mass loss here has been discussed (cf. (**26**)).

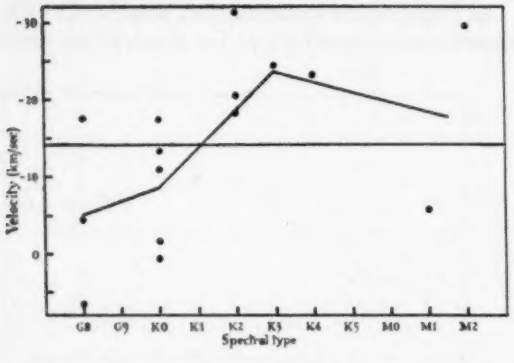

FIG. 3.—*Same as Fig. 1 but using only the d camera velocities from Table II.*

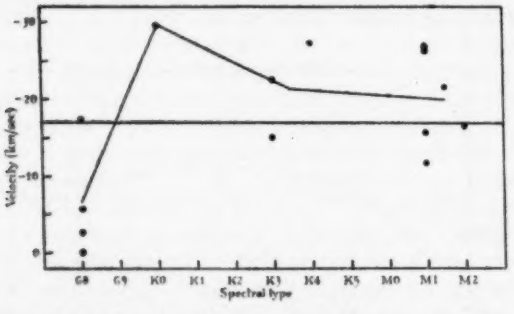

FIG. 4.—*Same as Fig. 1 but using only those c camera velocities determined with the Victoria system of wavelengths.*

It appears therefore feasible that an outward flow of matter in the atmosphere of the late K and M giants in 47 Tuc would explain the observations. If this is the case we might expect to find a relation between the velocity derived from any given line and the line's excitation potential (Deutsch (**25**) lists examples of such a relation for Me variables and some other stars). Unfortunately the present data, in particular the fact that so many lines are blends, is insufficient to test for this relationship.

If we accept the correlation of velocity and spectral type as real, whether instrumental or physical in origin, attention must be paid to it; for it will have a profound effect on the velocity dispersion and the mass deduced for the cluster. Bearing this

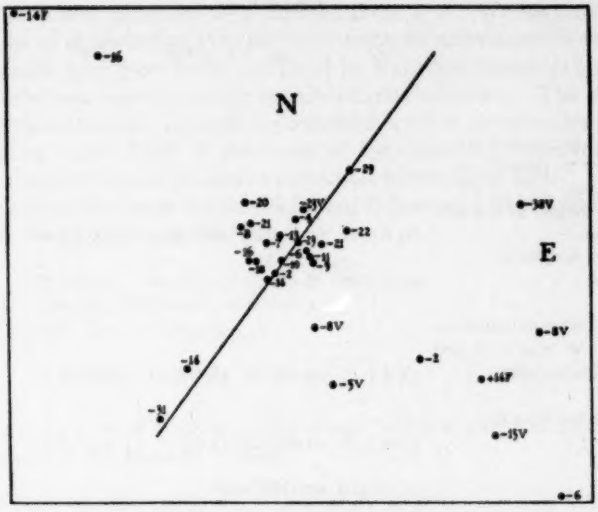

FIG. 5.—*Plot of the stars with measured radial velocity on the plane of the sky. The radial velocities to the nearest km/sec are indicated. The red variables are marked V and the two field stars F. The line represents the major axis of the cluster (H. Shapley and H. B. Sawyer, H.B.* 852 1927).

in mind we now proceed to a discussion of the velocity dispersion in 47 Tuc. We have 35 spectra of 22 red giants not known to be variable. For 2 stars there are 4 spectra, for 7 stars 2 spectra, and for 13 stars only 1 spectrum each. From these data we calculate the dispersions listed in Table V. In this table σ_e is the observed velocity dispersion obtained by giving equal weight to each star. σ_0 is the dispersion per spectrum of unit weight due to observational error (and possible real variation in the measured stellar radial velocity). This quantity is obtained from the 9 stars with more than one spectrum each. If σ is the true velocity dispersion then we have (**27**)

$$\sigma^2 = \sigma_e^2 - \sum^{i} \nu_i \sigma_0^2 / i \qquad (1)$$

where i = the number of plates of unit weight per star
ν_i = the fraction of stars with i plates of unit weight σ_w given in Table V is defined by

$$\sigma_w^2 = \sum^{i} \nu_i \sigma_0^2 / i.$$

The dispersions given in Table V have been calculated in the usual manner, that is, from the sums of the squares of the deviations from the means (suitably weighted) divided by the number of degrees of freedom in each case. The errors quoted are standard errors.

We have derived the true dispersion (σ) both ignoring and taking into account the variation of velocity with spectral type discussed above. In the case where we ignore the variation of velocity with type (i.e. where we regard it as a chance fluctuation in the velocities sampled) we give for comparison the results calculated giving equal weights to the c and d camera plates and those obtained giving doubled weight to the c camera plates. The results do not differ significantly. In taking

TABLE V

	σ_e^2	σ_0^2	σ_w^2	σ^2	Corresponding mass (cf. Table VI).
No correction applied for dependence of velocity on spectral type.					
(1) Equal weight to c and d plates.	$69{\cdot}6 \pm 22$	$62{\cdot}9 \pm 25$	$48{\cdot}6 \pm 19$	$21{\cdot}0 \pm 29$	M_1
(2) Double weight to c plates.	$65{\cdot}2 \pm 20$	$88{\cdot}9 \pm 35$	$50{\cdot}7 \pm 20$	$14{\cdot}5 \pm 28$	M_2
After correction for dependence of velocity on type. Equal weight to c and d plates.	$38{\cdot}5 \pm 13$	$62{\cdot}9 \pm 25$	$48{\cdot}6 \pm 19$	$-10{\cdot}1 \pm 23$	M_3
M92 reduced by the same method	$41{\cdot}2 \pm 16$	$21{\cdot}0 \pm 10$	$15{\cdot}4 \pm 8$	$25{\cdot}8 \pm 17$	

Units are (km/sec)²

into account the observed variation of velocity with type we have divided the stars into four groups (G8, K0, K2–4 and M1–2) and obtained a joint estimate of σ_e from these four groups. It will be noticed that in this case since $\sigma_e < \sigma_w$ the value of σ^2 (the true dispersion) derived is negative though of course not significantly less than zero. The considerable difference between the values of σ^2 obtained by ignoring or taking into account the variation of velocity with spectral type will be noted. It is therefore quite clear that any mass determination must be treated with reserve. However, it will be shown that a good upper limit to the mass may still be determined.

The only other work so far published on the velocity dispersion in globular clusters is the investigation of M92 by Wilson and Coffeen (**24**) whose results have also been re-discussed by Schwarzschild and Bernstein (**28**). For comparison with our results we have reduced the M92 results according to the procedure adopted for 47 Tuc and outlined above. From 23 spectra of 15 stars we deduce the dispersions given in Table V for M92. Our velocity dispersion and its error for M92 are somewhat larger than that given by (**24**) and (**28**) ($\sigma^2 = 19{\cdot}5 \pm 9$ (km/sec)²) for the following reasons. In the case of the dispersion itself we have derived σ_e and σ_0 from the squares of the deviations from the mean whereas Wilson and Coffeen (**24**) preferred to employ the modulus of these deviations. Further our result is obtained by combining σ_e and σ_0 according to equation (1). The error quoted for σ^2 by Schwarzschild and Bernstein (**28**) (viz. 9 (km/sec)²) is a probable error and therefore needs multiplying by 1·48 to be comparable with our quoted standard error. Apart from this trivial difference there is another more important difference. The variance, σ^2, is obtained as the difference of two variances and its standard error is thus determined from the standard errors of the two variances differenced. The manner in which these two standard errors are combined to form the standard error of σ^2 depends on whether or not the two variances differenced are correlated or not. Schwarzschild and Bernstein (**28**) assume a fairly high degree of correlation in deducing their uncertainty for σ^2. If they had taken the variances differenced as uncorrelated then the uncertainty

of σ^2 would have been increased by a factor of about $\sqrt{2}$. We have calculated the standard error of σ^2 assuming that the two variances differenced in equation (1) are uncorrelated, as appears to be indicated by statistical theory (**29**). Should correlation exist, our standard error is then an over-estimate. The matter is of some importance since the value of the standard error of σ^2 enters into the determination of an upper limit of the mass of the clusters. Schwarzschild and Bernstein's procedure would lead to a somewhat lower upper limit.

In determining the mass we have followed Schwarszchild and Bernstein (**28**) and used the virial theorem in the form

$$\bar{V}^2 = GM/\bar{r} \tag{2}$$

where G = the gravitational constant;
M = the mass of the cluster

$$\tfrac{1}{3}\bar{V}^2 = \sigma^2 \quad \text{and} \quad \bar{r} = 2\left(\int_0^R S\,dq\right)^2 \Big/ \int_0^R S^2 dq \tag{3}$$

$S(q)$ being the number of stars in a strip of unit width at perpendicular distance q from the centre of the cluster. Thus

$$S(q) = 2\int_q^R n(I)\,d(I^2 - q^2)^{1/2} \tag{4}$$

where $n(I)$ is the number of stars per unit area at distance I from the centre of the cluster.

For M92 Schwarzschild and Bernstein obtained $n(I)$ from published star counts and deduced $\bar{r}$ by numerical integration. For 47 Tuc we have used the surface photometry of Gascoigne and Burr (**13**) who tabulate the equivalent number of tenth magnitude stars per unit area at different distances from the cluster centre. We therefore assume a constant mass to light ratio throughout the cluster. Whilst this may not be strictly true, in view of the radial variation of colour in the cluster (**13**) the error thus introduced will probably be negligible for our purpose.

Then by numerical integration of (4) and (3) we find

$$\bar{r} = 409''.$$

The conversion of this to linear measure depends on the adopted distance modulus discussed above. For the two alternative distances we obtain the results listed in Table VI. This table also contains the mass deduced from the dispersions of Table V according to equation (2). Since the value of σ^2 derived if allowance is made for the dependence of velocity on type is negative we in principle derive a negative mass. The result is not significantly different from zero and has not been entered in Table VI. The result still however allows a determination of the upper limit of the mass and this is included in Table VI. The upper limits to the mass are determined from the quoted standard errors. If the distribution is normal there is 0·84 probability that the mass is not greater than the deduced mass by more than its standard error and 0·98 probability that it is not greater by more than twice its standard error.

Despite the problem of the variation of the velocity of the 47 Tuc stars with spectral type, Table VI shows that we can still deduce useful upper limits to the mass. Thus it would appear very unlikely under any assumption that the mass is greater than $6{\cdot}0 \times 10^5$ solar masses and on our most favoured distance there appears a good probability that it is less than about $4{\cdot}5 \times 10^5$ solar masses. If the variation

TABLE VI

Limits to masses of 47 Tuc and M92

47 Tucanae		
Adopted M_v of RR Lyrae stars	$0^m.0$	$+0^m.5$
$\bar{r}$	10·9 psc	8·6 psc
Mass (uncorrected for variation of velocity with spectral type and equal weight to c and d plates). Solar masses (M_1)	$(1.6 \pm 2.2) \times 10^5$	$(1.3 \pm 1.7) \times 10^5$
Mass (uncorrected for variation of velocity with spectral type and double weight to c plates). Solar masses (M_2)	$(1.1 \pm 2.2) \times 10^5$	$(0.9 \pm 1.7) \times 10^5$
Upper limits to mass:		
With 0·84 probability M_1	$< 3.8 \times 10^5$	$< 3.0 \times 10^5$
With 0·98 probability M_1	$< 6.0 \times 10^5$	$< 4.7 \times 10^5$
Mass (M_3) after correction for variation of velocity with spectral type and with equal weights to c and d plates.		
Upper limits to mass:		
With 0·84 probability M_3	$< 1.0 \times 10^5$	$< 0.8 \times 10^5$
With 0·98 probability M_3	$< 2.7 \times 10^5$	$< 2.2 \times 10^5$
Mass (M_1) to light ratio (solar units)	0.3 ± 0.4	0.3 ± 0.4
M92 re-reduced		
Mass of M92 (solar masses)	$(1.8 \pm 1.2) \times 10^5$	
Upper limit to mass of M92:		
With 0·84 probability	$< 3.0 \times 10^5$	
With 0·98 probability	$< 4.2 \times 10^5$	
Mass/light ratio (M92)	1.0 ± 0.7	

of velocity with type is considered established then we reduce the upper limit even more; the mass being unlikely to be more than about 2.5×10^5 solar masses. As shown in Table VI results of the same order of magnitude are found for M92 and the results may also be compared with the mass of M3 (1.4×10^5 solar masses) derived from the luminosity function (**30**).

The mass to light ratio in 47 Tuc is low (see Table VI). This confirms the previous estimates (**31**) that this ratio is much less in globular clusters than in elliptical galaxies. A recent analysis by Münch (**32**) suggests that mass/luminosity ratio may be the same in intermediate spirals and giant ellipticals and about 30 or 40. Hence it would appear that the ratio is significantly different in globular clusters from either of these two types of systems.

The radial velocity and spectral type of the bright blue star.—Star No. 1 which is easily the brightest star photographically has a visual magnitude of 10·26 (Wesselink, unpublished) and is quite blue. As seen in Table I, its velocity is -14.2 km/sec. This is in good agreement with the mean velocity of the red

giants (−14·2 km/sec), the exact agreement of course being fortuitous. There is therefore good reason to believe the star to be a cluster member especially as to the evidence of the radial velocity we may add the facts that the star lies quite close to the cluster centre and that blue stars of this magnitude are relatively rare at this galactic latitude. We have classified the star as B8 III (H, He I, Mg II, Ca II and Si II all being found) and no peculiarities were noted in the spectrum. Two blue stars such as this have been proved as members of M13 and M3 respectively from radial velocity considerations and more stars of this sort are believed to be members of other clusters (cf. (**33**)). The star in M13 is classified as B2V and that in M3 as O8. In neither case have peculiarities been noted either in the spectra or the colours. The presence of such stars has been generally regarded as a problem as it seems they must be considerably younger than the majority of the stars in the clusters. A similar situation is found to exist in young galactic clusters (**34**) where some stars are also found which are apparently younger than those of the main body of the cluster. Perhaps these bright blue stars in globular clusters represent a second generation of stars formed out of matter ejected by stars that have passed through the red giant phase. Further investigation of these stars is clearly desirable.

From the measured visual magnitude of Star No. 1, we deduce its absolute magnitude on our two alternative distances (Table VII).

TABLE VII

The absolute magnitude of the bright blue ★ *No. 1* (B8 III)

Adopted M_v of RR Lyrae stars	$0^m{\cdot}0$	$+0^m{\cdot}5$
Absolute visual magnitude of No. 1	$-3^m{\cdot}6$	$-3^m{\cdot}1$
Absolute visual magnitude from spectrum	$-3^m{\cdot}0$	

The spectral type gives the absolute magnitude shown according to the calibration of Morgan and Keenan (**18**). The result may be taken as another indication that the observations are better satisfied with the smaller distance.

Radial velocities and spectral types of the red variables.—47 Tuc contains several bright red variable stars and a considerable amount of time has been spent studying them spectroscopically. The red variables of greatest interest are Bailey Nos. 1, 2, 3 (**35**) which appear to be regular long period variables with periods near 200^d. The irregular variables Bailey Nos. 5 and 7 and the semi-regular variable Bailey No. 8 have also been observed. Altogether we have 22 spectra of the 6 stars, 16 of them on the c camera and the rest on the d camera with all but 4 of the spectra referring to variables 1, 2 and 3. The variables are identified on Plates 10 and 11 (i) and Table VIII is reproduced for convenience from data in Mrs Hogg's catalogue (**36**).

Consider first the three regular variables. Their nearly identical magnitudes and periods as well as their relative closeness to the centre of the cluster (distances of 2′·0, 3′·4 and 5′·5 respectively compared with an estimated radius of 47 Tuc of 26′·8 (**37**)) strongly suggests cluster membership. These points were all stressed by Shapley (**12**). We can make membership even more likely by computing the expected number of foreground long period variables. At this galactic latitude Shapley (**38**) finds 19 long period variables down to 14^m in 400 square degrees or 0·048 variables per square degree. Within a radius of 6′ we

TABLE VIII

Red variables in 47 Tucanae

Bailey No.	Mag (pg) Max.	Min.	Period
1	11·3	< 16·0	212^d40
2	11·55	15·3	202^d84
3	11·35	16·1	192^d34
5	13·0	14·0	Irr
7	13·3	13·8	Irr
8	12·7	14·7	$150^d \pm$ (cycles)

therefore expect only 0·0015 long variables and furthermore this refers to stars of all periods and of all magnitudes down to 14^m. Similar considerations apply to the irregular variables.

The radial velocities for the c camera spectra were obtained from measures with the projection micrometer using the absorption line wavelengths adopted by Merrill (**39**) in his extensive investigations of Me variables. Also following Merrill, laboratory wavelengths were adopted for the hydrogen emission lines. In the case of the few d camera spectra these were reduced using Kinman's globular cluster wavelengths (**23**), as discussed above, for the absorption lines and laboratory wavelengths for the emission lines. It may be mentioned that on account of their brightness the spectra of the regular variables at maximum are of better quality and the velocities derived are somewhat more accurate than those of the red giants. The velocities adopted are listed in Table II. As in the case of the red giants a correction of +10 km/sec was applied to the d camera velocities and the c and d camera results were given equal weight in taking the mean.

The velocities of the variables 5, 7 and 8 (viz. −15·0 −7·7 and −23·1 km/sec) agree with the cluster velocity of −14·2 km/sec within the limits to be anticipated from the velocity dispersion as discussed above. The measured radial velocities of the three long period variables are rather puzzling and require some discussion. Whilst the mean of the three radial velocities deduced from the absorption lines (−7·8, −5·2 and −37·7 km/sec) is −16·9 km/sec and clearly agrees as well as can be expected with the mean cluster velocity (−14·2 km/sec) yet the three velocities scatter rather widely about the mean. Examination of the velocities in Table II shows that whilst several red giant members have velocities as high or higher than variables 1 and 2, the velocity of variable 3 is lower algebraically than that of any other star measured in the cluster. We may note in this connection that the mean square space velocity in the cluster is $3 \times 21 = 63$ (km/sec)^2 taking the larger estimate of the velocity dispersion given above. According to Chandrasekhar ((**40**) eq. 5·306, p. 206) the mean square velocity of escape is four times this. Thus the root mean square velocity of escape is $\sqrt{63 \times 4} \div 16$ km/sec. The radial velocity of variable 3 differs from that of the cluster (−14·2 km/sec) by 23·5 km/sec which taken at its face value means that the variable could be (but is, of course, not necessarily) escaping from the cluster (though it is worth noting that Kurth (**41**) considers the above equation for the velocity of escape as "of little significance").

The question naturally arises, does this place the membership of variable 3 and perhaps also of variables 1 and 2 in doubt? The predicted numbers of field variables given above is so small that even allowing for a fairly large margin of error in the estimates we still find the probability of the stars being foreground variables as practically negligible. Further, besides the nearly identical magnitudes and periods of these three stars, we have the fact that so far as can be judged from the available data the median visual magnitudes of the variables are about the same as those of the stars at the tip of the giant branch. This result would probably be expected if the variables are really cluster members. Furthermore it is shown below that the variables are normal Me variables. Merrill's work (**42**) shows that the Me variables of about 200 day period have large peculiar motions so that even an approximate agreement of radial velocities for the three variables with that of the cluster is unlikely unless they are really members. It appears rather safe therefore to adopt the view that these variables are indeed cluster members. The rather high velocity dispersion indicated for these three stars and in particular the low velocity of variable 3 remains an outstanding problem. We have already discussed a possible dependence of velocity on spectral type for the red giants and perhaps we may see in the results for the variables an extension of this phenomenon. In this case the measured radial velocities may reflect mass motions in the atmospheres of the variables connected with the evolution of the stars from the top of the giant branch to the horizontal branch, an evolution which may be quite rapid (cf. (**26**)). On the other hand it is possible that variable 3 and perhaps variables 1 and 2 also may be members of binary systems showing orbital motion and it is intended to test this hypothesis by observing these three stars for radial velocity from time to time in the next few years.

We now turn to the spectral types of the variables. An earlier report (**43**) of the three regular variables was based on low dispersion Newtonian spectra. We find all six of the variables studied to be of M type with Ti O bands somewhat stronger than in the latest type non-variable giants and we classify them as M2 or 3. The irregular variables 5 and 7 do not show any emission lines on our spectra. H emission has been found in all three long period variables and in the semi-regular variable 8. The long period variables have luminosity classes in the range II—Ib whilst the other variables appear to be somewhat fainter (II—III).

The long period variables have not been found to show any other emission lines except H although these latter were often very strong. This is consistent with the known behaviour of the Me variables of moderately short period. We find no spectroscopic difference between these three stars and normal Me variables of comparable periods outside clusters. One slight peculiarity was, however, noted on some of the spectra. That is, the ratio Cr I 4254/Fe I 4250 indicated a slightly earlier type than the Ti O bands (i.e. Cr I 4254 is too weak for the assigned type). This effect was not noticed in any of the non-variable M stars in the cluster but Radcliffe spectra of several galactic Me variables also show this weakening of 4254 and it may possibly be a general phenomenon. Incipient emission is one possible cause. In Plate 11(i) and (ii) spectra of variables 1 and 3 are reproduced from 49A/mm($H\gamma$) plates. The normal galactic Me variable RV Pup of period 190^d is shown for comparison. It is known (**44**) that in Me variables there is a dependence on period of the difference between the absorption

and emission velocities. In the case of the three Me variables in 47 Tuc we find an average difference $A-E=+5{\cdot}6$ km/sec whereas Merrill gives a value of +9 km/sec, with a considerable scatter for this period. The agreement is satisfactory.

Since most of the spectra of the three Me variables were taken at or near maximum light there is little evidence of any variation in the spectra with phase. However the spectrum of variable 1 taken on 1953 November 20, when the star was judged to be near minimum light shows a weak apparently normal absorption spectrum and Hδ only in emission, the other H lines being absent.

A definitive determination of the absolute magnitudes must await accurate magnitudes and colours for the variables. However adopting the magnitudes at maximum given in Table VIII and a colour index of +1·7 as is indicated both by the preliminary colour magnitude diagram and by what is known of galactic stars of this type, we obtain the results of Table IX for our two assumptions as to the distance of 47 Tuc.

TABLE IX

Absolute magnitudes of the Me variables ($V1$, $V2$, $V3$)

Assumed M_V of the RR Lyrae stars	$0^m{\cdot}0$		$+0^m{\cdot}5$
Mean apparent photographic magnitude of Me variables at maximum		$11^m{\cdot}5$	
Adopted colour index		$+1^m{\cdot}7$	
Adopted visual magnitude at maximum		$9^m{\cdot}8$	
Deduced absolute visual magnitude at maximum	$-4^m{\cdot}1$		$-3^m{\cdot}6$
Absolute visual magnitude from the spectrum (luminosity class II–Ib)		$-3^m{\cdot}5$	
Absolute visual magnitude from galactic statistics (45)		$-2^m{\cdot}2$	

Irregular and semi-regular variables ($V5$, $V7$, $V8$)

Mean apparent photographic magnitude at maximum		$13^m{\cdot}0$	
Adopted colour		$+1^m{\cdot}7$	
Mean visual magnitude at maximum		$11^m{\cdot}3$	
Deduced absolute visual magnitude at maximum	$-2^m{\cdot}6$		$-2^m{\cdot}1$
Absolute visual magnitude from spectrum (luminosity class II–III)		$-2^m{\cdot}0$	

In the case of the irregular variables it is difficult to compare the deduced absolute magnitude with that of galactic irregulars as these have a rather large spread in absolute magnitude (cf. (46)). The assigned spectral types place the stars between luminosity classes II and III but probably near II. The estimated absolute magnitude from the spectrum was obtained from these luminosity classes and the calibrations of Keenan and Morgan (18). The agreement is satisfactory especially with the value derived from the smaller distance. Table IX also shows that in the case of the three Me variables the agreement between the absolute magnitude based on the distance of the cluster and that derived from the spectrum is best if the smaller distance is used. For Me variables of period about 200 days, Merrill and Wilson (45) derive an absolute magnitude of $-2^m{\cdot}2$ from space motions. In view of the uncertainties involved the difference from $-3^m{\cdot}6$ cannot be considered as significant. Studies in the Magellanic Clouds will probably eventually show whether all 200 day long-period variables are as bright as those in 47 Tuc.

The three 200-day Me variables in 47 Tuc appear to be the only known Me variables in globular clusters although the motions of the variables of this period in the general field suggest that these latter stars are related kinematically to the globular clusters. A number of variables of periods near 100^d exist in globular clusters and Arp (**33**, p. 124) has suggested that these stars represent the short period end of the Me sequence. Whilst it is possible that this is the case, the spectroscopic work on these 100^d variables in clusters (**47**) throws some doubt on such an interpretation. The observed spectra are quite different from normal Me spectra, being considerably earlier in type (early G). It is, of course, true that there are few Me variables with periods quite as short as 100 days in the general field. However SS Her(107^d, M3e) and T Cen (91^d, Moe) are two Me variables that lie in this range and yet they have much later types than the globular cluster variables.

Acknowledgments.—We should like to express our thanks to Dr A. J. Wesselink for placing his preliminary photometric results at our disposal. We are also greatly indebted to him and to Dr P. A. Wayman for some extremely helpful discussions of the statistical treatment of the data.

Radcliffe Observatory,
Pretoria:
1959 *September.*

References

(1) A. D. Thackeray, *Semaine d'Etude Populations Stellaire* Pont. Acad. Sci. (Rome) 1957, p. 69.
(2) M. W. Feast, A. D. Thackeray and A. J. Wesselink, *M.N.*, **120**, 64, 1960.
(3) A. J. Deutsch, *Principes Fondamentaux de Classification Stellaire* (Paris) 1955.
(4) P. C. Keenan and G. Keller, *Ap. J.*, **117**, 241, 1953.
(5) P. C. Keenan, *Ap. J.*, **95**, 461, 1942.
(6) P. C. Keenan, *Trans. I.A.U.*, **IX**, 405, 1955.
(7) T. D. Kinman, *M.N.*, **119**, 538, 1959.
(8) F. Hoyle and M. Schwarzschild, *Ap. J. Supp.*, **2**, 1, 1955.
(9) R. R. Kippenhahn, St. Temesvary and L. Biermann, *Zs. f. Ap.*, **46**, 257, 1958.
(10) M. and B. Schwarzschild, L. Searle and A. Meltzer, *Ap. J.*, **125**, 123 1957.
(11) P. C. Keenan, *Encyclopedia of Physics*, **50**, 100, 1958.
(12) H. Shapley, HR 228, *P.N.A.S.*, **27**, 440, 1941.
(13) S. C. B. Gascoigne and E. J. Burr, *M.N.*, **116**, 570, 1956.
(14) P. P. Parenago, *Per. Zvezd.*, **10**, 193, 1954.
(15) E D. Pavlovskaya, *Per. Zvezd.* **9**, 349, 1954.
(16) A. R. Sandage, *Semaine d'Etude Populations Stellaire*, Pont Acad. Sci. (Rome) 1957, p. 55.
(17) M. W. Feast, A. D. Thackeray and A. J. Wesselink, *Obs.*, **78**, 156, 1958.
(18) P. C. Keenan and W. W. Morgan (in) *Astrophysics*, Ed. Hynek (McGraw-Hill, New York, 1951) p. 23.
(19) H. C. Arp, *A. J.*, **60**, 317, 1955.
(20) R. O. Redman, *M.N.*, **99**, 686, 1939.
(21) S. G. Hacker, *Princeton Contributions* No. 16.
(22) J. K. McDonald, *J.R.A.S. Canada*, **42**, 220, 1948.
(23) T. D. Kinman, *M.N.*, **119**, 157, 1959.
(24) O. C. Wilson and M. F. Coffeen *Ap. J.*, **119**, 197, 1954.
(25) A. J. Deutsch, *Ap. J.*, **123**, 210, 1956.
(26) E. M. and G. R. Burbidge, *Encyclopedia of Physics*, **51**, 134, 1958.
(27) R. J. Trumpler and H. F. Weaver, *Statistical Astronomy* (University of California Press, 1953), p. 126.

(28) M. Schwarzschild and S. Bernstein, *Ap. J.*, **122**, 200, 1955.
(29) G. U. Yule and M. G. Kendall, *An Introduction to the Theory of Statistics* (Griffin: London), 13th Edition 1945. Section 23.32, p. 448.
(30) A. R. Sandage, *A. J.*, **59**, 162, 1954.
(31) M. Schwarzschild, *A. J.*, **59**, 273, 1954.
(32) G. Münch, *P.A.S.P.*, **71**, 101, 1959.
(33) H. C. Arp, *Encyclopedia of Physics*, **51**, 112, 1958.
(34) M. W. Feast, *M.N.*, **118**, 618, 1958.
(35) S. I. Bailey, *H.A.*, **38**, 1902.
(36) H. B. Sawyer, *Pub. David Dunlap Obs., Toronto*, Vol. **II**, No. 2, 1955.
(37) H. Shapley, HR 257, *P.N.A.S.*, **30**, 61, 1944.
(38) H. Shapley, HR 346, *P.N.A.S.*, **37**, 138, 1951.
(39) P. W. Merrill, *Ap. J.*, **93**, 380, 1941.
(40) S. Chandrasekhar, *Principles of Stellar Dynamics* (Univ. of Chicago Press, 1942), p. 206.
(41) R. Kurth, *The Mechanics of Stellar Systems* (Pergamon Press, London, 1957), p. 93.
(42) P. W. Merrill, *Ap. J.*, **94**, 171, 1941.
(43) A. D. Thackeray, *M.N.*, **100**, 45, 1950.
(44) P. W. Merrill, *Ap. J.*, **93**, 380, 1941.
(45) P. W. Merrill and R. E. Wilson, *Ap. J.*, **95**, 248, 1942.
(46) A. H. Joy, *Ap. J.*, **96**, 344, 1942.
(47) A. H. Joy, *Ap. J.*, **110**, 105, 1949.

A STUDY OF NEUTRAL HYDROGEN IN THE SOLAR NEIGHBOURHOOD OF THE MILKY WAY

R. D. Davies

(Communicated by A. C. B. Lovell)

(Received 1959 October 1)

Summary

The distribution of neutral hydrogen away from the galactic plane has been measured between Dec. $= +90°$ and Dec. $= -32°$. It shows a number of neutral hydrogen clouds which coincide in position with dust complexes. The major feature of the distribution is the excess of neutral hydrogen in the position of the local system (Gould's Belt) of early-type stars and dust. The system ($\sim 10^8 M\odot$) appears to represent a later formation in the local spiral arm. An extended region in Cepheus is probably similar.

---

1. *Introduction.*—Gould (1) noted that the brighter naked-eye stars of the northern and southern Milky Way formed a belt inclined at an angle of 20° to the galactic plane. Shapley (2) found this belt of stars to be a sub-system of the Galaxy localized within several hundred parsecs of the Sun. The B stars within 200 parsecs of the Sun have the spatial distribution shown in Fig. 1 with a semi-amplitude of 12°. These stars are mainly responsible for the naked-eye Gould Belt. Bright Be stars of magnitude less than 6·5 show the same distribution. Some constituents of the interstellar medium, notably reflection nebulae which are plotted in Fig. 1, also indicate a system inclined at about 20° to the galactic plane (3). These facts suggest that there is a galactic sub-system within which the Sun lies having the properties summarized in the following table (4, 5)

TABLE I

Properties of the Local System

N. Pole	$l' = 170°$	$b' = +74°$
Centre	$l' = 240°$	$b' = -3°$
Radius	~ 500 parsecs	
Mass	$\sim 10^8 M\odot$?	

The reality of this proposed sub-system has been questioned (e.g. 4, 3); it may be the observational effect of a dust density which falls at increasing distances or it may be the effect of a fortuitous irregular distribution of stars.

Strong new arguments in favour of the reality of a local system can be derived from the neutral hydrogen distribution away from the galactic plane. Lilley and Heeschen (6) have noted a correlation between neutral hydrogen gas and dust in the southern parts of the sub-system. A preliminary investigation of Jodrell Bank hydrogen-line records showed a much more extensive correlation between the neutral hydrogen distribution and the local system (7).

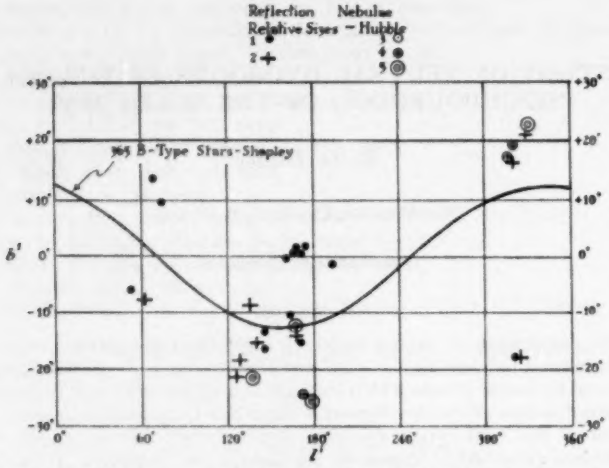

FIG. 1.—*The full-line represents in galactic coordinates the best fitting plane drawn through the bright B stars (after Shapley). The positions of large reflection nebulae (after Hubble) are also shown.*

2. *Programme of observations.*—During the course of the hydrogen-line programme of the 30 ft paraboloid (beamwidth $1°{\cdot}5 \times 1°{\cdot}7$) in 1955 and 1956 a large number of drift curves at constant frequency were taken at various declinations. These employed bandwidths of either 18 Kc/s or 40 Kc/s and showed a clear separation from the galactic plane of a broad feature centred about 20° away from the plane.

The preliminary analysis of this data and of Muller and Westerhout's (8) spectra taken near the galactic plane pointed to the desirability of a complete spectral survey of the sky visible from Jodrell Bank. This complementary survey consisted of setting the 30 ft paraboloid at various declination settings 5° apart and allowing the rotation of the Earth to sweep the beam through 24 hours in right ascension. During each drift the hydrogen comparison radiometer was constantly sweeping a frequency band 1·2 Mc/s in width so that spectra were obtained at least every 5° in the sky. The observing bandwidth was 100 Kc/s; this was adequate to measure the line integral of neutral hydrogen at each point. Each declination run was repeated. The survey covered declinations −32° to +90°. In all, 2500 spectra were taken and analysed.

The velocity characteristics of the neutral hydrogen in the local sub-system well away from the galactic plane were investigated by taking narrow-band spectra in sample regions. Bandwidths of 100, 25 and 3·5 Kc/s were used simultaneously; the 25 Kc/s channel gave the spectra required while the 3·5 Kc/s channel was used as a check to show that the 25 Kc/s channel produced no broadening in the observed profiles.

3. *Analysis and results*

(i) *Drift curves at a single frequency.*—In certain regions of the sky a drift curve across the galactic plane did not show a single broad peak but a broad peak centred on the radio galactic plane with a second fainter peak sometimes as much as 20° in galactic latitude from the first. Such constant declination drift curves

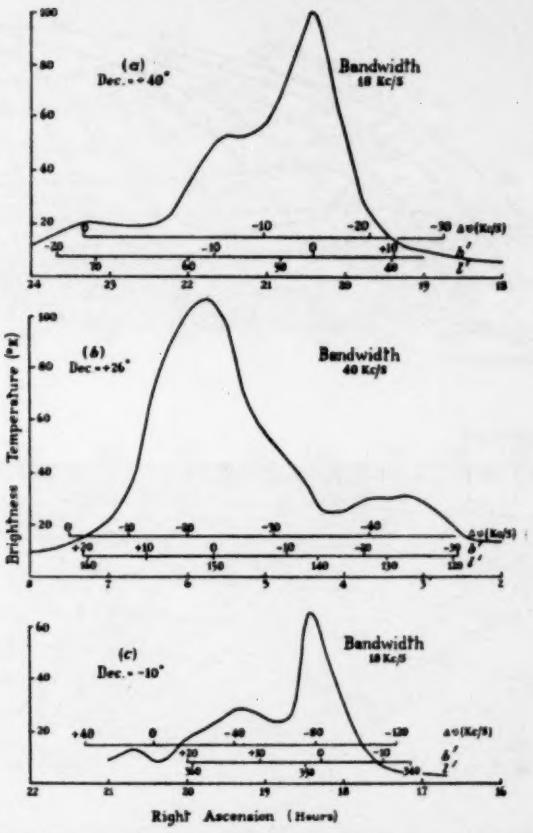

FIG. 2.—*Constant frequency drift curves across the galactic plane and the local system at (a) Dec.* = 40°, *(b) Dec.* = 26°, *(c) Dec.* = −10°. *Galactic coordinates and the frequency difference* Δv *from the l.s.r. are given.*

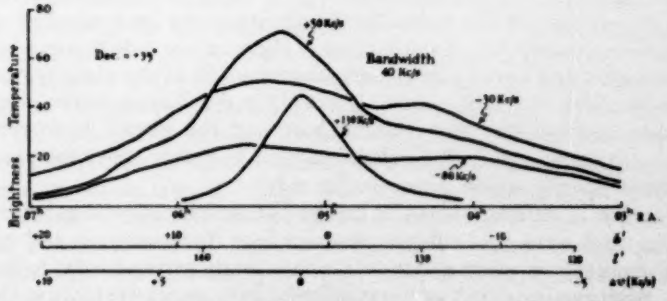

FIG. 3.—*Drift curves across the galactic plane and the local system at Dec.* = 39° *for various frequencies relative to the l.s.r.*

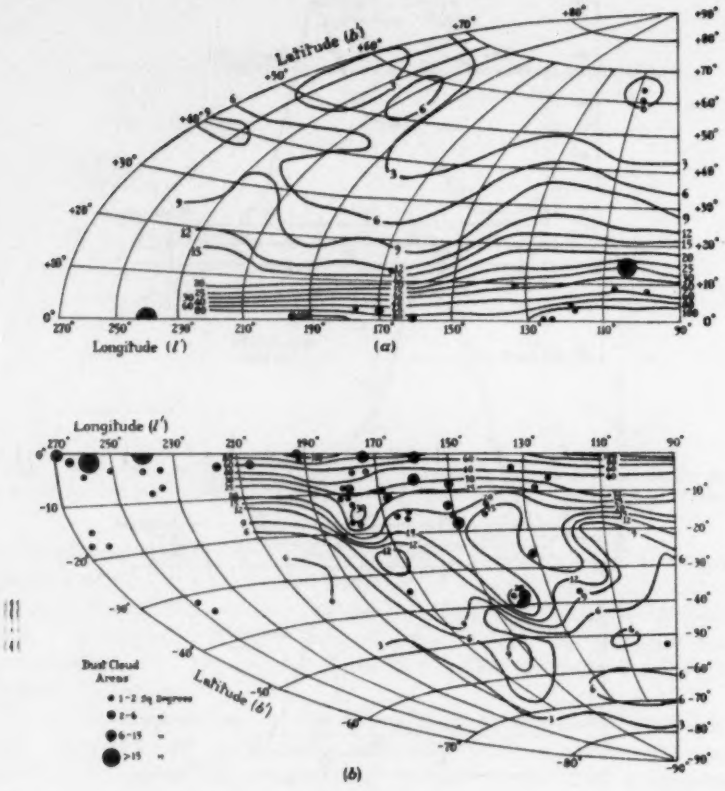

FIG. 4.—*The distribution of N (the integrated number of neutral hydrogen atoms per cm² in the line of sight) for the northern sky in units of* 10^{20} *cm*$^{-2}$.

taken at frequencies near the local standard of rest (l.s.r.) are shown in Fig. 2. The ordinates are brightness temperature while the abscissae show, as well as the right ascension, the galactic coordinates (l', b') and the changing frequency $\Delta\nu$ (although constant relative to the Earth) relative to the local standard of rest in the solar neighbourhood of the Galaxy. Fig. 2 (*a*) is a drift curve across the Cygnus region and shows a strong asymmetry south of the plane lying between galactic latitudes $-5°$ and $-15°$. Fig. 2 (*b*) in the Taurus region gives a clear separation between the main galactic peak and the neutral hydrogen belt at latitudes $-15°$ to $-30°$. A similar separation is visible above the plane in the Ophiuchus–Scorpio region shown in Fig. 2 (*c*).

Hydrogen at different distances can be distinguished due to galactic rotation by taking drift curves at different frequencies. This criterion still applies in the anticentre region where galactic rotation is nearly perpendicular to the line of sight. Such a series of drift curves at different frequencies was taken at Dec. $= 39°$ and the results are shown in Fig. 3. The frequency relative to the local standard of rest at any right ascension for a given curve is obtained by adding the frequency

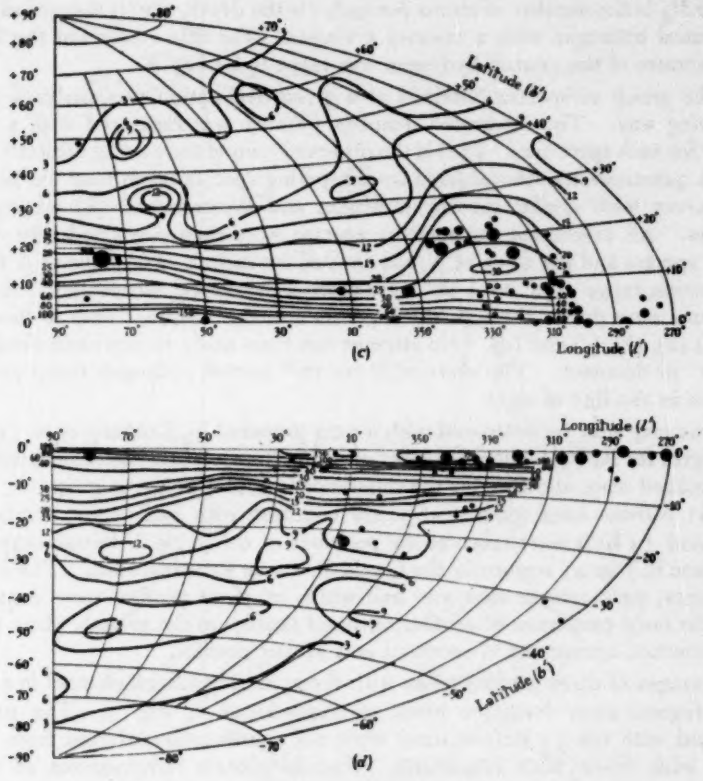

FIG. 4.—*Continued.*

correction $\Delta\nu$ at that right ascension to the frequency assigned to that curve. The H I spectrum in this region of the sky is a single line 160 Kc/s in width at the half temperature points. The drift curve for higher frequencies is narrow and consequently refers to more distant neutral hydrogen. The same phenomenon is observed in the absorption spectrum of Taurus-A (9) where absorption which occurs in nearby hydrogen is observed at the lowest frequencies. Hydrogen at negative frequencies (recession) relative to the local standard of rest has one broad peak on the galactic plane and a secondary maximum 5° to 10° below the plane. This local hydrogen some distance from the plane at zero or negative frequencies relative to the l.s.r. is visible over a range of galactic longitudes. It occurs above the plane around $l' = 330°$ and below the plane around $l' = 150°$.

(ii) *The survey of neutral hydrogen spectra in the Northern Sky.*—This survey, taken with a bandwidth of 100 Kc/s was designed to measure N, the integrated number of neutral hydrogen atoms in a 1 cm² column in the line of sight at each point.

$$N = \int N_H dl = 2{\cdot}3 \times 10^{15} \int \tau(v) dv$$

where N_H is the number of atoms per cm^3, l is the depth, $\tau(v)$ is the optical depth of neutral hydrogen with a velocity v cm/sec. For this evaluation the kinetic temperature of the neutral hydrogen was taken to be 125°K.

The group of spectra obtained at a given declination was analysed in the following way. The integrated quantity $\int T(v)dv$ was measured with a planimeter for each spectrum. $T(v)$ is the observed temperature on an arbitrary scale. These quantities are standardized by comparing spectra taken near the plane in the survey with similar spectra in Muller and Westerhout's (**8**) catalogue of profiles. All brightness temperature spectra were then converted into optical depth spectra and the value of N was derived for each. The value of N for the declination range $-32°$ to $+90°$ were plotted in galactic coordinates. Smooth contours were drawn through these points and the resultant map is shown in Figs. 4 (*a*), (*b*), (*c*) and (*d*). No attempt has been made to represent detail less than 5° in diameter. The units of N are 10^{20} neutral hydrogen atoms per cm^2 column in the line of sight.

This map may be compared with a map prepared by Erickson *et al.* (**10**) on a 10° grid for latitudes more than 20° from the plane. The agreement with this less detailed map, allowing for the difference in grid spacing, is good.

(iii) *Narrow band spectra.*—Spectra obtained with half-power bandwidths of 25 and 3·5 Kc/s were taken at the positions of enhanced N found away from the plane in Fig. 4; regions in the Gould Belt area were included. The central frequency, peak temperature and half-width of these profiles were compared with the same properties of profiles obtained nearby on the galactic plane which were checked against the Westerhout and Muller profiles.

Averages of three profiles taken with the 25Kc/s bandwith channel in each of eight regions away from the plane are reproduced in Fig. 5. The profiles obtained with the 3·5 Kc/s channel were not significantly different from those taken with the 25 Kc/s bandwidth. Peak brightness temperatures of up to 55°K were measured 20° off the plane along both axes of the Gould Belt system.

A number of the brightness temperature spectra show half widths to half temperature points of 7 km/sec. If the kinetic temperature is taken as 125°K the optical depth spectra indicate a value of halfwidth (η) of 5·8 km/sec. This may be compared with values of 12 to 10 km/sec for the galactic plane profiles at distances of 4 to 8·2 kiloparsecs from the galactic centre (**11**). The latter profiles probably include many neutral hydrogen clouds of the Gould Belt type in relative motion.

Other profiles in the present survey were broader and showed more complex structure. Those at $l' = 330°$, $b' = +20°$ and $l' = 330°$, $b' = +40°$ showed a broad base with a narrow bright peak. Some of these regions more than 20° away from the plane have values of η as large as 12 km/sec.

The centre frequency referred to the local standard of rest of the profiles plotted in Fig. 5 was determined to an accuracy of ± 5 Kc/s(± 1 km/sec) by referring spectra taken near the galactic plane to spectra in the catalogue of Muller and Westerhout. There is a significant departure of the centre frequency of most spectra from the zero of the l.s.r. The spectra representative of the Gould Belt region, i.e. near $l' = 330°$, $b' = +20°$ and $l' = 150°$, $b' = 20°$ show a centre frequency at -15 Kc/s($+3$ km/sec) which represents small but significant recession of this neutral hydrogen.

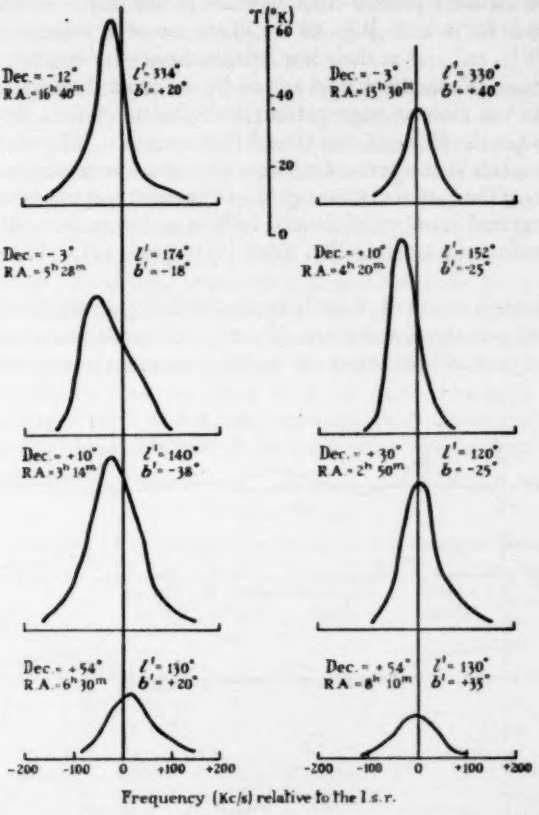

FIG. 5.—*Narrow band (25 Kc/s) profiles taken in regions away from the galactic plane.*

TABLE II

Properties of spectra taken in some regions of large N observed away from the galactic plane

Dec. °	R.A. (1958) h m	l'	b'	Peak temp °K	N units of 10^{20}cm^{-2}	Width of T spectrum, Kc/s	η Km/sec	centre freq. relative to l.s.r., Kc/s
−26	17 43	330	0	93	95	170	10·1	−13
−12	16 40	334	+20	53	20	70	6·0	−13
− 3	15 30	330	+40	27	9	70	7·4	+ 3
+26	5 43	150	0	106	80	105	9·0	− 5
− 3	5 28	174	−18	37	19	127	11·5	−15
+10	4 20	152	−25	55	16	67	5·8	−20
+10	3 14	140	−38	48	28	125	11·1	−10
+30	2 50	120	−25	42	16	80	7·6	− 3
+54	6 30	130	20	18	9	100	10·5	+13
+54	8 10	130	35	10	5	115	12·1	+10

Erickson *et al.* have plotted the departure of the centre frequency from the l.s.r. of spectra for which $|b'| > 20°$. These show a velocity contraction of 5 km/sec for $|b'| > 40°$ and at their low latitude limit of $b' = \pm 20°$ they check the present results. Thus there appears to be an inward movement of neutral hydrogen near the Sun at high galactic latitudes as distinct from an outward movement within the plane of the Gould Belt system. The properties of each of the spectra taken in the present 25 Kc/s survey are summarized in Table II.

4. *Features of the spatial contours of N.*—The main features of the distribution of N, the integrated number of neutral hydrogen atoms per cm² in the line of sight, are to be found plotted in Fig. 4 (*a*), (*b*), (*c*) and (*d*) and may be described as follows:

(i) The greatest values of N lie along the "radio" galactic plane ($b'' = 0$) which is inclined at 1°·5 to the Lund plane ($b' = 0$). The maximum value of N on the plane is about 150×10^{20} atoms per cm² and the minimum is 70×10^{20} atoms per cm²

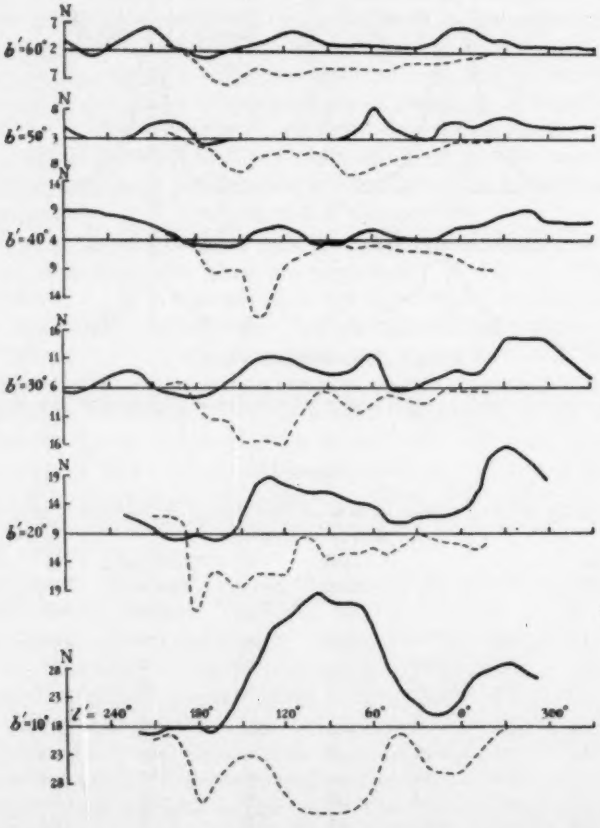

FIG. 6.—*The distribution of N in longitude between latitudes 10° and 60°. The plot for the northern hemisphere is a full line above, and that for the southern a broken line below a fiducial level for each latitude.*

assuming a kinetic temperature of 125°K. There are significant amounts of neutral hydrogen in both polar regions where values of N in the range 2 to 4×10^{20} atoms per cm^2 are found at $|b'| > 70°$.

(ii) The main departures from symmetry of N about the galactic plane and about the galactic centre are summarized in Fig. 6 which shows the distribution of N with galactic longitude plotted at 10° intervals of latitude. The values of N for the northern hemisphere are plotted above, and those for the southern hemisphere are plotted below a fiducial baseline. The major asymmetries are (*a*) a bulge about the galactic plane in the longitude range 60° to 120° extending from $b' = +15°$ to $b' = +5°$ and (*b*) the local sub-system of Gould's Belt seen above the plane from $l' = 220°$ to 350° and below the plane from $l' = 110°$ to 190°; it can be traced out to latitudes of 30° and 40° above and below the plane.

(iii) Concentrations of neutral hydrogen of limited extent were seen away from the galactic plane in a number of regions. Fourteen which were separated from the background distribution are listed in Table III. For each is assigned a position, extent and a value of ΔN, the increment of N above the surroundings. In addition the last three columns of the table show optical data which will be discussed below.

TABLE III

The properties of 14 regions of enhanced neutral hydrogen emission

H I region designation	l'	b'	Extent $l \times b$	N units of 10^{20} cm^{-2}	Obscuring clouds	Bright nebulae	Extragalactic absorption (mags)
			° °				
A	0	−20	35 × 10	5	Present ?		1–2
B	60	+35	10 × 7	6			1–2
C	65	+50	15 × 8	6			1–2
D	60	+ 5					
	to 120	to +15	60 × 10	15	Present	C	Avoidance
E	70	−28	10 × 5	6			0
F	70	−50	15 × 5	5			1–2
G	110	0					
	to 190	to −40	80 × 40	10	Present		Avoidance
H	120	−30	10 × 15	8	Present		1–2
I	140	−40	15 × 15	15	Present	C (Pleiades)	2
J	155	−55	10 × 10	5			0
K	175	−20	10 × 25	18	Present	C + E (Orion)	Avoidance
L	220	+ 5			Present	C (Scorpio etc)	Avoidance
	to 350	to +30	130 × 25	10			
M	320	+45	30 × 20	6	Present		1–2
N	340	−40	30 × 10	5			0 ?

5. *The distribution of N in latitude.*—A representative picture of the amount of neutral hydrogen at high galactic latitudes can be gained from a study of the latitude distribution of N. Accordingly the average value of N observed at each latitude was plotted against latitude for the northern and southern hemisphere in Fig. 7. To avoid any effect of the biasing of these plots by the sum of localized regions a second set of plots for each hemisphere was derived from the average of the ten lowest values of N (found in any 10° longitude interval) for each latitude. These are of similar shape to the former plots but are reduced by about 30 per cent in magnitude; they probably represent the broad distribution of neutral hydrogen at high galactic latitudes.

The plots were fitted to a uniform thickness model of the galactic neutral hydrogen using a secant-law analysis. The *minimal* distributions were fitted by layers above and below the Sun of $N = 2{\cdot}3 \times 10^{20}\,\mathrm{cm}^{-2}$ and $3{\cdot}1 \times 10^{20}\,\mathrm{cm}^{-2}$ respectively. The *average* distributions were equivalent to layers above and

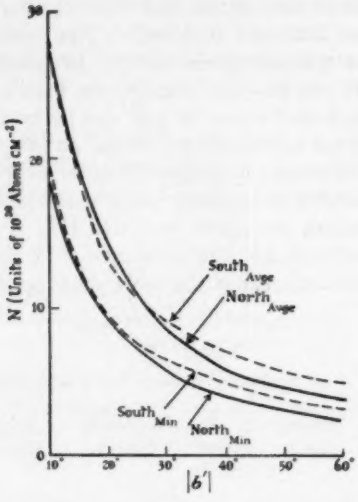

FIG. 7.—*The distribution of N in latitude averaged over all values of longitude. Minimal values are also plotted. The full line is for the northern hemisphere, the broken line for the southern.*

below the Sun of $N = 3{\cdot}5 \times 10^{20}\,\mathrm{cm}^{-2}$ and $4{\cdot}3 \times 10^{20}\,\mathrm{cm}^{-2}$ respectively. The difference between the *minimal* and *average* distributions may be ascribed to the effect of the non-uniform neutral hydrogen distribution near the Sun already discussed. Both distributions suggest that the Sun lies above the neutral hydrogen galactic plane with some 20 per cent more hydrogen below the plane than above it. If the distribution of neutral hydrogen in the solar neighbourhood is taken as uniform with a thickness of 220 parsecs (**12**) then the above 20 per cent difference would be accounted for if the Sun were about 22 parsecs above the neutral hydrogen plane. Analysis of stellar distributions indicates that the Sun is 13 parsecs above the stellar galactic plane (**13**).

The observed amount of neutral hydrogen at high galactic latitudes can be compared with that expected from the observed value of N within the galactic plane and the known dimensions of the galaxy as mapped in neutral hydrogen. For example, the value of N within the galactic plane in the Cygnus direction is $150 \times 10^{20}\,\mathrm{cm}^{-2}$ which is integrated over a depth of about 8 kpc. The value expected at high latitudes with a depth of about 100 parsecs is accordingly about $2 \times 10^{20}\,\mathrm{cm}^{-2}$ if we assume the H I density in the solar neighbourhood to be that of the average in the line of sight in the direction of Cygnus. In view of this assumption, the agreement is good with the value of $2-3 \times 10^{20}\,\mathrm{cm}^{-2}$ observed for the minimal distributions.

6. *A comparison of the neutral hydrogen distribution with optical features.*—The correlation between the density of neutral hydrogen and the existence of dust clouds has already been established for a number of regions within the galaxy (**14**, **15**, **16**). The present study has included an examination of types of Population I objects which are known to co-exist with neutral hydrogen in the spiral arms of the galaxy.

(i) *Obscuring clouds*

A map prepared by Lundmark (**17**) shows the positions and sizes of those dust regions in which the star density is less than 5 or 6 times the surroundings. In consequence the higher latitude regions may be in error, being only statistical fluctuations in star density. All those dust clouds greater than 1·0 degree in diameter have been plotted in the maps of N in Fig. 4 (*a*), (*b*), (*c*) and (*d*).

A correlation is visible between many features of the distribution of obscuring matter and the distribution of neutral hydrogen away from the galactic plane. There is an excess of obscuring matter in the plane of the local system (regions G and L) in the well-known dust regions of Taurus, Orion and Auriga which lie below the galactic anticentre and the regions of Ophiuchus, Scorpio and Scutum above the galactic centre. The bulge seen in the neutral hydrogen distribution above the plane between longitudes 60° and 120° in Cepheus (region D) also has a counterpart in Lundmark's map; this region is a dust complex about 500 parsecs distant (**4**). There also appears to be good evidence for an excess of obscuring matter in the small regions A, H, I, K and M. These correlations are indicated in column 6 of Table III.

Hubble's (**18**) measurements of the effect of galactic obscuring matter on counts of extragalactic nebulae give another indication of the distribution of local obscuring matter. The agreement with the general features of Lundmark's catalogue is good and in all cases where there was a correlation between the 21 cm measures and Lundmark's obscuring clouds there was a clear deficiency in the counts of extragalactic nebulae. Hubble's observed number deficiencies have been converted into magnitudes of absorption in column 8 of Table III. The zone of avoidance of extragalactic nebulae coincides with the shape of the local system and also with the Cepheus bulge.

(ii) *Bright nebulae*

Cederblad's (**19**) catalogue of continuous reflection and of emission nebulae gives the distance as well as the size of clearly distinguishable galactic nebulosities. Those nebulae with distances less than 1000 parsecs have been divided among the quadrants centred on the axis of the local system ($l' = 150°$, $l' = 330°$) in Fig. 8 (*a*) and the perpendicular axis in Fig. 8 (*b*). Their positions above or below the plane and their diameters have been plotted. The local system is clearly seen separated from the galactic distribution. It lies inclined at 20° to the radio galactic plane ($b^{r} = 0$). These clouds of dust and gas extend for 200 parsecs in the direction of $l' = 330°$ and 300 parsecs in the direction of $l' = 150°$. The more extensive bright complexes are noted in column 7 of Table III where their spectral character is given (E for gaseous emission and C for continuum reflection from dust). These regions are interwoven with the obscuring matter plotted on Lundmark's map and are at the same distance. The variation of N with galactic latitude integrated over each quadrant is given as a polar plot by the full-line in Fig. 8 (*a*) and (*b*). The correlation between N and the existence of interstellar dust is again marked.

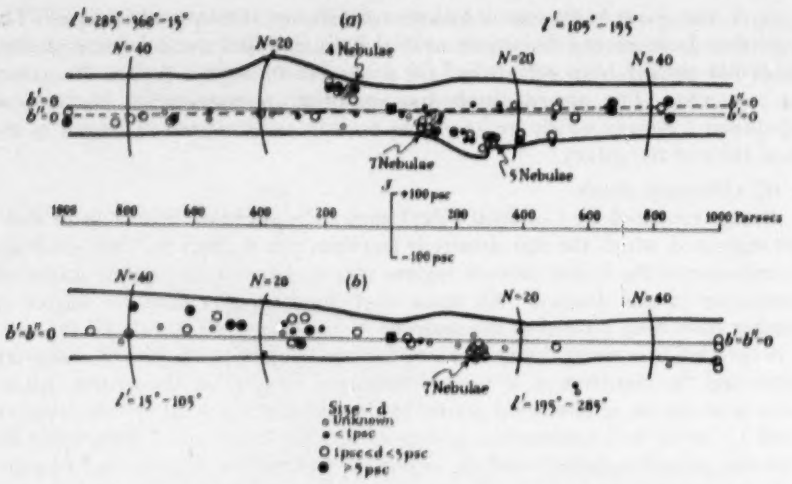

FIG. 8.—*The distribution in height (z) above the galactic plane of bright nebulae (after Cederblad) averaged for each quadrant of longitude. The corresponding distribution of N is given by the full line polar plot.*

(iii) *The distribution of stars*

The spatial distribution of stars in the solar neighbourhood has already been discussed in the introduction. The nearby early-type stars lie within the local system inclined at about 20° to the galactic plane. A large number of these are of spectral type B_5 to B_9 which indicates (**20**) an age of 20×10^6 years for the local system. This may be compared with $100–200 \times 10^6$ years for the bulk of the stars in the solar spiral arm.

7. *A comparison with radio continuum surveys.*—Recent publications have indicated that there may be some correlation between the distribution of neutral hydrogen and the brightness distribution of the continuum radiation from the Galaxy. Mills (**21**) has found 81 Mc/s radiation from spiral structure within the Galaxy and Blythe (**22**) has shown that some 38 Mc/s continuum details seen in the Taurus region are also visible in the neutral hydrogen contours. More evidence relating to this correlation was derived from a study of the present neutral hydrogen survey and from continuum surveys which have been made with beamwidths of less than about 10° i.e. comparable with the resolution of the present survey. The results are plotted in Fig. 9 (*a*) and (*b*) for frequencies of 38 (**22**), 200 (**23**), and 400 (**24**) Mc/s. The values are the average brightness temperatures within $\pm 5°$ of the latitudes indicated.

An examination of these plots shows that there is no close correlation between the continuum emission at any frequency and the neutral hydrogen distribution at galactic latitudes near $\pm 20°$. The only feature which produces an effect in both line and continuum radiation is the Orion complex of gas and dust. This is not unexpected since the continuum radiation comes from an extended region showing the Hα emission centred on the Orion Nebula. Moreover the continuum spur at $l' = 0°$ reaching to high positive latitudes has no counterpart in the neutral hydrogen distribution with the resolution of the present survey.

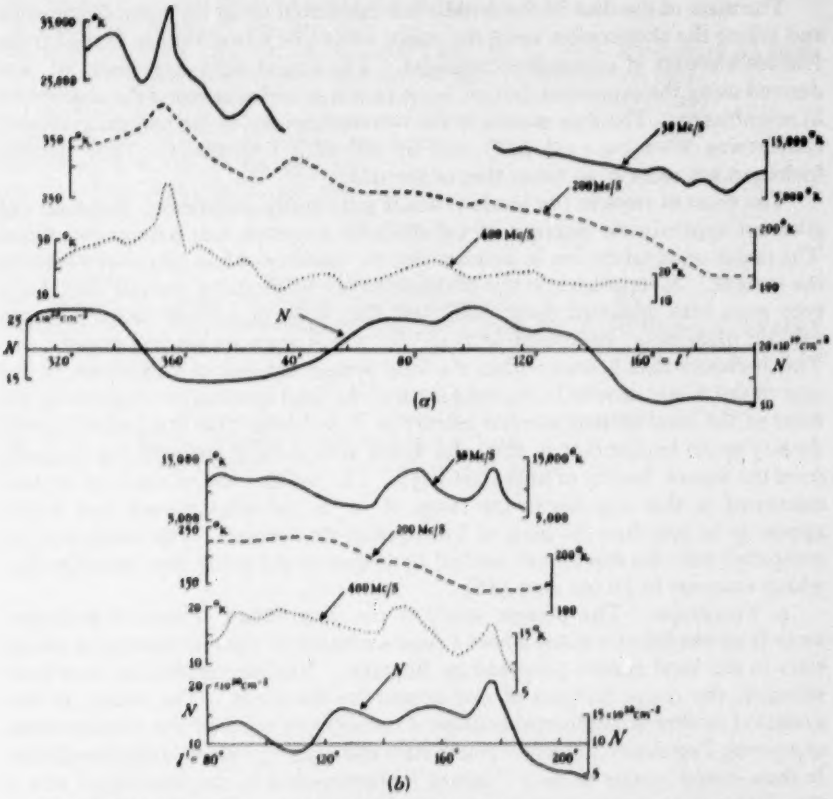

FIG. 9.—*The distribution in galactic longitude of N and continuum radiation for (a) b' = +15° and (b) b' = −20°.*

8. *The mass of gas, dust and stars in the local system.*—The mass of neutral hydrogen in the local system (Gould's Belt) can only be estimated if the dimensions of the system can be derived. Since the neutral hydrogen distribution is so closely correlated in position with the dust complexes of the local system, it will be assumed here that the hydrogen is distributed in depth the same way as the dust. Thus the hydrogen will be taken to have a uniform density towards $l' = 330°$ out to 200 parsecs (the Ophiuchus and Scorpio clouds) and towards $l' = 150°$ out to 300 parsecs (the Taurus, Orion clouds). The equivalent depth of the hydrogen perpendicular to the galactic plane is 30 parsecs as derived from the width to half-intensity in latitude of $\sim 15°$. The corresponding breadth in the direction $l' = 60°$ to $l' = 240°$ is estimated at 150 parsecs (width $\sim 70°$) although it is difficult to determine because the local system here crosses the galactic plane and might just as well have been taken as 500 parsecs i.e. making the region a circular disk. The neutral hydrogen in the former case is 10^5 solar masses ($M\odot$) and in the latter $2{\cdot}6 \times 10^5 M\odot$. The hydrogen gas density in this idealized representation of the local system is 2·0 atoms per cm^3 in excess of the gas density within the local spiral arm.

The mass of the dust in the system was calculated using the same dimensions and taking the obscuration along the major axis to be 2 magnitudes as read from Hubble's counts of extragalactic nebulae. The line of sight dust mass, m', was derived using the expression (16) $m' = 3 \times 10^{-5} m$ gr cm^2 where m is the absorption in magnitudes. The dust masses of the two models used in the neutral hydrogen calculations were $2{\cdot}5 \times 10^3$ $M\odot$ and 6×10^3 $M\odot$ respectively. The neutral hydrogen gas mass is 40 times that of the dust.

The mass of stars in the local system is not readily calculable. Schmidt (**5**) gives an approximate estimate of 10^8 $M\odot$ for a system 500 parsecs in radius. The major uncertainty lies in determining the number of low luminosity stars in the system. An approach to the problem can be made using the fact that the A type stars with apparent magnitudes less than 6 lie in a plane inclined to the galactic plane at 4° compared with 16° for the B stars within 200 parsecs (**2**). This indicates that A stars within the local system amount to only about 30 per cent of the A star density in the field stars of the local spiral arm. Assuming the mass of the local system consists mainly of A and later type stars with a space density 30 per cent of that in the local spiral arm, a useful estimate can be made from the known density of field stars (**25**). The stellar mass of the local system calculated in this way lies in the range of 10^4 to 10^5 solar masses, and would appear to be less than the mass of hydrogen in the system. This result may be compared with the fraction of neutral hydrogen in the spiral arm near the Sun which amounts to 10 per cent (**26**).

9. *Conclusion.*—The present study of the distribution of neutral hydrogen away from the galactic plane shows a close similarity to the distribution of young stars in the local system proposed by Shapley. Neither distribution is smooth although the major features of one appear on the other. The reality of this system is further strengthened because it consistently exhibits the characteristics of a young Population I object—young stars and a high percentage of gas and dust. It then would appear to be a "recent" phenomenon in the local spiral arm if this data can be interpreted in an evolutionary sense. The "bulge" seen in the dust and neutral hydrogen distributions in the direction of Cepheus may be a similar type of system. This can only be substantiated if data on the type and distance of the stars embedded within it become available.

Acknowledgments.—The author wishes to thank Dr R. C. Jennison, who played a major part in the development and operation of the equipment used in the spectral survey described in Section 3(ii).

Jodrell Bank Experimental Station,
Lower Withington,
Cheshire:
1959 *September.*

References

(1) Gould, B. A., *Uranometria Argentina*, 335, 1879.
(2) Shapley, H., *Ap. J.*, **49**, 311, 1919.
(3) Hubble, E., *Ap. J.*, **56**, 162, 1922.
(4) Bok, B. J., *The Distribution of Stars in Space*, Chicago, 1937.
(5) Schmidt, H., Bonn. Univ. Veroff, No. 35, 1949.
(6) Lilley, A. E., and Heeschen, D. S., *Pub. Nat. Acad. Sci.* **40**, 1095, 1954.
(7) Davies, R. D., Paris Symposium on Radio Astronomy, Ed. R. N. Bracewell, Stanford Univ. Press, Stanford, 1959.

(8) Muller, C. A., and Westerhout, G., *B.A.N.*, **13**, 151, 1957.
(9) Muller, C. A., *Ap. J.*, **125**, 830, 1957.
(10) Erickson, W. C., Helfer, H. L., and Tatel, H. E., Paris Symposium on Radio Astronomy, Ed. R. N. Bracewell, Stanford Univ. Press, Stanford, 1959.
(11) Kwee, K. K., Muller, C. A. and Westerhout, G., *B.A.N.*, **12**, 211, 1954.
(12) Schmidt, M., *B.A.N.*, **13**, 247, 1957.
(13) van Tulder, J. J. M., *B.A.N.*, **9**, 315, 1942.
(14) Lilley, A. E., *Ap. J.*, **121**, 559, 1955.
(15) Heeschen, D. S., *Ap. J.*, **121**, 569, 1955.
(16) Davies, R. D., *M.N.*, **116**, 443, 1956.
(17) Lundmark, K., Med. fr. Astron. Obs. Upsala, No. 30, 1927.
(18) Hubble, E., *Ap. J.*, **79**, 8, 1934.
(19) Cederblad, S., Med. fr. Astron. Obs. Lund, Ser. II, 119, 1946.
(20) Sandage, A., *Stellar Populations*, Vatican Observatory, p. 41, 1958.
(21) Mills, B. Y., Paris Symposium on Radio Astronomy, Ed. R. N. Bracewell, Stanford Univ. Press, Stanford, 1959.
(22) Blythe, J. H., *M.N.*, **117**, 652, 1957.
(23) Droge, F., and Priester, W., *Z. f. Ap.*, **40**, 236, 1956.
(24) Seeger, C. L., Westerhout, G., and Conway, R. G. (in preparation).
(25) Allen, C. W., *Astrophysical Quantities*, London, 1955.
(26) Kerr, F. J., and Hindman, J. V., *P.A.S.P.*, **69**, 558, 1957.

CONVERGENCE OF CHANDRASEKHAR'S METHOD FOR THE PROBLEM OF DIFFUSE REFLECTION*

Philip M. Anselone

(Communicated by Z. Kopal)

(Received 1959 October 8)

Summary

Let $I(\tau, \mu)$, $J(\tau)$ and $\mathfrak{J}(\tau)$ denote the intensity, average intensity and source function for radiation in a semi-infinite, plane-parallel, isotropically scattering atmosphere, with albedo $\varpi_0 \leqq 1$ and the only external source due to an incident parallel beam. Let $I_m(\tau, \mu)$, $J_m(\tau)$ and $\mathfrak{J}_m(\tau)$ denote the corresponding Chandrasekhar approximations, derived with the aid of either the Gauss or double Gauss quadrature formula. It is proved that $I_m \to I$, $J_m \to J$ and $\mathfrak{J}_m \to \mathfrak{J}$ uniformly as $m \to \infty$. Error bounds are obtained in the non-conservative case ($\varpi_0 < 1$).

---

1. *Introduction.*—The general problem of the diffuse reflection of a parallel beam of radiation by a plane-parallel atmosphere is formulated by Chandrasekhar in ((1), pp. 20–23). In this paper we are concerned with the important special case of a semi-infinite atmosphere which scatters radiation isotropically. Our notation is standard. Let $I(\tau, \mu)$, $J(\tau)$ and $\mathfrak{J}(\tau)$ denote, respectively, the intensity, average intensity and source function of diffuse radiation. Let ϖ_0 ($0 < \varpi_0 \leqq 1$) denote the albedo for single scattering, πF ($F > 0$) the net flux of the beam per unit area normal to itself, and $-\mu_0$ ($\mu_0 > 0$) the direction cosine of the beam relative to the outward normal to the atmosphere. The functions I, J and $\mathfrak{J}$ are positive, bounded, and satisfy the equations

$$\mu \frac{\partial I(\tau, \mu)}{\partial \tau} = I(\tau, \mu) - \mathfrak{J}(\tau), \tag{1}$$

$$\mathfrak{J}(\tau) = \varpi_0 J(\tau) + \tfrac{1}{4}\varpi_0 F e^{-\tau/\mu_0}, \tag{2}$$

$$J(\tau) = \tfrac{1}{2}\int_{-1}^{1} I(\tau, \mu)\, d\mu, \tag{3}$$

$$I(0, \mu) = 0 \text{ for } \mu < 0. \tag{4}$$

The method of discrete ordinates used by Chandrasekhar in ((1), pp. 80–87), involves replacing the integral in (3) by the Gauss quadrature formula sum of order $2m$, $m = 1, 2, 3, \ldots$, and solving the resulting problem. For each m the Chandrasekhar approximations I_m, J_m and $\mathfrak{J}_m$ are the unique bounded functions which satisfy the equations

$$\mu \frac{\partial I_m(\tau, \mu)}{\partial \tau} = I_m(\tau, \mu) - \mathfrak{J}_m(\tau), \tag{5}$$

$$\mathfrak{J}_m(\tau) = \varpi_0 J_m(\tau) + \tfrac{1}{4}\varpi_0 F e^{-\tau/\mu_0}, \tag{6}$$

$$J_m(\tau) = \tfrac{1}{2}\sum_{i=\pm 1}^{\pm m} a_{mi} I_m(\tau, \mu_{mi}), \tag{7}$$

$$I_m(0, \mu) = 0 \text{ for } \mu < 0. \tag{8}$$

* Presented to the American Mathematical Society, 1959 September 3.

We make a slight generalization. The constants a_{mi} and μ_{mi} in (7) pertain either to the Gauss formula or to the "double Gauss" formula used by Sykes (2). In either case,

$$0<\mu_{m1}<\ldots<\mu_{mm}<1, \quad \mu_{m,-i}=-\mu_{mi}, \quad a_{m,-i}=a_{mi}>0. \tag{9}$$

For a general discussion of numerical integration see Kopal (3), especially Chapter VII.

This is a statement of our principal results.

Theorem.—As $m\to\infty$,

$$I_m(\tau,\mu)\to I(\tau,\mu), \quad J_m(\tau)\to J(\tau), \quad \mathfrak{S}_m(\tau)\to\mathfrak{S}(\tau),$$

uniformly for $0\leqq\tau<\infty$ and $-1\leqq\mu\leqq 1$.

In (4), (5) and (6) this writer derived analogous results for the "classical transfer problem"—no incident radiation, pure isotropic scattering, and constant net flux. The same general approach that was adopted in those papers is also used below, but with important differences and extensions. Most of the analysis is expressed in terms of $\mathfrak{S}$ and $\mathfrak{S}_m$. Estimates of the deviation of $\mathfrak{S}_m$ from $\mathfrak{S}$ are obtained in the non-conservative case ($\varpi_0<1$).

2. *Integral equations for* $\mathfrak{S}$ *and* $\mathfrak{S}_m$.—It follows from equations (1) and (4) that

$$\left.\begin{aligned} &I(0,\mu)=\mathfrak{S}(0);\\ &I(\tau,\mu)=\int_0^\tau e^{(\tau-t)/\mu}\mathfrak{S}(t)\frac{dt}{-\mu}, \quad \mu<0;\\ &I(\tau,\mu)=\int_\tau^\infty e^{(\tau-t)/\mu}\mathfrak{S}(t)\frac{dt}{\mu}, \quad \mu>0. \end{aligned}\right\} \tag{10}$$

Equations (10), (3) and (2) yield

$$\mathfrak{S}(\tau)=\tfrac{1}{2}\varpi_0\int_0^\infty E_1(|\tau-t|)\mathfrak{S}(t)\,dt+\tfrac{1}{4}\varpi_0 F e^{-\tau/\mu_0}, \tag{11}$$

where E_1 is the exponential integral function of order one; more generally,

$$E_r(x)=\int_0^1 e^{-x/\mu}\mu^{r-2}\,d\mu, \qquad x\geqq 0, \quad r\geqq 1. \tag{12}$$

It follows from equations (5) and (8) that

$$\left.\begin{aligned} &I_m(0,\mu)=\mathfrak{S}_m(0);\\ &I_m(\tau,\mu)=\int_0^\tau e^{(\tau-t)/\mu}\mathfrak{S}_m(t)\frac{dt}{-\mu}, \quad \mu<0;\\ &I_m(\tau,\mu)=\int_\tau^\infty e^{(\tau-t)/\mu}\mathfrak{S}_m(t)\frac{dt}{\mu}, \quad \mu>0. \end{aligned}\right\} \tag{13}$$

Equations (13), (7) and (6) yield

$$\mathfrak{S}_m(\tau)=\tfrac{1}{2}\varpi_0\int_0^\infty E_{m1}(|\tau-t|)\mathfrak{S}_m(t)\,dt+\tfrac{1}{4}\varpi_0 F e^{-\tau/\mu_0}, \tag{14}$$

where E_{m1} is a special case of

$$E_{mr}(x)=\sum_{i=1}^{m} a_{mi}\,e^{-x/\mu_{mi}}(\mu_{mi})^{r-2}, \quad x\geqq 0, \; r\geqq 1. \tag{15}$$

3. *Neumann series representations of* $\mathfrak{H}$ *and* $\mathfrak{H}_m$.—Let S denote the set of bounded measurable functions f defined on the interval $0 \leqq \tau < \infty$. With the norm of uniform convergence, $\|f\| = \sup |f(\tau)|$, S is a Banach space. Let Λ and Λ_m, $m \geqq 1$, be the integral operators on S such that if $f \epsilon S$ then Λf and $\Lambda_m f$ are the functions defined for $0 \leqq \tau < \infty$ by

$$(\Lambda f)(\tau) = \tfrac{1}{2} \int_0^\infty E_1(|\tau - t|) f(t) dt, \tag{16}$$

$$(\Lambda_m f)(\tau) = \tfrac{1}{2} \int_0^\infty E_{m1}(|\tau - t|) f(t) dt. \tag{17}$$

The following statements are easily verified. If $f \epsilon S$ then $\Lambda f \epsilon S$ and $\Lambda_m f \epsilon S$. For each $f \epsilon S$, $\|\Lambda f\| \leqq \|f\|$ and $\|\Lambda_m f\| \leqq \|f\|$, so that Λ and Λ_m are bounded operators. More specifically, $\|\Lambda\| = \|\Lambda_m\| = 1$, where the operator norms have the usual definitions, $\|\Lambda\| = \sup\{\|\Lambda f\| : \|f\| = 1\}$ and similarly for $\|\Lambda_m\|$. If $f \epsilon S$ and $f \geqq 0$ then $\Lambda f \geqq 0$ and $\Lambda_m f \geqq 0$. For further properties, see (4) and the monograph (7) by Hopf, where classes of integral operators which include Λ and Λ_m are considered.

The integral equations (11) and (14) are expressed equivalently as

$$(\mathbf{I} - \varpi_0 \Lambda)\mathfrak{H} = h, \qquad (\mathbf{I} - \varpi_0 \Lambda_m)\mathfrak{H}_m = h, \tag{18}$$

where $\mathbf{I}$ is the identity operator on S and

$$h(\tau) = \tfrac{1}{4} \varpi_0 F e^{-\tau/\mu_0}. \tag{19}$$

Note that $h \epsilon S$ and

$$\|h\| = \tfrac{1}{4} \varpi_0 F. \tag{20}$$

Suppose that $0 < \varpi_0 < 1$. Then $\|\varpi_0 \Lambda\| = \|\varpi_0 \Lambda_m\| = \varpi_0 < 1$, so that the operators in parentheses in (18) have the unique bounded inverses given by the uniformly convergent Neumann operator series,

$$(\mathbf{I} - \varpi_0 \Lambda)^{-1} = \sum_{n=0}^{\infty} \varpi_0^n \Lambda^n, \qquad (\mathbf{I} - \varpi_0 \Lambda_m)^{-1} = \sum_{n=0}^{\infty} \varpi_0^n \Lambda_m^n. \tag{21}$$

It follows from a cursory examination of the effect of these inverse operators on constant functions and from the Neumann series that

$$\|(\mathbf{I} - \varpi_0 \Lambda)^{-1}\| = \|(\mathbf{I} - \varpi_0 \Lambda_m)^{-1}\| = 1/(1 - \varpi_0). \tag{22}$$

These results imply that the equations in (18) have the unique solutions in S given by the Neumann series

$$\mathfrak{H} = \sum_{n=0}^{\infty} \varpi_0^n \Lambda^n h, \qquad \mathfrak{H}_m = \sum_{n=0}^{\infty} \varpi_0^n \Lambda_m^n h, \tag{23}$$

at least if $0 < \varpi_0 < 1$, and in this case equations (18), (20) and (22) yield

$$\|\mathfrak{H}\| \leqq \frac{\varpi_0 F}{4(1 - \varpi_0)}, \qquad \|\mathfrak{H}_m\| \leqq \frac{\varpi_0 F}{4(1 - \varpi_0)}. \tag{24}$$

Now let $\varpi_0 = 1$. Hopf (7) proved that the equation $(\mathbf{I} - \Lambda)\mathfrak{H} = h$ has a unique bounded solution in the form of the Neumann series. His reasoning applies, *mutatis mutandis*, to the equation $(\mathbf{I} - \Lambda_m)\mathfrak{H}_m = h$. Therefore, for each value of the albedo ϖ_0, $0 < \varpi_0 \leqq 1$, the integral equations in (18) have the unique bounded solutions given by the Neumann series in (23). It follows from (23) and (19) that $\mathfrak{H}$ and $\mathfrak{H}_m$ are positive functions, which was to be expected. For a quite different representation of $\mathfrak{H}_m$, see Chandrasekhar (p. 83, formula (98)(1)).

4. *Convergence of* $\mathfrak{S}_m$ *to* $\mathfrak{S}$ *in the non-conservative case.*—Throughout this section assume that $0<\varpi_0<1$.

It follows from (18) that

$$\mathfrak{S}-\mathfrak{S}_m=\varpi_0\Lambda\mathfrak{S}-\varpi_0\Lambda_m\mathfrak{S}_m=\varpi_0(\Lambda-\Lambda_m)\mathfrak{S}+\varpi_0\Lambda_m(\mathfrak{S}-\mathfrak{S}_m),$$

$$(\mathbf{I}-\varpi_0\Lambda_m)(\mathfrak{S}-\mathfrak{S}_m)=\varpi_0(\Lambda-\Lambda_m)\mathfrak{S},$$

$$\mathfrak{S}-\mathfrak{S}_m=\varpi_0(\mathbf{I}-\varpi_0\Lambda_m)^{-1}(\Lambda-\Lambda_m)\mathfrak{S}. \tag{25}$$

By (25), (22) and (24),

$$\|\mathfrak{S}-\mathfrak{S}_m\|\leqq\frac{\varpi_0}{1-\varpi_0}\|\Lambda-\Lambda_m\|\,\|\mathfrak{S}\|, \tag{26}$$

$$\|\mathfrak{S}-\mathfrak{S}_m\|\leqq\frac{\varpi_0^2F}{4(1-\varpi_0)^2}\|\Lambda-\Lambda_m\|. \tag{27}$$

The definitions of Λ and Λ_m imply that

$$(\Lambda f-\Lambda_m f)(\tau)=\tfrac{1}{2}\int_{-\infty}^{\tau}[E_1(|x|)-E_{m1}(|x|)]f(\tau-x)dx,$$

$$\|\Lambda f-\Lambda_m f\|\leqq\tfrac{1}{2}\|f\|\int_{-\infty}^{\infty}|E_1(|x|)-E_{m1}(|x|)|dx,$$

$$\|\Lambda-\Lambda_m\|\leqq\int_0^{\infty}|E_1(x)-E_{m1}(x)|dx. \tag{28}$$

The inequalities (27) and (28) yield

$$\|\mathfrak{S}-\mathfrak{S}_m\|\leqq\frac{\varpi_0^2F}{4(1-\varpi_0)^2}\int_0^{\infty}|E_1(x)-E_{m1}(x)|dx. \tag{29}$$

We prove now that the sequence of integrals appearing in (28) and (29) converges to zero as m tends to infinity. According to equations (24) and (26) of (5),

$$E_2(y)=\int_y^{\infty}E_1(x)dx,\quad E_{m2}(y)=\int_y^{\infty}E_{m1}(x)dx,\quad y\geqq 0, \tag{30}$$

and $E_2(0)=E_{m2}(0)=1$. Hence, if $0<t<\tau<\infty$ then

$$\int_0^{\infty}|E_1(x)-E_{m1}(x)|dx=\left\{\int_0^t+\int_t^{\tau}+\int_{\tau}^{\infty}\right\}|E_1(x)-E_{m1}(x)|dx$$

$$\leqq 2-E_2(t)-E_{m2}(t)+\int_t^{\tau}|E_1(x)-E_{m1}(x)|dx+E_2(\tau)+E_{m2}(\tau).$$

According to Theorem 1 of (5), $E_{m1}(x)\to E_1(x)$ uniformly for $t\leqq x\leqq\tau$ and $E_{m2}(y)\to E_2(y)$ uniformly for $y\geqq 0$, as m tends to infinity. Thus,

$$\limsup_{m\to\infty}\int_0^{\infty}|E_1(x)-E_{m1}(x)|dx\leqq 2[1-E_2(t)+E_2(\tau)]$$

for $0<t<\tau<\infty$. Let $t\to 0$ and $\tau\to\infty$ to obtain

$$\int_0^{\infty}|E_1(x)-E_{m1}(x)|dx\to 0\quad\text{as } m\to\infty. \tag{31}$$

By (28), (29) and (31),

$$\|\Lambda-\Lambda_m\|\to 0\quad\text{as } m\to\infty, \tag{32}$$

$$\|\mathfrak{S}-\mathfrak{S}_m\|\to 0\quad\text{as } m\to\infty. \tag{33}$$

Thus, $\mathfrak{S}_m(\tau)\to\mathfrak{S}(\tau)$ uniformly for $0\leqq\tau<\infty$ as $m\to\infty$.

Since the functions E_1 and E_{m1} are known explicitly, (29) furnishes an estimate for the deviation of $\mathfrak{B}_m$ from $\mathfrak{B}$. However, it is not satisfactory to have to evaluate the integrals for each m. These integrals can be estimated by means of the standard error formula for the Gauss quadrature formula (cf. Kopal [(3), p. 372]). Unfortunately, this procedure yields estimates which tend to infinity as $m \to \infty$. Another approach, which involves the Weierstrass approximation theorem and utilizes the fact that the Gauss formula of order $2m$ integrates correctly polynomials of orders up to $4m-1$, leads to a sequence of estimates which does converge to zero as $m \to \infty$. However, this sequence of estimates is of doubtful value because the convergence to zero is very much slower than experience would lead one to predict. Efforts to obtain practical numerical estimates are continuing.

Exchange the pairs $(\Lambda, \mathfrak{B})$ and $(\Lambda_m, \mathfrak{B}_m)$ in the analysis leading to (26) to obtain the "relative" estimates,

$$\|\mathfrak{B}-\mathfrak{B}_m\| \leqq \frac{\varpi_0}{1-\varpi_0}\,\|\Lambda-\Lambda_m\|\,\|\mathfrak{B}_m\|, \tag{34}$$

$$\|\mathfrak{B}-\mathfrak{B}_m\| \leqq \frac{\varpi_0}{1-\varpi_0}\,\|\mathfrak{B}_m\| \int_0^\infty |E_1(x)-E_{m1}(x)|dx. \tag{35}$$

Whenever $\|\mathfrak{B}_m\|$ is known or available in good approximation, (34) and (35) may be used. Since there is reason to think that the first inequality in (24), which was used in the derivation of (27), is a poor estimate of $\|\mathfrak{B}\|$, it is likely that the "relative" estimates for $\|\mathfrak{B}-\mathfrak{B}_m\|$ derived above are better than the "absolute" estimates, (27) and (29).

5. *Convergence of* $\mathfrak{B}_m$ *to* $\mathfrak{B}$ *for the conservative case.*—In this section assume that $\varpi_0 = 1$.

The average intensity in the classical transfer problem is a constant multiple of $\tau + q(\tau)$, where $q - \Lambda q = \frac{1}{2}E_3$,

$$q = \tfrac{1}{2}\sum_{n=0}^{\infty} \Lambda^n E_3, \tag{36}$$

and $0 < q < 1$. In Theorem XII of (7), Hopf expressed the source function for the problem of diffuse reflection in terms of q. With appropriate notational changes, Hopf's formula (182′) becomes.

$$\mathfrak{B}(\tau) = \tfrac{3}{4}F\left[\mu_0^2 + \int_0^\infty e^{-t/\mu_0} q(t)dt\right] \times \left[1 - e^{-\tau/\mu_0} + \frac{q(\tau)}{\mu_0} - \frac{1}{\mu_0^2}\int_0^\tau e^{(t-\tau)/\mu_0} q(t)dt\right]. \tag{37}$$

Let q_m denote the Chandrasekhar approximation to q or order m, which is given by formula (46) on page 75 of (1). According to results reported in (5), $q_m - \Lambda_m q_m = \frac{1}{2}E_{m3}$,

$$q_m = \tfrac{1}{2}\sum_{n=0}^{\infty} \Lambda_m{}^n E_{m3}, \tag{38}$$

and $0 < q_m < 1$. The same reasoning by which Hopf derived (37) leads to the analogous equation,

$$\mathfrak{B}_m(\tau) = \tfrac{3}{4}F\left[\mu_0^2 + \int_0^\infty e^{-t/\mu_0} q_m(t)dt\right] \times \left[1 - e^{-\tau/\mu_0} + \frac{q_m(\tau)}{\mu_0} - \frac{1}{\mu_0^2}\int_0^\tau e^{(t-\tau)/\mu_0} q_m(t)dt\right]. \tag{39}$$

It was proved by this writer in (6) that $\|q-q_m\|\to 0$ as $m\to\infty$. It therefore follows from (37) and (39) by routine arguments that

$$\|\mathfrak{I}-\mathfrak{I}_m\|\to 0 \text{ as } m\to\infty. \tag{40}$$

This procedure also yields an estimate of $\|\mathfrak{I}-\mathfrak{I}_m\|$ in terms of $\|q-q_m\|$. Since no estimates of $\|q-q_m\|$ have been obtained, there is as yet no "absolute" estimate of $\|\mathfrak{I}-\mathfrak{I}_m\|$ in the conservative case.

A consequence of (40) is that

$$\mathfrak{I}_m(\infty)\to\mathfrak{I}(\infty) \text{ as } m\to\infty, \tag{41}$$

where $\mathfrak{I}(\infty)$ and $\mathfrak{I}_m(\infty)$ are the (positive) limits of $\mathfrak{I}(\tau)$ and $\mathfrak{I}_m(\tau)$ as $\tau\to\infty$.

6. *Final remarks.*—We have proved that $\|\mathfrak{I}-\mathfrak{I}_m\|\to 0$ as $m\to\infty$ whenever $0<\varpi_0\leqq 1$. By (2) and (6), $\mathfrak{I}-\mathfrak{I}_m=\varpi_0(J-J_m)$. Therefore,

$$\|J-J_m\|\to 0 \quad \text{as } m\to\infty. \tag{42}$$

The expressions in (10) and (13) for I and I_m in terms of $\mathfrak{I}$ and $\mathfrak{I}_m$ can be used to prove that, as $m\to\infty$.

$$I_m(\tau,\mu)\to I(\tau,\mu) \text{ uniformly for } 0\leqq\tau<\infty \text{ and } -1\leqq\mu\leqq 1. \tag{43}$$

Since the proof of (43) is formally identical with that of Theorem 2 of (5), it is omitted. The estimates derived for $\|\mathfrak{I}-\mathfrak{I}_m\|$ imply corresponding estimates for the deviations of J_m and I_m from J and I.

This completes the proof of the theorem stated in Section I.

Mathematics Research Centre,
U.S. Army,
University of Wisconsin:
1959 *October.*

References

(1) S. Chandrasekhar, *Radiative Transfer*, Oxford University Press, 1950
(2) J. B. Sykes, *M.N.*, **111**, 337–386, 1951.
(3) Zdenek Kopal, *Numerical Analysis*, Chapman and Hall, Ltd., London, 1955.
(4) Philip M. Anselone, Integral Equations of the Schwarzschild-Milne Type, *Journ. of Mathematics and Mechanics*, **7**, 557–570, 1958.
(5) Philip M. Anselone, *Ap.J.*, **128**, 124–129, 1958.
(6) Philip M. Anselone, *Ap.J.*, **130**, 881–883, 195.
(7) Eberhard Hopf, *Mathematical Problems of Radiative Equilibrium*, Cambridge University Press, 1934.

NOTICE TO AUTHORS

Presentation of Papers at Meeting

At some meetings of the Society the background and conclusions of selected papers are presented and then discussed. In order to assist the Secretaries in the selection of papers for such meetings, authors are asked to let the Society know, when submitting papers, whether they would be willing to give an account of their paper, if requested.

The attention of authors resident abroad is drawn to the fact that the Society welcomes information about their work. The Secretaries would be happy to consider having such work described at a meeting, in accordance with the author's wishes, either by a Secretary or other Fellow.

Publication of Papers

1. *General.*—It is the aim of the Society to be of the greatest possible service in disseminating astronomical results and ideas to the scientific community with the utmost possible speed. Contributors are accordingly urged to give the most careful consideration to the presentation of their work, for attention to detail will assuredly result in a substantial saving of time.

It is the practice of the Society to seek a referee's opinion on nearly every paper submitted for publication in *Monthly Notices*; experience has shown that frequently the comments of referees have enabled authors to improve the presentation of their work and so increase its scientific value.

2. *Communication.*—Papers must be communicated to the Society by a Fellow. They should be accompanied by a summary at the *beginning* of the paper conveying briefly the content of the paper, and drawing attention to important new information and to the main conclusions. The summary should be intelligible in itself, without reference to the paper, to a reader with some knowledge of the subject; it should not normally exceed 200 words in length. Authors are requested to submit MSS. in duplicate. These should be typed using double spacing and leaving a margin of not less than one inch on the left-hand side. Corrections to the MSS. should be made in the text and not in the margin. By Council decision, MSS. of accepted papers are retained by the Society for one year after publication; unless their return is then requested by the author they are destroyed.

3. *Presentation.*—Authors are allowed considerable latitude, but they are requested to follow the general style and arrangement of *Monthly Notices*. References to literature should be given either in the traditional form of a numbered list at the end of the paper, or as prescribed in *Notes on the Preparation of Papers to be Communicated to the Royal Society*.

4. *Notation.*—For technical astronomical terms, authors should conform closely to the recommendations of Commission 3 of the International Astronomical Union (*Trans. I.A.U.*; Vol. VI, p. 345, 1938). Council has decided to adopt the I.A.U. 3-letter abbreviations for constellations where contraction is desirable (Vol. IV, p. 221, 1932). In general matters, authors should follow the recommendations in *Symbols, Signs and Abbreviations* (London: Royal Society, 1951) except where these conflict with I.A.U. practice.

5. *Diagrams.*—These should be designed to appear upright on the page, drawn about twice the size required in print and prepared for direct photographic reproduction except for the lettering, which should be inserted in pencil. Legends should be given in the manuscript indicating where in the text the figure should appear. Blocks are retained by the Society for 10 years; unless the author requires them before the end of this period they are then destroyed. Rough copies or prints of the diagrams should accompany each manuscript.

6. *Tables.*—These should be arranged so that they can be printed upright on the page.

7. *Proofs.*—Authors are liable for costs of alteration exceeding 5 per cent of composition. It is therefore in their own and the Society's interests to seek the maximum conciseness and simplification of symbols and equations consistent with clarity.

CONTENTS

PAGE

A. A. Weiss, Radio-echo observations of southern hemisphere meteor shower activity from 1956 December to 1958 August 387

E. J. Öpik, The lunar surface as an impact counter 404

P. J. Treanor, The spatial analysis of magnetic fields in sunspots 412

Olin J. Eggen, Stellar groups, V. Luminosities, motions and masses of the late-type subgiants 430

Olin J. Eggen, Stellar groups, VI. Space motions of the dwarf A-type and giant M-type stars in the solar neighbourhood... 448

M. W. Feast and A. D. Thackeray, 47 Tucanae: radial velocities and spectral types of individual stars 463

R. D. Davies, A study of neutral hydrogen in the solar neighbourhood of the Milky Way 483

Philip M. Anselone, Convergence of Chandrasekhar's method for the problem of diffuse reflection 498

Printed in London by Taylor & Francis, Ltd., 1960 June